The Electromyography, Electronics and Sensory System for a Mechatronics Integrated Touch Hand 3

By

Andrew Mangezi (211543957)

Submitted in partial fulfillment of academic requirements of

Masters of Science in Mechatronics Engineering

In the College of Agriculture, Engineering and Science

University of KwaZulu-Natal

Howard College

South Africa

July

PREFACE

The research contained in this dissertation was completed by the candidate while based in the discipline of Mechanical Engineering, School of the College of Agriculture, Engineering and Science, University of KwaZulu-Natal, Howard College, South Africa. The research was financially supported by Technology Innovations Agency.

The contents of this work have not been submitted in any form to another university and, except where the work of others is acknowledged in the text, the results reported are due to investigations by the candidate.

_____

Signed: Professor Riaan Stopforth

Date:

DECLARATION: PLAGIARISM

I, Andrew Mangezi, declare that:

I. The research reported in this dissertation, except where otherwise indicated or acknowledged, is my original work;

II. This dissertation has not been submitted in full or in part for any degree or examination to any other university;

III. This dissertation does not contain other persons' data, pictures, graphs or other information, unless specifically acknowledged as being sourced from other persons;

IV. This dissertation does not contain other persons' writing, unless specifically acknowledged as being sourced from other researchers. Where other written sources have been quoted, then:

   i. their words have been re-written but the general information attributed to them has been referenced;

   ii. where their exact words have been used, their writing has been placed inside quotation marks, and referenced;

   iii. where I have used material for which publications followed, I have indicated in detail my role in the work;

V. This dissertation is primarily a collection of material, prepared by myself, published as journal articles or presented as a poster and oral presentations at conferences. In some cases, additional material has been included;

VI. This dissertation does not contain text, graphics or tables copied and pasted from the Internet, unless specifically acknowledged, and the source being detailed in the dissertation and in the references sections.

Signed: _____

Date: _____

DECLARATION 2 – PUBLICATIONS

Details of contribution to publications to be submitted that form part and/or include research presented in this dissertation:

- Mangezi, A., Stopforth, R., "Comparison of the Contact and Non-Contact Embroidery EMG Electrodes for the Prosthetic Control.", to be submitted
- Mangezi, A., Stopforth, R., "Contactless EMG Electrodes Design and Development for Prosthetics.", to be submitted

Signature: . . . . . .

ACKNOWLEDGEMENTS

Foremost, I would like to express my heartfelt gratefulness to my Supervisor Prof. R. Stopforth of the uninterrupted support of my master's research, for his serenity, inspiration, enthusiasm, and knowledge.

Many thanks also go to my fellow labmate, for the courage, wonderful collaboration and sleepless nights we were working together before deadlines. In addition, I thank all my friends for their encouragement and motivation.

I would like also to convey my special thanks to my family: Baba naMai Mangezi for their wise counsel, sympathetic ear, and support throughout my life.

Above all, I give thanks and praise to the highest God, Jehovah for the completion of this master's thesis.

ABSTRACT

This research presents the EMG, electronics and sensory system for a mechatronics integrated Touch Hand 3. This unique myoelectric hand was driven by EMG signals captured at the surface of the skin in order to achieve a more robust grasp. The research consisted of different configurations and types of electrodes to be used for an EMG device, with the research analysis of the different candidates to control the Touch Hand 3. In addition, the EMG experimental results to compare contact and non-contact electrodes were carried out to find a correlation between the EMG electrodes and an antenna. These results determined the number of layers that the EMG sensor will need to obtain the best reading in a patch-yagi antenna. Stick-on electrodes were used to monitor two muscle groups in the arm at the same time. Contact and non-contact electrode tests were conducted, which used a combination of the embroidery electrodes and the stick-on electrodes. The flexion-extension muscles were tested in the experiments, by letting each volunteer lift a 2.5 kg weight. The electronics and sensor system had to be researched, designed, developed and optimized to allow for a successful integration of the Touch Hand 3. The artificial arm is fitted with palpable sensors to read the object temperature, force, and vibration. A number of constraints were considered in designing the system including the modularity of the system, cost, weight, and its grip strength in comparison with the Touch Hand 2. The modular electrical system was designed to accommodate full control and integration with the mechanical system to form a myoelectric mechatronics prosthetic system to be used by the amputees more effectively in a quicker response.

TABLE OF CONTENTS

LIST OF FIGURES

1.0. INTRODUCTION AND LITERATURE REVIEW

2.0. ANTENNAS AND EMG CORRELATION

3.0. RELATIONSHIP OF EMG TO PHYSICAL PARAMETERS

4.0. ELECTRONICS AND MECHANICAL

5.0. TESTS AND RESULTS

LIST OF TABLES

CHAPTER 1: INTRODUCTION AND LITERATURE REVIEW

1.0. INTRODUCTION

Development of a myoelectric prosthetic hand with the capability of the human hand is one of the grand challenges of robotics. A Biomimetic study of the human hand has become important to duplicate the functionality and gesture features of the physical human hand. In order to improve the life quality of amputees, many researchers provide an estimated use capability of a human hand to that of a robotic hand. Earlier research works developed so far on the prosthetic limb failed to consider its modularity (Gregory Kyle Jones, 2015). Modularity failed in that it did not consider the contributions of the advanced technology, many modern electronic devices that are known as microcontrollers, EMG sensors and micro actuators (Atkins *et* al., 1998). Additionally, the advancement of a flexible artificial hand, the NTU Hand III proved the modularity (Han *et* al., 2014). The modularity of the EMG, electronics, and sensory systems is vital in the designing of the Touch hand 3. The milestone of this research focuses on designing a low-cost (to the value of approximately USD 1000), lightweight, functional, upgradable and aesthetically pleasing modular hand system. The improvements of this Touch hand system are based on the commercially made artificial hands for amputees and Touch Hand 2 developed at UKZN.

The research conducted at the University of KwaZulu-Natal allowed for the implementation of electromyography electrodes to use in prosthetic devices, specifically the Touch Hand prosthetic system. The aim was to find a correlation between the electromyography electrodes and an antenna, thus obtaining the number of layers that the embroidered electrodes need to obtain the best reading in a patch-Yagi antenna configuration. Implementation of the capacitive electrode was done to compare them to the conventional contact electrodes. The capacitive electrodes were coated with a cloth as the conductor. These electrodes can be embedded in clothing not sensitive to skin. They can also eliminate the risk of delivering high currents to the test study since they are capacitive and non-contact.

1.1. LITERATURE REVIEW

Several advances in technology and research resulted in the advent of myoelectric prosthetic hands that perform many tasks with a high similarity to that of a human hand such as Bebionic3 prosthetic hand shown in figure 1-1 (RSLSteeper, 2013a).

Figure 1-1: Bebionic3

This robotic hand uses biosignals based approach to perform human-like characteristics (RSLSteeper, 2013a). The research focused on these bio signal approaches namely the EMG, electrooculography (EOG) and electroencephalogram (EEG) signals and how they could assist the disabled and amputee people to restore their missing parts full functionality. The contributions of the research include design, development, testing and optimization of EMG electrodes. These EMG electrodes improved readings in a non-contact manner, generic and modular electronic system for the control, sensory readings, and investigating different decoding methods to identify different motions the user wants to perform.

1.1.1. Electromyography (EMG) signal

Amputee and people with disabilities (Alsayegh, 2000) use electromyography technology in many applications. The human's limb muscle actions induce electrical activity to read and alter into processer's control instructions as shown in figure 1-2.

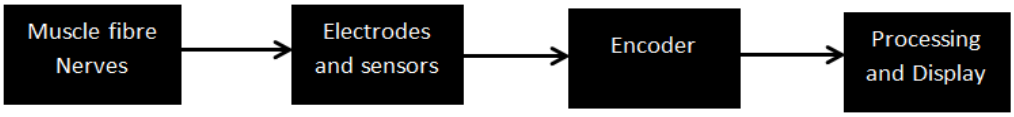

Figure 1-2: Electromyography process

Additionally, the EMG signals can be read on the person’s skin through suitable electrodes as shown in figure 1-3 (Antonios *et* al., 2008). The system based on the electrooculography (EOG) provides preferred options for mouse indicator mechanism, and are useful and valued for people with backbone injury, unlike optical systems.

As a result, their sophisticated erudition and standardization methods present the main restrictions and extra improvement (Surdilovic, 2005).

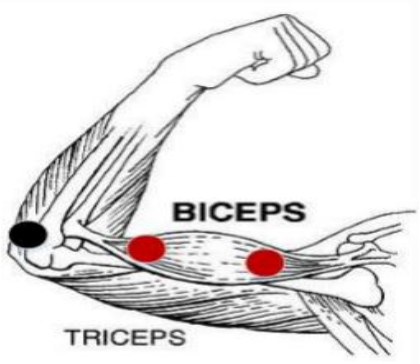

Figure 1-3: Placement of the EMG electrode

The brain-computer systems provide one major limitation because of its probable EMG contagion. The electroencephalogram (EEG) signals begin in the brain nerve cells and spread through the head and muscles to get to the surface electrodes. In addition, the EEG electrophysiological devices are made up to include extraordinary amplification since their signals are lesser in amplitude (Taberner *et* al., 1998). Therefore, any muscle actions can generate outsized noise contagion matching EMG signal. If the user has neurological disorders, this noise can be a huge problem. Furthermore, brain-computer interface scholars superlatively attempted to eradicate electromyography noise, particularly eye winks and neck actions (Pfurtscheller *et* al., 1996). The EEG is a non-invasive monitoring technique of recording brain activities on the scalp (Millan *et* al., 2004).

This technique represents the numerous activities of many cortical nerve cells, decreased spatial resolution and a low signal to noise ratio (SNR). However, intrusive techniques of monitoring assess individual activities of cortical brain nerve cells (Wessberg *et* al., 2000). Additionally, interface approaches based on brain nerve cells require high levels of training (Cheng *et* al., 2002). For the diagnosis of neurological and neuromuscular complications, researchers normally adopt EMG technology (Kamen *et* al., 2004). It was also used diagnostically by gait laboratories and by clinicians trained in the use of biofeedback assessment. In addition, electromyography was also used in many types of research laboratories, including those involved in biomechanics, movement disorders, postural control and physical therapy technology (Barreto *et* al., 1999). Moreover, it was used in medical tests to measure electrical activity in a person's muscles. It is also vital in amputees because it enhances mobility and extends the functionality of prosthesis (Berniker *et* al., 2008).

The human body produces potential difference on the skin because of electric events to coordinate with electromyography embroidery electrodes.

The differences can be measured with the embroidered electrodes, which are electrochemical transducers. The transducer changes the potential differences due to the ion flows within the muscles into visible voltage differences. These currents result from the flow of ions from one muscle fiber membrane to another. They intrinsically form part of the integrated signals, which in turn inform the muscle when to contract. Accurate EMG measurements are contingent on a diversity of aspects. The embroidered EMG signal amplitude ranges between a few microvolts to a few millivolts. The real time and frequency domain properties of these signals depend on the timing and strength of contractions, the overlying tissue characteristics, the electrode and amplifier properties (Neumann *et* al., 1995). The study of the capability of living cells, tissues, and organisms to generate electrical fields and the response of cells to the electromagnetic field was vital in this paper (Malmivuo *et* al., 1994). One such good example is muscle fibers which enable the generation of small electrical currents with respect to the production of muscle force and transmit to the EMG electrodes which act as antennas according to the human body actions.

1.1.2. Electrooculography (EOG) signal

The formation of modern communication interactions between computers and humans is suitable in bio signals. The inception of bio signals offers new prospects in comparison with conventional ones, in most cases audio-visual brain-computer interface. The eye movement is the most frequent of all human movements (Jonghwa *et* al., 2008). In addition, it was regarded as one of the main subsystems of the body, which directly relates with the visual information of interest. The position of the eye can be measured using optical, mechanical, and electrical means while providing intuitive assistive devices. In order to determine the position of the eye, the electrical technique of measurement, which is EOG, was considered the least invasive (Doyle *et* al., 2006). The EOG is the electrical recording corresponding to the direction of the eye. One of the advantages of adopting the EOG method to record eye movements is that no direct attachment to the eye itself is required (Quipping Ding *et* al., 2005) as shown in figure 1-4. As a result, this makes the adaptation of EOG for applications such as man-machine interaction very attractive.

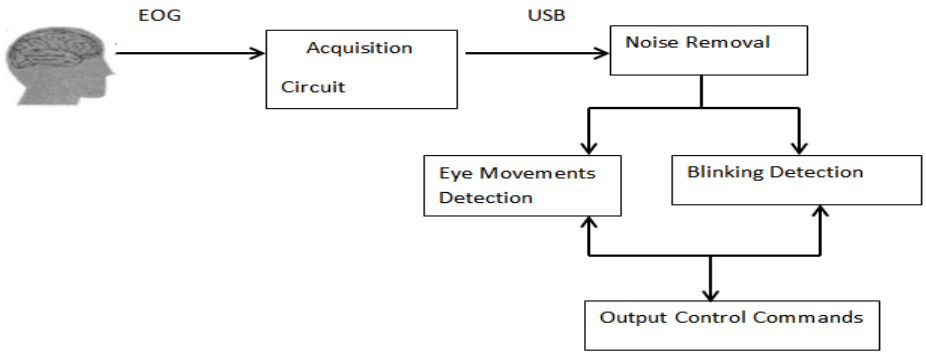

Figure 1-4: The EOG interface

1.1.3. Electroencephalogram (EEG) signal

It was observed through a number of studies that individuals with intense neuromuscular disabilities could practice Brain Computer Interface (BCI). This was done by integrating numerous features into their EEG (Wolpaw *et* al., 2002). Additionally, the EEG is of interest to the BCI community since it is among various brain signal acquisition (Ebrabimi *et* al., 2003). The interface is a developing multidisciplinary technology that enables the monitoring of the computer directly by the brain, thereby reducing dependence on normal neuromuscular pathways (Dornhege *et* al., 2007) as shown in figure 1-5.

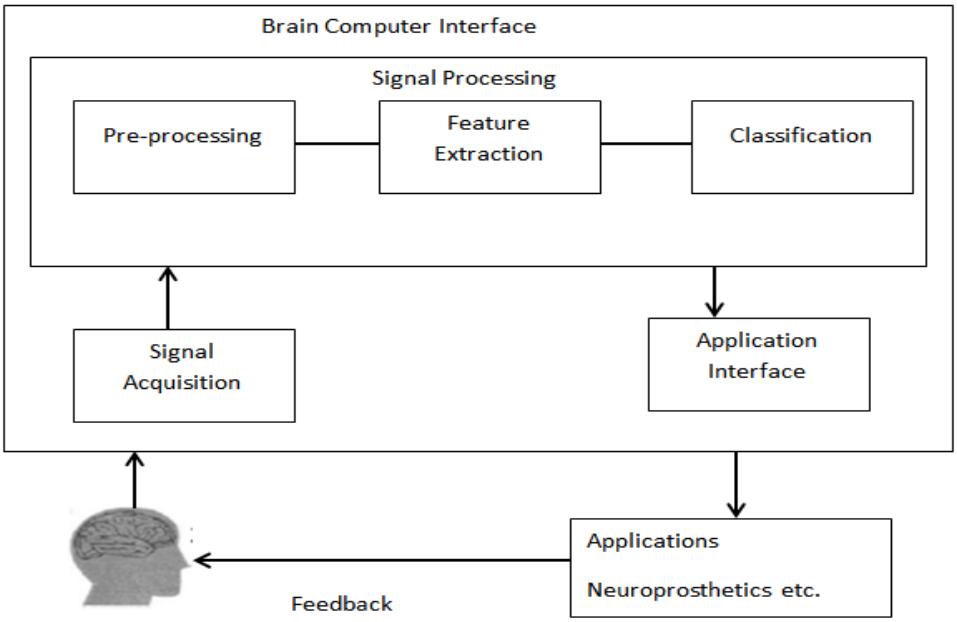

Figure 1-5: The EEG interface

The application of the technology for people with different paralysis is very important especially for those who suffer from intense neuromuscular disorders. The Brain Computer Interface has the ability to equip them with communication, control, or rehabilitation tools to assist in the full recovery of their disability. The EEG works by acquiring the brain electrical signal from the scalp, which originates from postsynaptic potentials. These signals combine at the cortex and transmit through the skull to the scalp (Fisch *et* al., 1999). The EEG-based device requires the extraction of raw data from the brain and transforms it to the device control commands through proper signal processing methods. After the recording of the cerebral electrical activities, these signals are measured and become amplified, filtered and digitized for processing in a computer (Gopi *et* al., 2006). Modulation is one of the phenomena used for BCI control of mu (8 Hz - 12 Hz) and beta (18 Hz - 25 Hz) rhythms via motor imagery (Palaniappan, 2005).

The motor imagery movements often result in the reduction in amplitude with respect to the sensorimotor cortex. As a result, BCI users are able to control magnitude through the modulation of these rhythms by switching between motor imagery tasks (Rasmussen *et* al., 2006). The EEG is often credited as being non-invasive and as a less demanding system in terms of usage thus giving it an added advantage in terms of affordability (Wolpaw *et* al., 2006). Despite these advantages, it poses challenges concerning signal processing and pattern recognition in that, it has comparatively poor signal-to-noise ratio, frequency range and restricted topographical resolution (Wolpaw *et* al., 2006). These signals of interest are normally hidden in the extremely noisy environment. However, spatial filtering (Bufalari *et* al., 2006), can improve the signal-to-noise ratio. On the contrary, the amount of training required by the user to gain a high level of control may prove to be a limitation for practical applications of brain-computer interface such as artificial control and daily computer use for disabled individuals (Guger *et* al., 2003).

1.2. BIOLOGICAL ANALYSIS OF THE FOREARM

The network of nerves and fibers forms the regulatory and communications structure of the human body (Bear *et* al., 1996). This system comprises of nerve cells that interconnect through diverse parts of the human body using electrical signals (Kandel *et* al., 2000). The network of nerves and fibers comprises of three key portions that include the cerebrum, the backbone and the peripheral network of nerves and fibers (Dalley *et* al., 2010). Nerves cells are extremely specialized cells that transmit nerve impulses messages within the different parts of the human body (Kandel *et* al., 2000). The muscle consists of groups of specific cells with the capability to contract and relax as shown in figure 1-6 (Lippert *et* al., 2006).

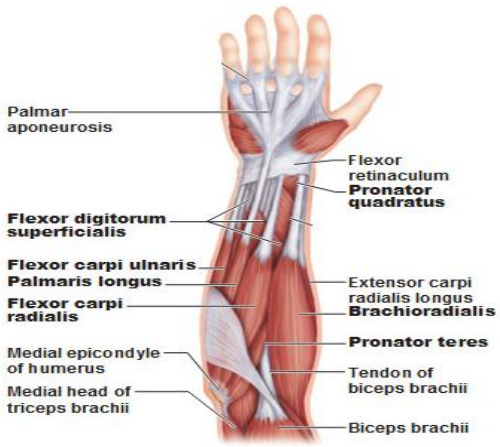

Figure 1-6: Structure of the forearm

These specific cells have the capability to transmit speech or writing and produce forces and movements. Furthermore, the muscle's capability to encode and decode stimuli results in its contraction (Andersen *et* al., 2000). The four main functions of the muscle include motion production, movement of the substance within the body, providing balance, and producing heat (Baldwin *et* al., 2014). In addition, the muscle tissues can be classified into three categories that include the skeletal muscle, smooth muscle, and cardiac muscle (Marieb *et* al., 2007). The bone attaches the skeletal muscle and its contraction is to support and move the skeleton. This contraction originates from impulses in the neurons to the muscle under controlled movement (Dalley *et* al., 2010). The EMG signal is normally proven as a filtered neuron pulses and appears random in nature (Basmajian *et* al., 1985).

1.2.1. Bones

A hand is a terminal part of the forearm with a tactile and prehensile function and a thumb opposable to the other fingers as shown in figure 1-7 (Almecij *et* al., 2009). The skeleton of the hand comprises of 27 bones, excluding the sesamoid bone in which the number differs between people, 14 of which are the phalanges (Almecij *et* al., 2009). Each human hand consists of eight carpal bones and five metacarpals, which connects the fingers and wrist (Austin, 2005). The anatomy of four of the digits namely the index, middle, ring, and small finger are the same, except for the thumb. The former fingers begin with the metacarpals, which are attached to the proximal phalanges via the proximal interphalangeal joints (PIP), followed by the distal phalanges, attached through the distal interphalangeal joints (DIP) (Austin, 2005). However, the thumb is different in that it does not contain a second phalangeal, and, secondly, there is more freedom of movement in the carpometacarpal articulation (Taylor, 1955).

The thumb was made up of two (2) bones and three (3) muscles (Almecij *et* al., 2009). The middle finger was made up of three (3) bones and four (4) muscles (Almecij *et* al., 2009). Moreover, the ring finger was made up three (3) bones and four (4) muscles and little finger consists of three (3) bones and four (4) muscles (Almecij *et* al., 2009). The wrist consists of two (2) rigid bodies (palm rigid body, which has 14 bones, and the forearm rigid body, which has two (2) bones) and six (6) muscles splines (Almecij *et* al., 2009). All the muscles are attached to the palm rigid body (Almecij *et* al., 2009).

Figure 1-7: Bones of the hand

1.2.2. The fingers and wrist

The human fingers can be flexed and extended naturally as shown in figure 1-8 (Mansfield *et* al., 2009). The wrist can be flexed, extended, abducted and adducted. These poses are achieved by giving each muscle certain activation levels. The muscle applies forces at their bone insertion points in accordance with the specified activation levels since each was attached to a bone (Lippert, 2011). Every finger has two muscles running along the top and two along the bottom while the thumb has only one muscle running along the bottom (Lippert, 2011). This muscle configuration for the fingers allows the fingers to perform flexing and extending (Lippert, 2011). Fingers are capable of abducting and adducting, but the muscles required for this range of motion are not simulated. The wrist has six muscle attachments, inserted all around the wrist, allowing it to flex, extend, abduct, and adduct. The wrist is capable of supination and pronation but the muscles and bones required for this range of motion are not simulated. In each pose, certain muscles are contracted while others are stretched, particularly those opposing the contracted muscles (Mansfield *et* al., 2009). When a finger is flexed, it is evident that the bottom two muscles are contracted and the top two are stretched.

When a finger is extended, the top two muscles are contracted and the bottom two is stretched (Mansfield *et* al., 2009). The same concept of contraction and stretching applies to the wrist for each pose that was achieved.

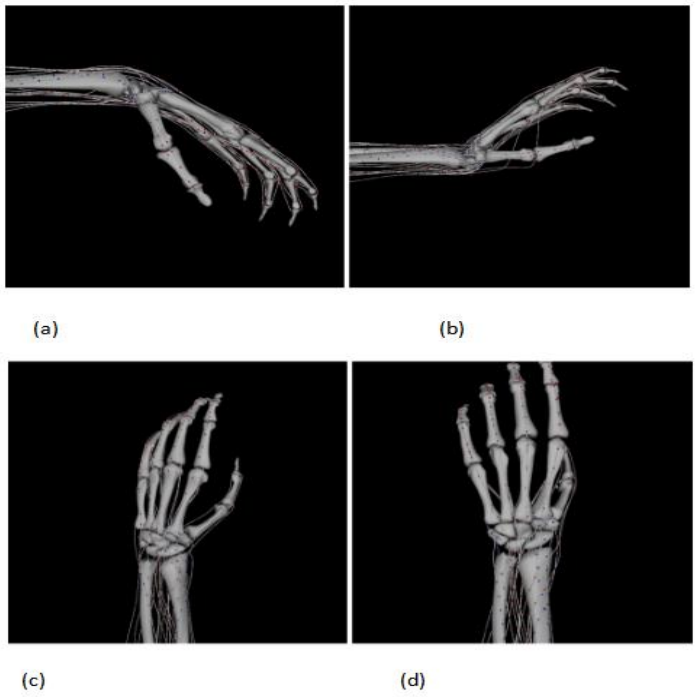

Figure 1-8: (a) Flexion (b) Extension (c) Abduction (d) Adduction

1.2.3. Action potential and excitable tissue

The network of nerves and fibers has two main types of tissues namely the excitable and non-excitable tissue. The non-excitable nerve is made up of glial cells, which are unable to react to a physical stimulus due to their non-conducting as they only work to maintain cells in the network of nerves and fibers. Excitable tissues consist of nerve cells to respond and convey nerve impulses as shown in figure 1-9 (Esther Wednesday, 2005). These nerves are made up of four parts namely the muscle fibers, axons, sensory receptors and neurons cell bodies (Esther Wednesday, 2005). On contact with high-temperature surfaces, sensory receptors can convey harmful stimulus, which may end in pressure and pain (Esther Wednesday, 2005). More so, the receptor can convey pain. The receptor potential, which results from inner current movement, conveys the potential of the membrane of the sensory receptor. In addition, the sensory receptor produces high receptor potential that rapidly decreases to a lower stable level when a nerve is stimulated by a constant high-pressure stimulus resulting in adaptation (Esther Wednesday, 2005). The nerve cells transmit messages along the axon of the nerve to the backbone base to step off that pebble. The electrical signals are carried away from the nerve cell body by nerve fiber (Esther Wednesday, 2005).

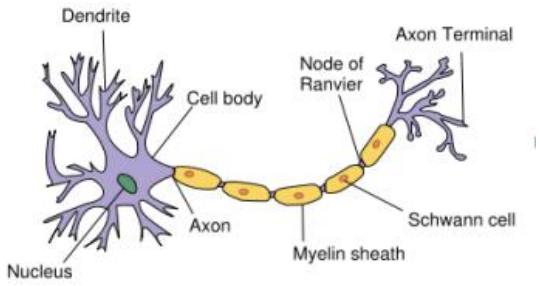

Figure 1-9: Excitable nerve cell

The nerve fiber comprises of sensory and motor axons. Distinctive time variations related to an unexpected, steady stimulus are shown in figure 1-10 (Esther Wednesday, 2005). More so, the network of nerves and fibers transmits information from sensory receptors to the brain. The high-speed messages that are transmitted by motor axons to the different parts of the body are to stimulate the contraction of the muscles (Esther Wednesday, 2005). However, the normal axons are entirely responsible for simple activities such as fluctuations in temperature and exposure pain. The motor axon transmits the action potential rupture from the nerve cells to the inner nerve cells that respond to motor neuron only (Esther Wednesday, 2005). This results in synapses, which is a chemical transmitter that was produced between thin fluid gaps. The gland is the ultimate specific junction that allows nerve cells to send signals to their target cells (Esther Wednesday, 2005). The muscle contracts when the signal gets to the muscle tissue, which is as result of lifting small objects (Esther Wednesday, 2005).

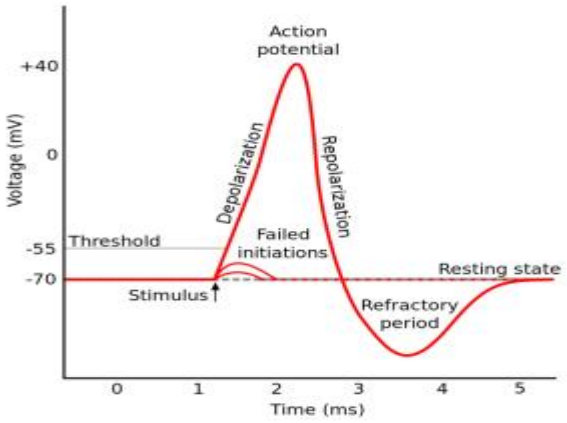

Figure 1-10: Action potential

1

1.3. POSSIBLE IMPROVEMENTS ON TOUCH HAND 2

Touch hand 3 is an improved version of Touch hand 2, which was designed at the UKZN. It was noted that the previous design had its own flaws in the electronic hardware, motor control, grip forces and user interface.

1.3.1. Electronic hardware

According to the design objectives, the electronic hardware that was designed for Touch hand 3 was modular to allow for easy maintenance and repair. In addition, the aim was to create an aesthetically pleasing and compatible electronic board. Touch hand 2 designed an all in one circuit board as shown in figure 1-11 (Jones, 2015). This means that all the components were mounted on one circuit board, which makes it difficult to identify the faults and repair.

Figure 1-11: Printed Circuit board (PCB)

1.3.2. Control

The control of the Touch hand 3 was similar to how the normal human hand functions. This myoelectric hand uses EMG signals to perform different grasping tasks with human–like futures whilst Touch hand 2 was based on the commands send from the Graphical user interface. In addition, Touch hand 3 aims to reduce the maximum grip type selection time by speeding the movement of the hand. More so, the mechanism for the grip force was used in the design of the Touch hand system. This could also include the automatic grip force control through slip detection the grip force on an arbitrarily shaped object would change such that it does not slip out of the grasp (Jones, 2015).

1.3.3. Motor and grip force

Grip strength of the hand was crucial in designing a myoelectric prosthetic hand. Many designers focus on aesthetic instead of functionality.

Hence, the Touch hand 3 was designed to give a tighter grip to the objects in contact. This was achieved mainly by the choice of the motor with a higher torque and speed.

1.4. RESEARCH OBJECTIVES AND CONTRIBUTIONS

The design objectives for the EMG, electronics and sensory system were:

(1) Controlling the prosthetic hand using only two EMG channels.
(2) Investigation of the non-contact and contact electrodes for the Touch hand system.
(3) Designing a modular integrated EMG, electronics, and sensory system.
(4) To measure the temperature of objects, slippage, and texture of the hand.
(5) The hand should be intelligent to auto-detect modules communicate useful information to amputees.
(6) The communication protocol must be developed to work with touch hand and be capable of e.g. 2-4 sensory channels communicating simultaneously.
(7) The system should be aesthetically pleasing, low-cost and lightweight.

1.5. CHAPTER SUMMARY

This chapter gives detailed background information of the different bio signals that were considered in trying to restore full functionality of the disabled and amputee people. Upon comparison of these biosignals to use in the Touch hand system, EMG proved to be the most effective and advantageous signals to consider. In addition, the EMGs were chosen because the myoelectric signals are generated on the forearm of an amputee in Touch hand design. The EOG and EEG signals are generated on the head and eye respectively, which was not in the Touch design objectives, hence they were less prioritized. The study of the biological human analysis of the forearm particularly the muscles, wrist and fingers helped in designing a myoelectric prosthetic hand with human-like features. The objectives of the design were understood and mark the initial development of a myoelectric Touch hand 3 for amputees.

CHAPTER 2: ANTENNAS AND EMG CORRELATION

2.0. INTRODUCTION

The vital parts of industrial wireless systems are antennas. An antenna was recognized as a device, with identical impedance and can be used to link the transmitter to any medium (Milligan, 2005). They are the means for coupling the transmitter to the medium. These are electromagnetic radiators, which generate an electromagnetic field between the transmitting device to the receiver's antenna (Milligan, 2005). Electromagnetic waves are converted into electrical signals that can be utilized at the initial stages. Antennas have three broad categories namely Omni-directional, directional and semi-directional (Milligan, 2005). The study of patch-Yagi antenna effects was also an interesting focus of the research.

2.1. YAGI ANTENNA

Yagi antenna is one example of directional antennas. The antenna consists of multiple parallel elements in a line (Graf *et* al., 1999). Reflectors are the additional driven elements, which are linked to the receiver with a transmission line (Balanis *et* al., 2011). The Yagi antenna was extensively used in high gains antenna frequencies such as High Frequency (HF), Ultra High Frequency (UHF) and Very High Frequency (VHF) (Wolf *et* al., 2010). It consists of a reasonable gain, which relies on the different elements, and it is lightweight, inexpensive and simple to construct (Wolf *et* al., 2010). The bandwidth of the Yagi antenna is narrow and decreases with the increasing gain (Wolf *et* al., 2010).

2.2. YAGI ANTENNA ANALYSIS

To achieve a full analysis of a system one has to take into consideration the possible delay which is because of the limited spacing between elements (Kai, 1984). These elements require certain levels of calculation between dipole elements and mutual impedances. The model element number j as having a feed point at the center with a voltage V_j and a current I_j flowing initially. Considering two such elements the voltage at each feed point in terms of the currents using the mutual impedances Z_{ij} can be expressed as:

$$V_1 = Z_{11}\, I_1 + Z_{12}\, I_2 \qquad (2.1)$$

$$V_2 = Z_{21}\, I_1 + Z_{22}\, I_2 \qquad (2.2)$$

Z_{11} and Z_{22} are simply the ordinary driving point impedances of a dipole. Due to reciprocity $Z_{21} = Z_{12}$ .Assuming that V_1 and I_1 are the voltage and current supplied by the transmitter. Since it is shorted at its feed point implied that $V_2 = 0$. Using the above relationships, then, one can solve for I_2 in terms of I_1:

$$0 = V_2 = Z_{21}\ I_1\ +\ Z_{22}\ I_2 \tag{2.3}$$

and so

$$I_2 = -\frac{Z_{21}}{Z_{22}} I_1 \tag{2.4}$$

This is the current induced in the parasitic element due to the current I_1 in the driven element. The voltage V_1 can be solved at the feed point of the driven element using the earlier equation as

$$V_1 = Z_{11}\ I_1\ +\ Z_{12}\ I_2\ = Z_{11}\ I_1\ - Z_{12}\frac{Z_{21}}{Z_{22}} I_1 \tag{2.5}$$

Where $Z_{12} = Z_{21}$ is substituted. The ratio of voltage to current at this point is the driving point impedance Z_{dp} of the 2-element Yagi:

$$Z_{dp} = \frac{V_1}{I_1} = Z_{11}\ - \frac{Z_{21}^2}{Z_{22}} \tag{2.6}$$

The driven element present the driving point impedance would have simply been Z_{11}, but has now been modified by the presence of the parasitic element. The phase and amplitude of I_2 in relation to I_1 as computed above allows the determination of the radiation pattern due to the currents flowing in these two elements. A solution of such an antenna with more than two elements proceeds along the same lines, setting each $V_j = 0$ for all but the driven element and solving for the currents in each element and the voltage V_1 at the feed point (Uda, 1954).

2.2.1. Yagi antenna analysis calculations

Using the Yagi antenna analysis one can calculate the performance given a set of parameters and adjust them to optimize the gain to allow lower strength signals to be received. This can be explained in equation (2.6) when the Z_{22} is decreased resulting in increasing this ratio $\frac{Z_{21}^2}{Z_{22}}$. When this ratio increases to approximately Z_{11} the output Z_{dp} is minimised. It also allows the interference of the signals from the muscles to be minimised since patch Yagi antenna has a directivity. The Yagi antenna spacing, length and a variety of other factors all affect the feed impedance represented by the dipole to the feeder.

In addition, the construction of the non-contact electrodes for Touch hand system was Yagi antenna spacing and length effects. The antenna is easy to construct resulting in applying the concept to the construction of the EMG non-contact electrodes for Touch hand system.

2.3. PATCH ANTENNA THEORY

The patch antenna is a narrow band, wide beam antenna fabricated by etching an antenna element pattern in a metal trace bonded to an insulating dielectric substrate such as a printed circuit board (Bancroft, 2004). Patch antennas have different types namely the microstrip, array wire, aperture and reflectors antennas. The understanding of these different types of antennas assisted in determining the correlation between the patch antenna and EMG electrodes. In addition, it also helped in applying the principles of a particular antenna in construction of the non-contact electrodes for Touch hand System

a) Wire antenna

This type of antenna is effectively on automobiles, buildings, aircraft and various spacecraft (Winder *et* al, 2002). This comes in different shapes such as a dipole, helix, and loop (Basu, 2010). In addition, loop antennas are not necessarily circular in shape but it is the most common because of its simple design as shown in figure 2-1 (Winder *et* al, 2002).

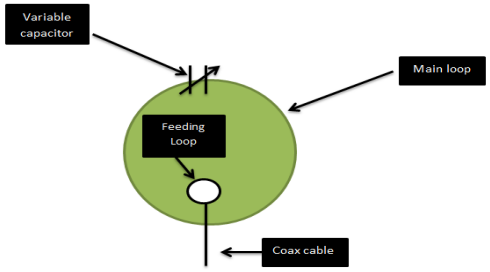

Figure 2-1: Wire antenna

b) Aperture antenna

The aperture antennas are mostly common today due to the growing demand for the utilization of very high frequencies and forms that are more enlightened (Stutzman et al., 1998). These types of antennas are considered to be of use in machines such as airplanes because they can be mounted on the skin of the crafts (Balanis, 2005). Additionally, they are enclosed with an electrical insulator to protect them from different harmful conditions. An aperture antenna (loop antenna) is as shown in figure 2-2 (Balanis, 2005).

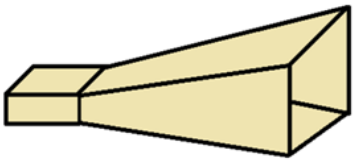

Figure 2-2: Aperture antenna

c) Microstrip antenna

They are made up of a metallic patch on a substrate that is grounded as shown in figure 2-3 (Basu, 2010). These antennas are simple and cost effective to design (Basu, 2010). One advantage of these antennas is their mechanical strength and durability when weighed on the rigid surfaces such as cars and satellites missiles (Ramesh, 2001).

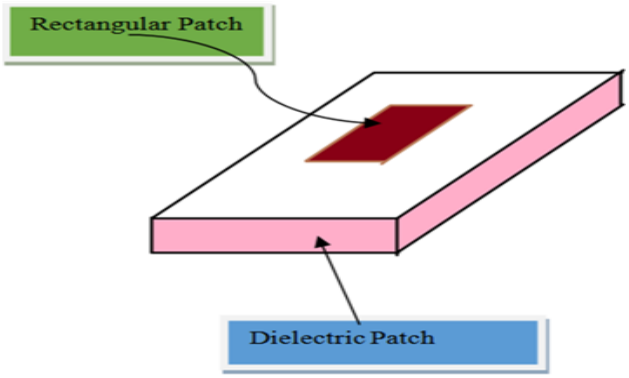

Figure 2-3: Microstrip

d) Array antenna

These are made up of a combination of numerous antennas (Balanis, 2005). The array antennas are arranged so that the radiations from the elements add up to give high radiation in a specific direction and low in other directions (Balanis, 2005).

e) Reflector antenna

The reflector antenna has the largest applications. These antennas combine feed antenna, which was known as secondary antennas, and a metallic plate, which acts as a primary antenna (John, 1998). They are mostly common in satellites, broadcasting TV, and broadcasting radio. A reflector antenna is as shown in figure 2-4 (John, 1998).

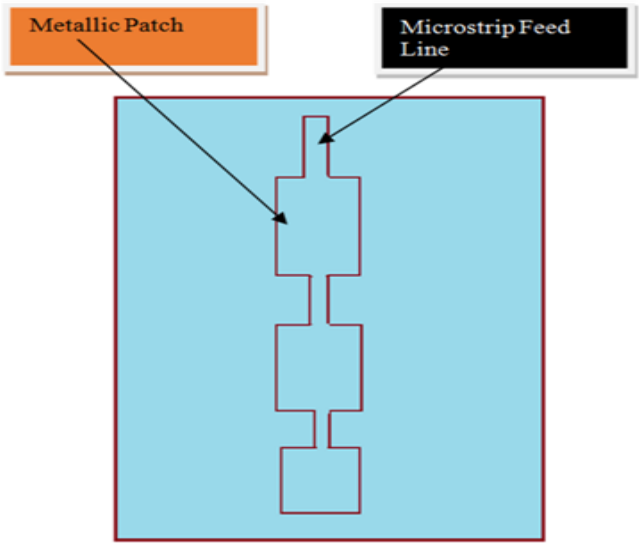

Figure 2-4: Reflector antenna

2.3.1. Patch antenna parameters

The various parameters are required to clarify the functionality and features of antennas. These essential parameters for the antenna include the beam width, directivity, gain, radiation pattern and return loss. When two similar points on opposite side of the maximum pattern of the lobe forms angular separation, this was called beam width of the pattern (Stutzman et al., 1998). The antenna pattern has a number of beam widths, for example, the half - power beam widths (HPBW). In addition, the angular separation between the initial patterns nulls (First Null Beam Width) is another vital beam width. Figure 2-5 shows the beam width of an antenna (Stutzman et al., 1998).

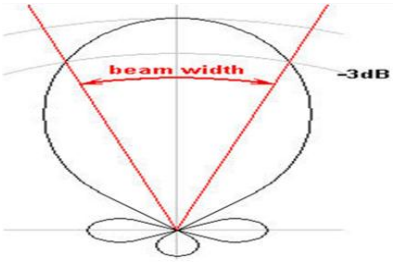

Figure 2-5: Antenna beam

The ratio of the intensity of radiation in a specified way from the antenna to the intensity of radiation averaged over all directions forms antenna directivity (Stutzman et al., 1998). The intensity of radiation was known as the ratio of total antenna power radiated to four (John, 1998). In addition, directivity was also known as antenna figure of merit. The density of the power, which an antenna emits in the direction of its powerful, was measured by directivity.

More so, the capability of the antenna to direct energy of radio frequency in a specific direction is a result of the gain of the antenna and was measured in decibel. The comparative field strength was transferred from the antenna or received by the antenna in a graphical illustration resulting in patterns of radiation (John, 1998). These antennas patterns of radiation were observed at one cut, polarization, and frequency. The reflection produced due to a disturbance in a transmission line results in signal power loss (John, 1998). This disturbance can be a mismatch with a device introduced in the transmission line.

2.3.2. Patch antenna equations

The parameters in a rectangular patch antenna, for example, the length L, width W, height H and permittivity controls the properties of the antenna as shown in figure 2-6 (Fawwaz, 2007).

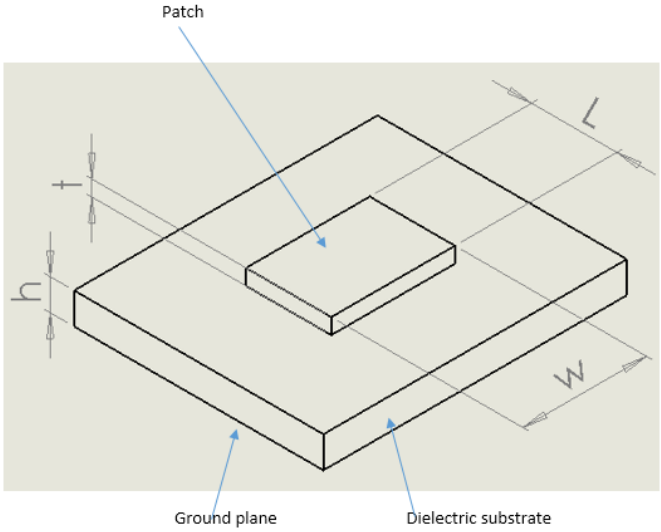

Figure 2-6: Rectangular patch antenna

An overall indication of the way the performance of the antenna was affected by parameters was well explained to comprehend the process of their design. The equations were formulated to understand how these parameters affect performance on the antenna. The patch length L controls the frequency of resonant and equation (2.7) shows the connection between length of patch and frequency of resonant (David, 1989). The impedance input was controlled by the width of the antenna and patterns of the radiation. In addition, the lowering of the impedance input results in broader patch. In order to obtain improved radiation, the permittivity ε_r has to lower which results in broader fringes. In addition, the reduction in permittivity results in increase in the bandwidth and efficiency of the antenna. However, the antenna impedances rise with higher values of the permittivity, which permits shrinking of the patch antenna.

One method that can be used to obtain half wavelength of the antenna is to consider substrate with extreme permittivity. Equation (2.8) was obtained by solving equation (2.7) to find *L*.

$$f_c = \frac{C}{2L\sqrt{\varepsilon_r}} = \frac{1}{2L\sqrt{\varepsilon_0 \varepsilon_r \mu_0}} \tag{2.7}$$

$$L = \frac{1}{2f_c\sqrt{\varepsilon_0 \varepsilon_r \mu_0}} \tag{2.8}$$

Moreover, the quadruples of the permittivity lowers the length required by a factor of two (Fawwaz, 2007). Furthermore, the bandwidth was controlled by the substrate height h, which indicates that when the height increases, the bandwidth also increases. The principle states that an antenna occupying additional space in a spherical volume results in a broader bandwidth (Fawwaz, 2007). This applies when stating that increasing the thickness of the dipole antenna increases its bandwidth. Additionally, the increase in the height results in the increase of the antenna efficiency. The increased height prompts surface waves that move within the substrate. The equation (2.9) describes how the bandwidth works with these parameters:

$$B\ \alpha\ \frac{\varepsilon_r}{\varepsilon_r^2}\frac{W}{L}\ h \tag{2.9}$$

2.3.3. Antenna and EMG electrodes construction

After carefully understanding the different types of the antennas and their properties, investigations were carried out to determine the correlation between the EMG electrodes and the patch antenna. The construction of the non-contact EMG electrodes for Touch hand system used the principle of the microstrip antenna. This was because the antennas possess well matched to planar and non-polar surfaces, easy, low profile and affordable to design. The low cost and simple non-contact electrodes were constructed using the Ag/AgCl chloride and Aluminium to create different layered electrodes. The other antennas principle was not applied in the construction of the electrodes because of their various applications in buildings, automobiles, and various spacecraft. The parameters that affect the antenna performance were used to investigate the performance of different layered non-contact EMG electrodes. The construction of the EMG electrodes was based the Yagi-patch antenna. Equation (2.1) shows how the frequency of resonant controlled the patch length. The equation shows that resonant frequency and length of the patch antenna increases and decreases inversely. This information is important in the construction of the non-contact electrodes because it helps in determining the appropriate length of the electrodes to be constructed. Additionally, when the bandwidth increases, the dipole antenna thickness also increases. This principle was used in the construction of the different electrode layers.

2.4. EMG ELECTRODES

For the myoelectric prosthetic hand to properly function, EMG electrodes were placed on the forearm muscle of the amputees. The electrode's positive and negative connections were placed on the two forearm muscles and the ground connection was placed on the neutral body part. There are many different types of electrodes used by amputees in the myoelectric process. In this regard, the investigations focused mainly on contact and non-contact embroidered electrodes. The idea on how the Yagi antenna relates to the electrodes was in cooperated in this dissertation.

2.4.1. Contact electrodes

Contact electrodes are used where there is in fact little noise recording (Fernandez, 2000). Additionally, these contact electrodes are not polarized and have a steady half-cell. However, there are large amounts of excess noise present in recordings in biological signals. The source of extra noise is as result of the equilibrium processes localized at the surface of the skin and residual EMG signal from nearby muscles (Huigen *et* al., 2002). The skin was abraded in order to lower extra noise. The electrode type used determines the level of noise. In addition, amplifiers, capacitive and inductive interference and motion artifacts also reduce the signal noise ratio. One of the type of the contact electrodes that were used in the touch hand system was the covidien electrodes shown in figure 2-7.

Figure 2-7: Contact electrodes

2.4.2. Non-contact electrodes

The non-contact electrodes are covered with conducting layers attached to the person skin. The non-contact electrodes that were investigated and tested for touch hand system include the developed contactless and embroidered electrodes shown in figure 2-8 and figure 2-9 respectively.

These electrodes were free of noise, easy to use and affordable. As a result, these electrodes were used in the experiment to determine the correlation between EMGs and antenna, taking into consideration the Yagi- patch antenna configuration.

Depending on the type of application, different electrodes and electrode placing might be used. The type of embroidery electrodes that were used in this experiment is shown in figure 2-8. These electrodes were made up of the combination of the sewn electrodes and cloth as the conducting layer.

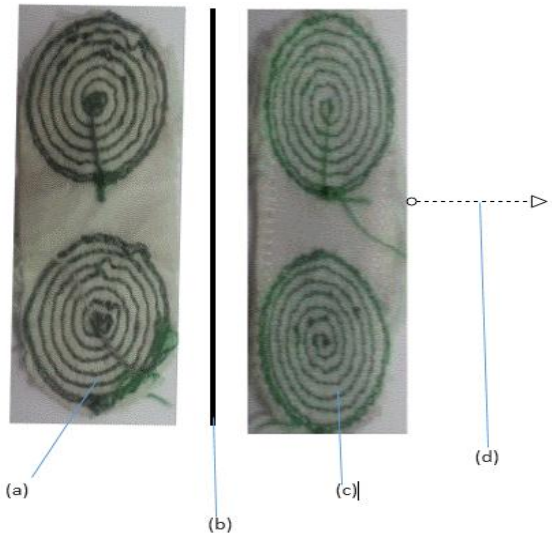

Figure 2-8: Embroidered electrodes layering- (a) under layer (b) cloth (c) upper layer (d) increasing the number of electrodes layers.

Another type of non-contact electrodes that was coupled with aluminum foil as a conductor is shown in figure 2-9.

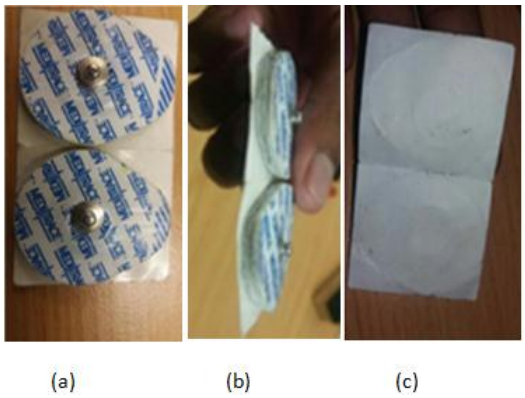

Figure 2-9: Non-contact developed contactless electrodes showing (a) top view (b) side view showing the different layers (c) a bottom view.

The aluminum foil layer was used in the construction of the developed contactless electrodes because of easy availability, very light and thin, and its metallic features (Ferris, 1972).

Different electrodes layers were constructed and tested to determine the best electrode to be used for the Touch hand system. These electrodes were tested with the silicon layer placed on the person skin and compare the results with the other EMG electrodes. The idea behind the construction of these electrodes was to prove the existence of the antenna, in particular, the Yagi- patch antenna.

2.5. SOURCE OF NOISE

One of the problems identified in designing myoelectric hands is the noise due to the EMG electrodes and amplifiers. In addition, the two kinds of the source of noise include the direct current and alternating current, which results from the transfer of an ionic to an electronic form (Duchene & Goubel, 1993). The variations between the electrode sensor and the person's skin due to chemical reactions of electrode gel and the skin results in direct current (Gerdle *et* al., 1999). However, alternating current results from various factors such as variations in impedance between the person skin and conductive transducer. The impedance effects can be reduced by using non-contact electrodes, which are noise free. These electrodes were made up of silver chloride and aluminum foil as a conducting layer.

In addition, the two types of noise that need to be considered in designing the Touch hand system were transducer and ambient noise. The noise that was produced by electromagnetic devices such as force plates, power lines, and computers was known as ambient (Day, 1997). Any device that was plugged into the outlet of the wall alternating current can permit ambient noise and has an extensive range of frequencies. However, the junction of the electrode-skin generates transducer noise. Amputees often find difficulties in decoding and encoding EMG readings due to unwanted noise resulting in poor performance of the prosthetic hand.

The designing of the Touch hand 3 aims to reduce these kinds of noise in order to get the full functional hand for the amputees. Therefore, understanding the different sources and types of noise was a logical step towards the development of the myoelectric artificial hand. To reduce these noises, a number of factors were considered that includes construction of non-contact electrodes, ensuring that the amplifiers connected to the electrodes were not close to the computers in case of ambient noise and the introduction of filtering methods in decoding and encoding EMG signals.

2.6. CHAUVENET'S CRITERION

This technique theoretically retrieves a portion of statistics as an outlier from a usual of observations (William, 1891).

The notion behind this criterion is to get a probability range from the normal distribution centered mean as illustrated in figure 2-10 that would sensibly comprise of all *n* samples of a statistical set (Aicha, 2003).

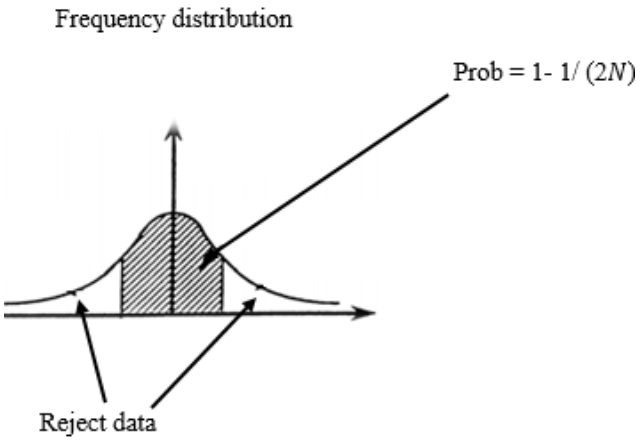

Figure 2-10: Normal distribution

Any outliers refer to any statistical points that have n samples that lie outside this probability range. These statistical points can be eliminated from the information set, and new standard deviation and mean based on the outstanding values and new sample size can be calculated. This was accomplished by calculating standard deviations number that match to the limits of the probability range around the mean D_{max} and equating that value to the exact value of the difference between the assumed outliers and the mean divided by the sample standard deviation.

$$D_{max} \geq |(x - \mu)|/\sigma \qquad (2.10)$$

Where

D_{max} = highest acceptable deviation.

x = assumed outlier value

μ = mean sample

σ = standard deviation sample

In order to be considered as including all n observations in the sample, the probability band (centred on the mean) must only account for $(n - ½)$ samples (if $n = 3$ then only 2.5 of the samples must be accounted for in the probability band) (William, 1891). In reality, partial samples cannot be achieved so $(n - ½)$ that is (2.5 for $n = 3$) is approximately n.

Anything less than $(n - ½)$ is approximately $n - 1$ that is (2 if $n = 3$) and is not valid because the aim to find the probability band that contains n observations, not $(n - 1)$ samples. In short, the probability P is equal to $(n - ½)$ out of n samples (William, 1891).

$$P = (n - ½)/n \quad (2.11)$$

Where

P = probability band centred on the sample mean,

n = sample size.

The quantity $(1/(2n))$ corresponds to the combined probability represented by the two tails of the normal distribution that fall outside of the probability band P. In order to find the standard deviation level associated with P, only the probability of one of the tails of the normal distribution needs to be analysed due to its symmetricity.

$$Pz = (1/(4n)) \quad (2.12)$$

Where

Pz = probability represented by one tail of the normal distribution,

n = sample size.

$$Z = (x - \mu)/\sigma \quad (2.13)$$

Where

Z = z-score,

x = sample value,

μ = 0 (mean of standard normal distribution),

σ = 1 (standard deviation of standard normal distribution).

2.6.1. Chauvenet's application and its relevance to the touch hand system

This criterion was used to find the probability band of the results that were obtained in the experiment that was carried out at the University of KwaZulu-Natal.

The aim was to determine the type of the electrode to be used in the Touch hand system, particularly the Touch hand 3. The flexion-extension muscles were tested in the experiments, by letting each volunteer lift a 2.5 kg weight. Nine volunteers did the experiment. In addition, 9 samples of data were recorded and from these statistical points, outliers obtained were considered to be outside this probability range. In practice, not all the readings obtained from the experiment are correct due to the human errors such as systematic and random errors in lifting the weight. In this case, errors were due to the improper positioning of the hand on picking up the weight. In addition, the errors were due to the inconsistent force exerted on the flexion muscles by the volunteers. The errors were also due to muscle fatigue because of the repeated and continuous lifting of the weight for five different layers by the volunteers. The incorrect readings were regarded as outliers and to get rid of the outliers, Chauvenet's criterion was used. The outlier data points were eliminated from the statistical set, a new standard deviation and mean obtained from the outstanding values, and new sample size was calculated. As the result of the chauvenet's criterion, smooth and clear graphs were obtained.

2.7. CHAPTER SUMMARY

This chapter summary the possibility of combining a patch-Yagi antenna configuration with the embroidered EMG electrodes. The results obtained from this investigation shows that embroidered electrodes work best with 2 layer electrodes. It was also an important aspect to reduce noise in order to get the full functional hand for the amputees. Therefore, understanding the different sources and types of noise was a logical step towards the development of the myoelectric artificial hand. This led to the construction of the non-contact electrodes for the Touch hand system. It was noted that the non-contact electrodes have many advantages over contact electrodes. The first advantage was that non-contact method is that they are durable and can be placed comfortably onto the person skin. Less noisy and smoother graphs were observed for non-contact electrodes than contact electrodes. The feature implementations of non-contact electrodes for amputees have been obtained, because of their sophisticated, comfortable and non-obtrusive EMG measurements.

CHAPTER 3: RELATIONSHIP OF EMG TO PHYSICAL PARAMETERS

3.0. INTRODUCTION

The design of the Touch hand considered quite a number of physical parameters and their relationship with the EMG technology. These biomechanical variables include the force, velocity and muscle fatigue. The study of the relationship of EMG and these physical parameters is vital in the design development of the Touch hand system.

3.1.1. Force

During the limb movement patterns, one can derive the EMG signals amplitude, which could be interpreted as an extent of the comparative tension of the muscle. When the tension varies with time, the linear envelope to process the EMG was broadly used to find the relationship between the tension and EMG signal. The tension measured was described as the mean value of the corrected EMG signal for constant tension experiments (Huigen *et* al., 2002). The force due to muscles was approximated by recording the EMG signals. The approximated force was usually calculated based on the corrected signal or after proper low pass filtering of the corrected EMG signal. The muscle fibers generate a distinguished waveform that comprises of the space-time addition of the action potentials of the separate muscle fiber (Basmajian *et* al., 1985).

3.1.2. Velocity

The increase in velocity extends the time of the activity of the muscle resulting in earlier or longer lasting activity. The person's mobile speed can increase the amplitude of the EMG signals. However, the relaxed person's mobile speed can reduce the activity of the EMG (Broman, 1985). The person's mobile speed was a vital constraint in designing a myoelectric artificial hand particularly the Touch hand 3 so as to understand the state of the activity of muscle and relate it to the EMG signal.

3.1.3. Muscle fatigue

When a muscle is performing an activity, it gets tired and starts to underperform. This results in fatigue in muscles, which is due to the discharge of lactic acid (De Luca, 1984). It was believed that the movement of the calcium between the muscle cells seems to restore the issue of the muscle fatigue (De Luca, 1984). The motor action potentials shape could be modified from the point of view of an EMG because of fatigue. Furthermore, fatigue can decrease because of the decrease in EMG spectrum components with higher frequency.

3.2. RELATIONSHIP OF THESE PHYSICAL PARAMETERS TO TOUCH HAND 3

It was important in Touch hand design to study these physical parameters and their relationship to an EMG. The study proved that muscle tension and EMG signal amplitude increases positively with respect to isotonic movements. The amplitude of the EMG is not directly proportional to the accumulation of isometric tension during muscle contraction because of the lag period. As a result, it is challenging to approximate the force produced from EMG recordings. More so, there is an uncertainty in validating the amplitude and force relationship while numerous muscles are crossing the same or multiple joints. Concerning concentric and eccentric contractions, and considering the activity of the muscle, one can conclude that eccentric contractions release limited muscle activity than concentric contraction while operating against equivalent force (De Luca, 1984). When the muscle gets tired, one observes that the tension reduces and the amplitude increases. Furthermore, fatigue lowers the component of the EMG signal with high frequency, which could be observed by the median frequency reduction of the muscle signal. On the other hand, the movement velocity and strength production with concentric contractions have inverse proportionality while the movement velocity and strength of production with eccentric contractions have positive proportionality. In summary, eccentric contractions can accommodate extra weight at greater speed. The muscle fibers generally produce not greater force to pick up a heavy load but the muscle EMG activity holding the load could be smaller. This results in the inverse proportionality for concentric contractions and positive relationship for eccentric contractions with respect to the speed of movement.

3.3. RECOMMENDATIONS FOR CONTACT AND NON-CONTACT ELECTRODES

The recommendation for the construction of the non-contact electrodes includes the shape, size, distance, materials used and construction of the electrodes.

3.3.1. Shapes of the electrodes

The electrode shape was defined as the conductive area. Electrodes come in several shapes from circular to the square to bar-shaped electrodes. The comparison was carried out between the big and small electrodes in both contact and non-contact electrodes. Although the conductive was the same size, the small electrodes produced better EMG signals than the bigger electrodes. The graph in figure 3-1 showed the average voltage of 0.172 V.

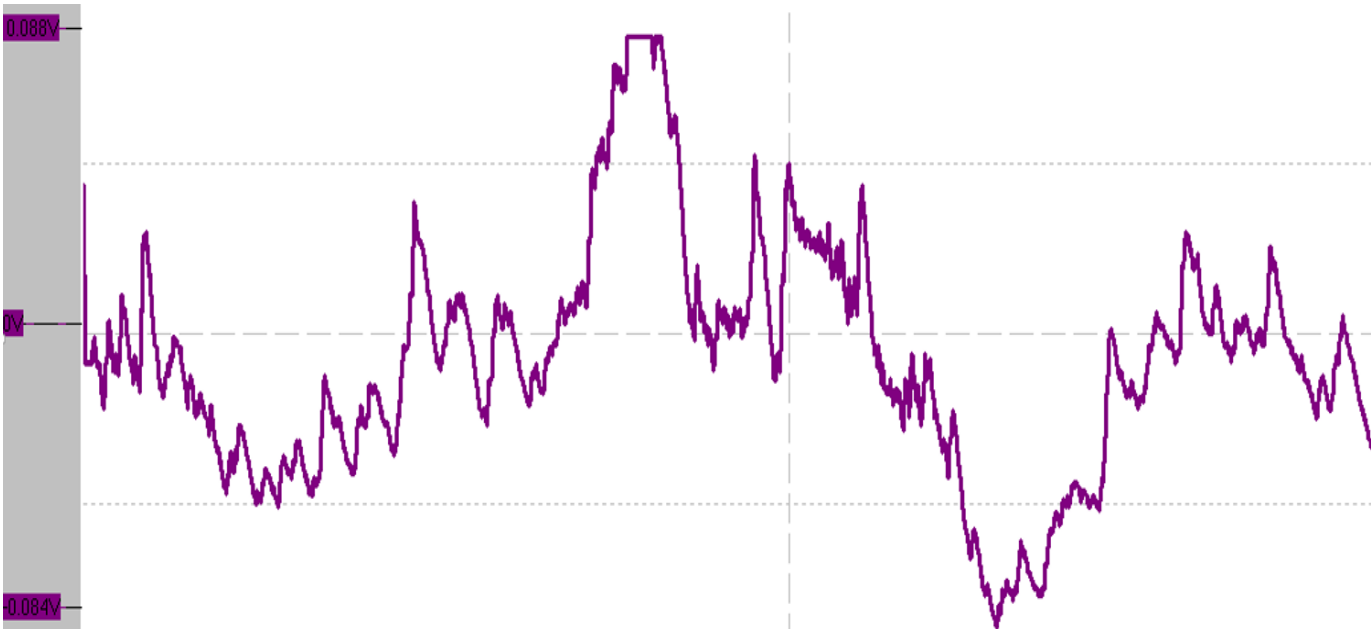

Figure 3-1: Small stick-on electrode

Furthermore, figure 3-2 shows the average voltage of 0.14 V that was obtained from the big stick-on electrodes. Comparing the average voltages of the two electrodes, one could conclude that small electrodes produced best EMG readings, as it produced higher amplitude in voltage for the same action performed.

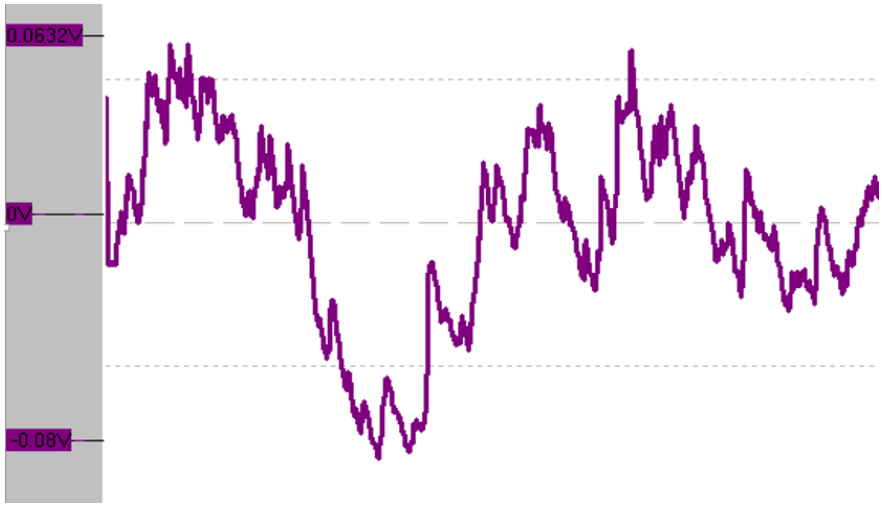

Figure 3-2: Big stick-on electrodes

3.3.2. Size of the electrodes

The electrode size refers to the surface area size of a contact or non-contact electrode as illustrated in figure 3-3. According to the patch antenna theory, the greater the size of the electrode surface area the better the EMG signals obtained from the amputee's muscle.

However, the theory contrasts with the investigations carried out to compare the average voltages of the big and small stick-on electrodes. The average voltages values of the obtained from the graphs in figure 3-1 and figure 3-2 were 0.17 V and 0.14 V respectively. The results obtained from these investigations conclude that the smaller electrodes size the better the EMG signals.

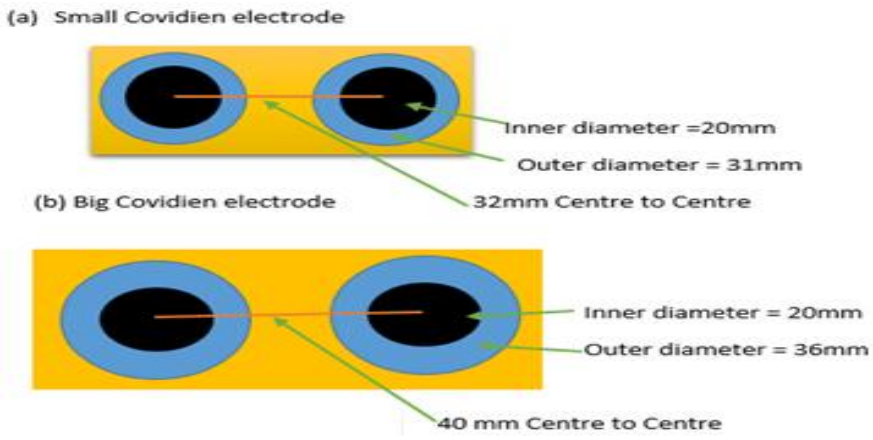

Figure 3-3: Electrode Size – (a) Smaller stick-on electrode (b) Big stick-on electrode

3.3.3. Distance between the electrodes

This refers to the distance between two centers of the EMG electrodes as shown in figure 3-4. It was important to understand the relevance of the inter-distance and cross talk to the construction of the Touch hand system electrodes. The developed contactless electrodes were made up to be used by the amputees. The objective was to find the best electrode layer that can be easily affordable, cheap and durable. With regard these electrodes that were constructed as shown in figure 3.5, the inter-electrode distance was put in consideration. The center to center was kept as close together as possible to avoid cross-talk between the two electrodes as shown in figure 3-4, hence avoiding incorrect readings during the experiment.

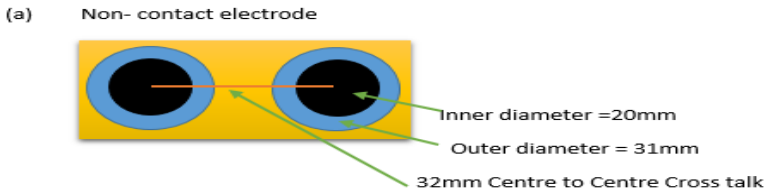

Figure 3-4: Illustration of inter-electrode distance for a non-contact electrode

3.3.4. Materials used for the electrodes

The contact electrodes that were used in the experiment were the disposable Silver/Silver chloride electrodes.

The materials used for the EMG electrodes which form the skin contact layer needs to realize a good electrode-skin contact, a low electrode-skin impedance and steady behavior in time. The impedance of the electrode-skin was reduced by electrode paste and gel. The non-contact electrodes were made up of a combination of disposable Ag/AgCl electrodes with Aluminium foil in between as an insulator. The different layers of non-contact were constructed as shown in figure 3-5.

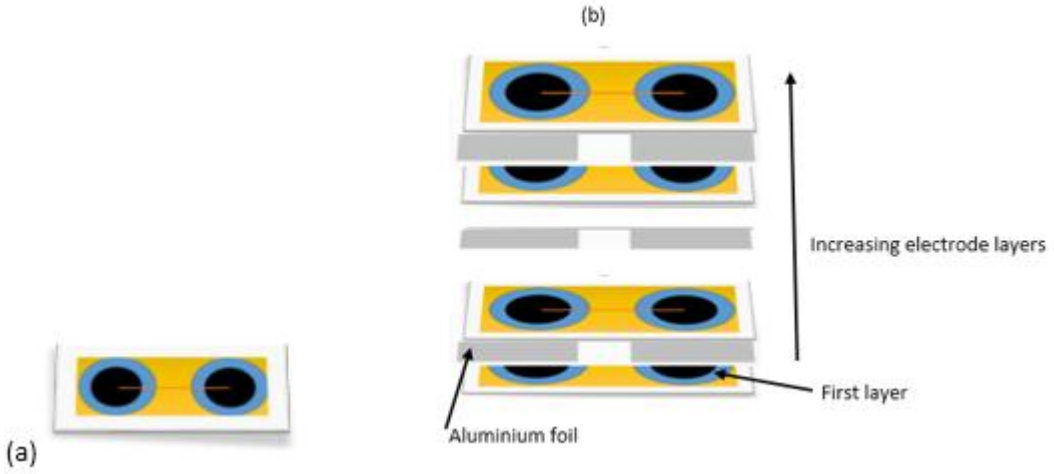

Figure 3-5: Construction of non-contact electrodes (a) Top view of single layer (b) Layer 4 combination of developed contactless electrodes

3.4. REQUIREMENTS AND SPECIFICATIONS

The experiment was carried out to find a correlation between the EMG electrodes and antennas. In addition, the aim was to obtain the number of layers that the EMG embroidered electrodes would need for best readings in a patch-Yagi antenna configuration. The idea was also to eliminate noise generated on the skin of a person. Volunteers were allowed to lift a 2.5 kg weight so to minimize errors obtained in carrying out the experiment. Furthermore, the EMG investigations were done to monitor two muscles groups in the arm at the same time as shown in figure 3-6.

(a)

(b)

Figure 3-6: (a) Positioning of the hand flexing the flexion muscle (b) Positioning of the hand after flexing the flexion muscle

3.5. PROCEDURE AND TESTING STEPS TAKEN TO FIND THE BEST NON-CONTACT EMBROIDERED ELECTRODES LAYERS

The experiment was carried out basing on the benchmark procedural steps to find the best non-contact embroidered electrodes layers for the Touch Hand system. The following steps were carefully followed sequentially during the experiment so as get correct readings from the digital oscilloscope.

(1) The five different layer electrodes were placed on the flexion-extension muscles of each volunteer, one at a time.
(2) The forearm was kept in a position and facing downwards. The volunteer was given a 2.5 kg to lift as shown in figure 3-6.

(3) The change in EMG signal amplitude was observed on the oscilloscope as the volunteer lifts the weight.
(4) The change in amplitude of EMG signals from the oscilloscope was noted and compared amongst the volunteers.
(5) The same experiment was repeated on 9 volunteers.

Most importantly, the experiment was done using the same weight and no another weight was used. In addition, the volunteers were required to repeat the same experiment for two times to find the best readings. In terms of the age groups, the volunteers who did the experiment were ranging between 20 years and 33 years. Furthermore, half of the volunteers were females and the other half were males.

3.6. EMG DECODING

The capability to interpret EMG signals can demonstrate very valuable in giving back some or all of functionality in amputees and partially paralyzed. The EMG signals were recorded from the forearm and hand muscles of the behaving individuals depending on the grasping tasks. The decoding and encoding of signals for the Touch hand system were based on neural networks related to artificial intelligence methods. The neural network involves modeling of the nervous system and nerve cells mathematically (Ascoli, 2002). Kalman filtering that uses Gaussianity assumption was the proposed approach to EMG prediction. It was formulated as an optimized framework and non-negativity constraint. Touch hand designs adopt various ways of training EMG signals such as Hidden Markov Model. The approach was introduced for designing and neuroelectric interfaces to control virtual devices (Wheeler, 2003).

3.7. KALMAN FILTERING

The Kalman filter refers to the scientific control device, which plays a significant part in computer designs and calculations (Antonis *et* al., 2010). A significant toolbox could be used for stochastic approximation from sensor measurements. Fundamentally, a set of equations that uses a predictor-corrector type estimator that is optimal in the sense that it reduces the predictable error covariance when some presumed conditions are met. The Kalman filter has been the topic of broad study and application, mainly in the prosthesis area. This is possibly due in great part to improvements in digital computing that made the use of the filter practical, but also to the comparative simplicity and robust nature of the filter itself.

3.7.1. Advantages and disadvantages of Kalman filter

For Gaussian models with limited non-linearity, extended Kalman filter was appropriate. For non-Gaussian and nonlinear models, particle filtering was the most appropriate approach since was able to provide arbitrarily posterior probability distribution. The reasons why Kalman filters were used in amplifiers signal filtering is shown in table 1.

Table 1: Advantages and disadvantages of Kalman filters of noise

Advantages of Kalman filters	Disadvantages of Kalman filters
(1) Excellent outcomes in practice due to optimality and structure.	It gives precise outcomes only for linear models of Gaussian.
(2) Appropriate form for online real time processing.	It assumes that the state belief is Gaussian distributed
(3) Easy to express and implement given a simple understanding.	Inaccurate initialization of the filter (providing an initial state estimate and covariance that is inconsistent with the true system state). This is easily overcome using a Weighted Least Squares (WLS) initialization procedure.
(4) Measurement equations need not be inverted.	Imprecise/incorrect knowledge of the state dynamics and measurement models.
(5) The filter takes into account quantities that are partially or completely neglected in other techniques (such as variance of the initial estimate of the state and the variance of the model error).	Incorporating measurements that are statistical "outliers" with respect to the system dynamics model. This can cause the Kalman Gain to have negative elements, which can lead to a non-positive semi-definite covariance matrix after update. This can be avoided using "gating" algorithms, such as ellipsoidal gating, to validate the measurement prior to updating the Kalman Filter with that measurement.

Advantages of Kalman filters	Disadvantages of Kalman filters
(6) It provides information about the quality of the estimation by providing, in addition to the best estimate, the variance of the estimation error.	
(7) Its recursive structure allows its real time execution without storing observations or past estimates.	
(8) It permits one to adjust a model to some physical process.	

3.7.2 Kalman filters equation

The filter was a recursive estimator, which implies that the only predictable state from the preceding time step and the current measurement were needed to compute the estimate for the current state. The filter state was denoted by means of two variables:

$\boldsymbol{X}_{k|k}$, approximation state at period *k* specified interpretations involved at period *k*.

$\boldsymbol{P}_{k|k}$, covariance matrix error.

This filter is conceptualized as two distinct phases that are predict and update (Mital *et* al., 2010). The predicted phase utilizes the approximate state from the preceding step time to generate an approximation of the state at the present step time. The current a priori estimate was combined with present observation data to improve the approximate state in the update phase.

(1) Predict

$$\boldsymbol{X}_{k|k-1} = \boldsymbol{F}_k \boldsymbol{X}_{k-1|k-1} + \boldsymbol{B}_k \boldsymbol{u}_k \quad (3.1)$$

$$\boldsymbol{P}_{k|k-1} = \boldsymbol{F}_k \boldsymbol{P}_{k-1|k-1} \boldsymbol{F}_k^T + \boldsymbol{Q}_k \quad (3.2)$$

(2) Update

$$\boldsymbol{y}_k = \boldsymbol{z}_k - \boldsymbol{H}_k \boldsymbol{X}_{k|k-1} \quad (3.3)$$

$$\boldsymbol{S}_k = \boldsymbol{H}_k \boldsymbol{P}_{k|k-1} \boldsymbol{H}_k^T + \boldsymbol{R}_k \quad (3.4)$$

$$\boldsymbol{K}_k = \boldsymbol{P}_{k|k-1} \boldsymbol{H}_k^T S_k^{-1} \quad (3.5)$$

$$\boldsymbol{X}_{k|k} = \boldsymbol{X}_{k|k-1} + \boldsymbol{K}_k \boldsymbol{y}_k \quad (3.6)$$

Update estimate covariance $\boldsymbol{P}_{k|K} = (I - \boldsymbol{K}_k \boldsymbol{H}_k) \boldsymbol{P}_{k|k-1}$ (3.7)

Where,

$\boldsymbol{F}_k$ = is the transition model

$\boldsymbol{X}_{k|k-1}$ = Predicted state estimate

$\boldsymbol{P}_{k|k-1}$ = Predicted estimate covariance

$\boldsymbol{y}_k$ = Measurement residual

$\boldsymbol{S}_k$ = Innovation covariance

$\boldsymbol{K}_k$ =Optimal Kalman gain

$\boldsymbol{X}(k|k)$ = Updated state estimate

$\boldsymbol{Q}_k$ = Estimation of the noise covariance

The predict and update equation alternate as time and readings are obtained.

3.8. EMGS PSEUDO AND ALGORITHM

The algorithms to control the Touch hand 3 were divided into three (3) main categories namely opening, closing, and wrist motion. The other grasping methods were derived from those three main categories resulting in the formulation of the pseudo code and algorithm for the prosthetic hand system. Furthermore, the EMG signal was used to control the sensory system namely the temperature, force, and vibration sensor. The EMG stimulates the temperature sensor to differentiate hotness and coldness of the object they are touching. In addition, the EMG signal would control the force that the artificial hand applies to a gripped object thereby avoiding the complete crush. Furthermore, the vibration sensor would measure the bearing absolute vibration based on the piezoelectric effect depending on the EMG signal levels.

The flow diagram shown in figure 3-7 represent the opening and closing of the hand based on the EMG signals from the forearm muscle. The irregularity in the grasping gesture is due to the variations in the levels of EMG signals on amputees because of magnitude and strength of the enduring muscles. The C code needs to be standardized to each amputee's distinctive signals to interpret for this difference in the strength of the EMG signal. The Kalman filter, which generates approximations of the present state variables, alongside with uncertainties, was used to eliminate unwanted EMG noise from the amplifier and electrodes. The Kalman variables were introduced in the C code to accommodate the raw data read from the sensors. The initial step was to generate random raw data by placing the electrodes on the two forearm muscles and use the data to calculate the variance. Effective use of this mechanism system required hard testing in order to get a successful outcome**.**

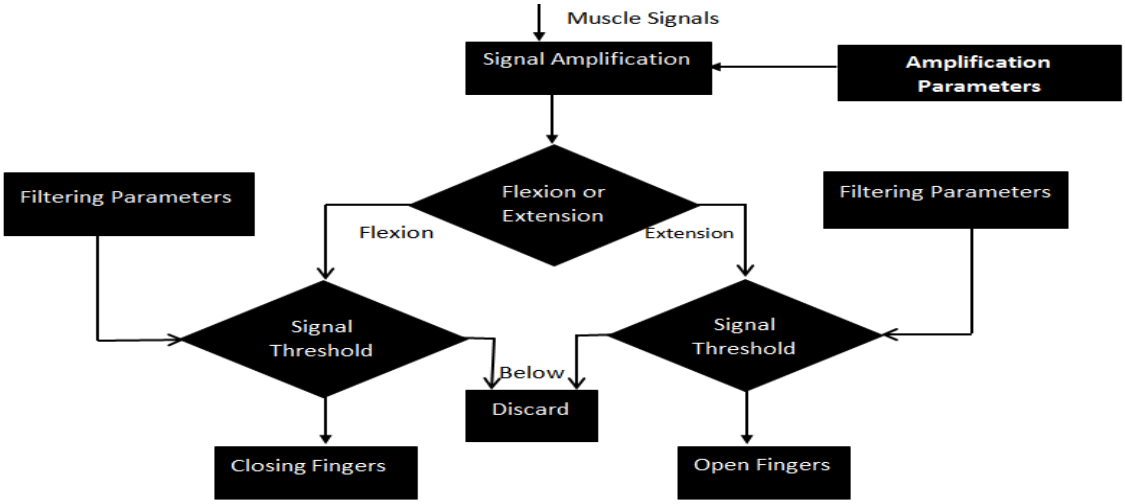

Figure 3-7: Single grasp controlled by muscle flexion and extension

3.8.1. Temperature sensor pseudo and algorithm

According to the Touch hand design objectives, implementation of the temperature sensor was essential to avoid damage to the system when exposed to heat. The temperature sensor was positioned inside the middle fingertip of the myoelectric artificial hand to sense hotness or coldness of the object on contact as shown in figure 3-8.

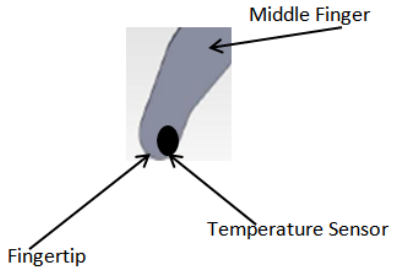

Figure 3-8: Positioning temperature sensor on the fingertip

An algorithm was formulated in order to achieve the design objectives as shown in figure 3-9.

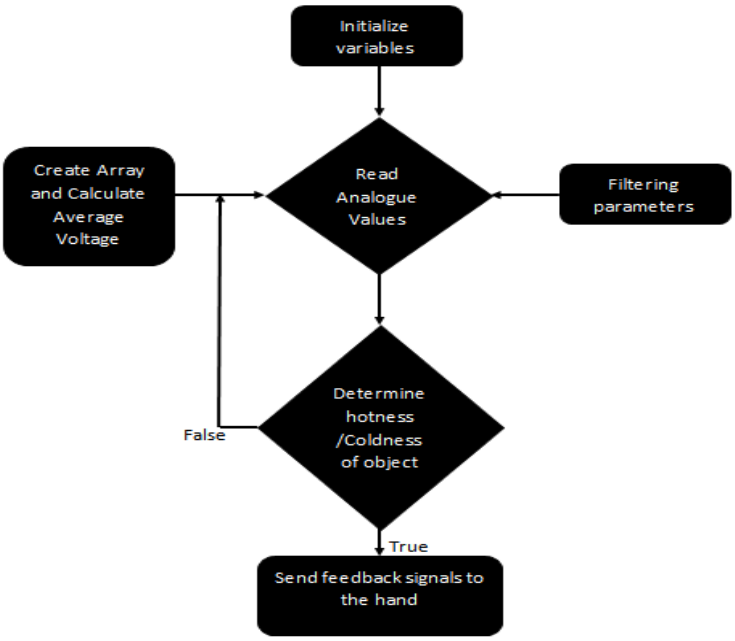

Figure 3-9: Temperature sensor algorithm

The pseudo code for the temperature sensor implementation was formulated as shown in table 2.

Table 2: Temperature sensor pseudo code

Temperature sensor pseudo code
(1) Defines the variables to hold the temperature value.
(2) The sensor output variable was defined.
(3) The input voltage and ground are set to high and low respectively.
(4) Read the analogue values and convert them to temperature readings in degrees Celsius or Fahrenheit.
(5) Create an array of values and calculate the averages.
(6) Using Kalman filtering parameters to eliminate noise from the analogue.
(7) Wait for the EMG signals to stimulate the sensor so that the hand will sense hotness or coldness of the object in contact.

3.8.2. Force sensor pseudo and algorithm

The force sensor was implemented in order to design a system, which can control the force exerted by the myoelectric artificial hand on the gripping object. The force sensor was positioned on the outside of the index fingertip as shown in figure 3-10.

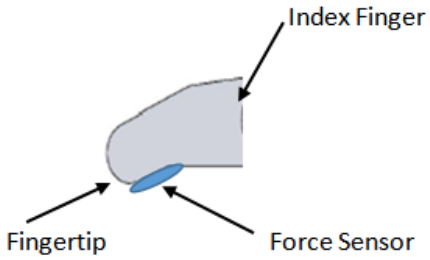

Figure 3-10: Positioning force sensor on the fingertip

The algorithm that was used to implement this force sensor is shown in figure 3-11.

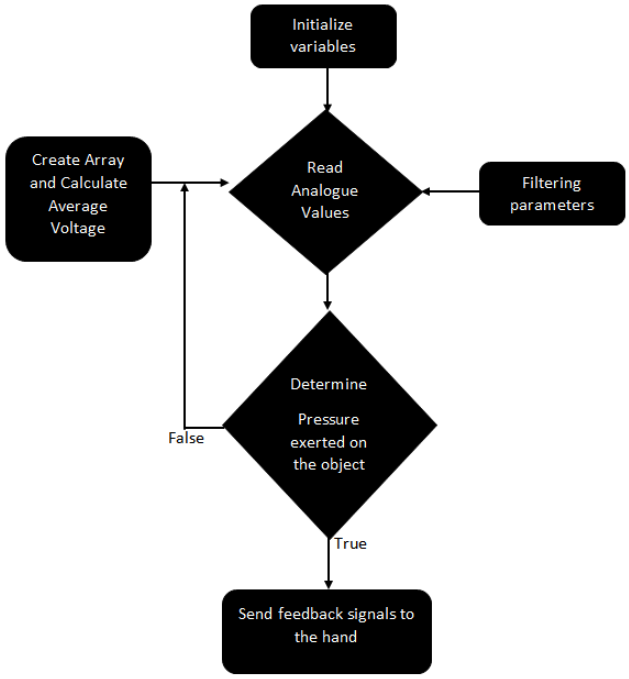

Figure 3-11: FSR sensor algorithm

Furthermore, the pseudo code for the force sensor was stated as shown in table 3:

Table 3: FSR pseudo code

FSR pseudo code
(1) Defines the variables to hold the FSR value.
(2) The sensor output variable is defined.
(3) The input voltage and ground are set to high and low respectively.
(4) Read the analogue values and convert them to voltage readings.
(5) Create an array of values and calculate the averages.
(6) Using Kalman filtering parameters to eliminate noise from the analogue.
(7) Wait for the EMG signals to stimulate the sensor so that the hand will sense hotness or coldness of the object in contact.

3.8.3. Vibration sensor pseudo and algorithm

The vibration sensor was crucial in the Touch hand system to measure the bearing entire vibration due to the effect of the piezoelectric. The vibration sensor was placed on the ring fingertip as shown in figure 3-12.

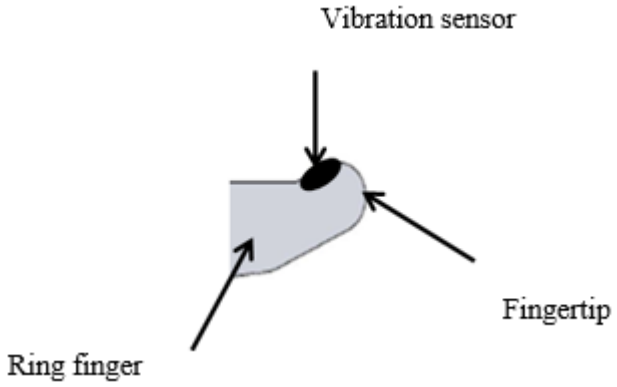

Figure 3-12: Positioning vibration sensor on the fingertip

The algorithm that was used to implement this vibration sensor is shown in figure 3-13.

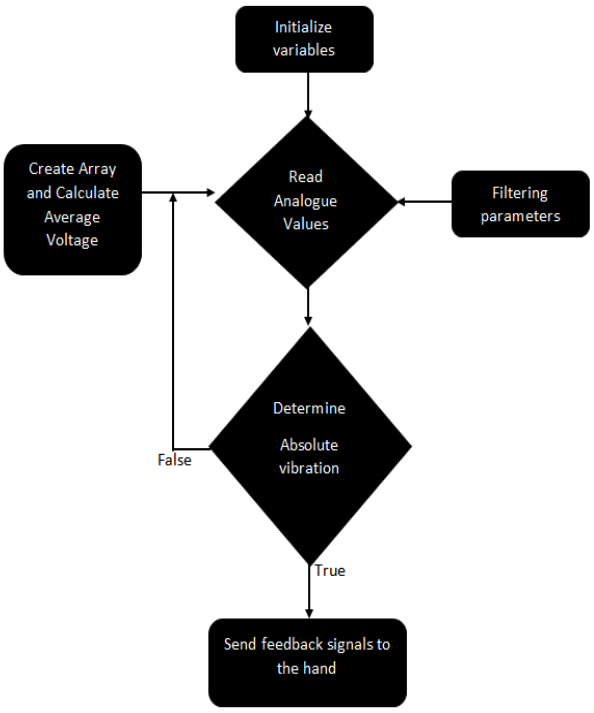

Figure 3-13: Vibration sensor algorithm

Furthermore, the pseudo code for the vibration sensor was stated as shown in table 4.

Table 4: Vibration sensor pseudo code

Vibration sensor pseudo code
(1) Defines the variables to hold the vibration sensor value.
(2) The sensor output variable was defined.
(3) The input voltage and ground are set to high and low respectively.
(4) Read the analogue values and convert them to voltage readings.
(5) Create an array of values and calculate the averages.
(6) Using Kalman filtering parameters to eliminate noise from the analogue.
(7) Wait for the EMG signals to stimulate the sensor so that the hand will sense hotness or coldness of the object in contact.

3.8.4. Motors pseudo and algorithm

The Touch hand system uses two different types of motors for actuation. The linear servomotors are used to actuate the fingers and the DC motor is for the wrist motion.

The motors move according to the EMG signals generated by the forearm muscles. The algorithm formulated for both the motors is shown in figure 3-14.

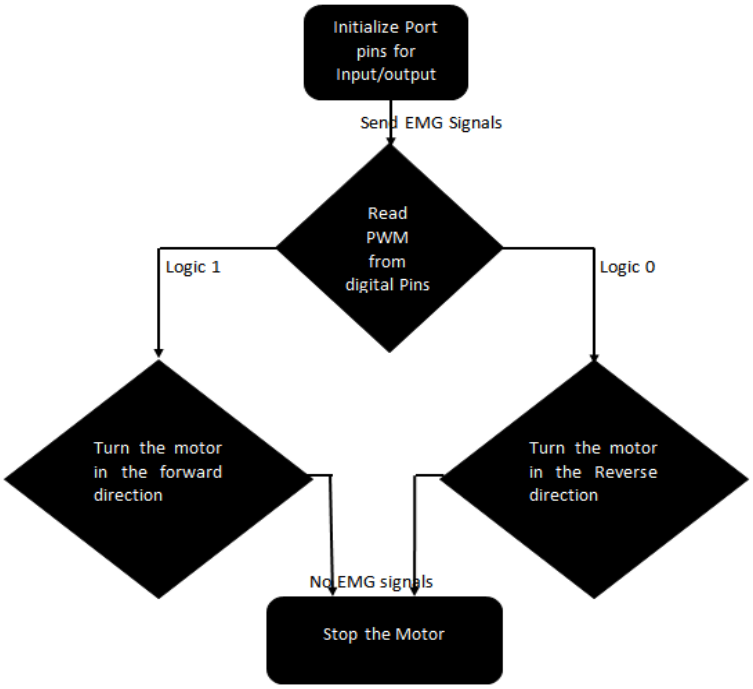

Figure 3-14: Touch hand system motor's algorithm

The linear actuator pseudo code was formulated as shown in table 5.

Table 5: Linear actuator pseudo code

Linear actuator pseudo code
(1) Set the pulse width modulation (PWM) pins as outputs.
(2) The PWM was read from the digital pins for desired motor's position.
(3) The preferred value is set from the PWM registers.
(4) The PWM module was initiated for the particular PWM channel pin to go high and it goes low once the essential width was attained.
(5) The PWM was initiated to start a timer with a delay of approximately 19 ms and delay until the timer overflows.
(6) Go to step II.

3.9. CHAPTER SUMMARY

The relation between EMG and biomechanical variables were studied. These biomechanical variables include the joint motion, force, muscle fatigue, and velocity.

The person's mobile speed is a vital constraint in designing a myoelectric artificial hand particularly the Touch hand 3 since one can understand the state of the activity of muscle and related it to the EMG. The force due to muscles was approximated by recording the EMG signals. The construction of the non-contact electrodes for Touch hand system was successful, taking into account the size of the electrode, electrode material etc. Furthermore, the objectives to investigate the correlation between EMG and antenna configuration were met. More so, EMG decoding was done using Kalman filtering that uses Gaussianity assumption was the proposed approach. The algorithms for the temperature, pressure, and vibration sensors were formulated.

CHAPTER 4: ELECTRONICS AND MECHANICAL

4.0. INTRODUCTION

The biomechatronic technique entails the design of a myoelectric prosthetic hand that duplicates essentially the structure of the hand of the human (Dalley *et* al., 2010). In turn, it reproduces important tasks such as grasping. To design a dependable structure following the important necessities the electronics, control and mechanical solutions must be simple. Figure 4-1 below shows the eight canonical hand postures that the artificial hand should perform (Dalley *et* al., 2010). The design of the Touch hand 3 aims to develop a hand with human-like features. The functionality of this hand has to be proved on testing stage, marking the different grasping tasks achieved.

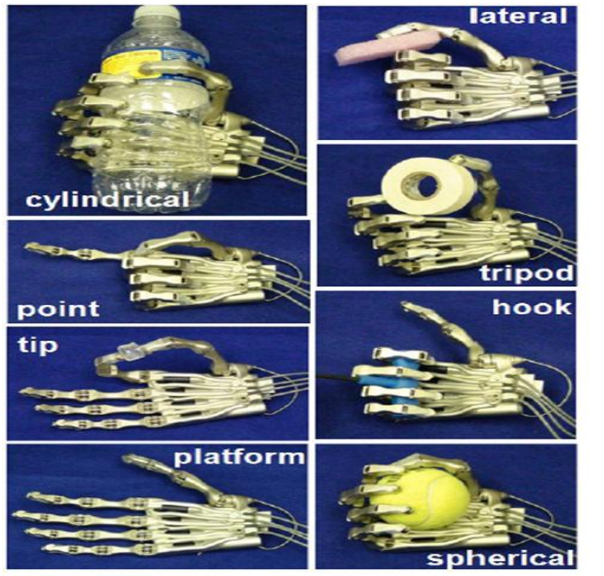

Figure 4-1: Eight hand canonical postures

4.1. ELECTRONICS

The aim was to create a modular electrical design capable of handling the full scope of modularity, from non-existent in the mechanically actuated system to full system integration of the motors, EMG sensors, external sensors and sensory feedback system. The electrical circuits include the motors, H-bridge, EMG sensors, external sensors (temperature, pressure, vibration and resistive), sensory feedback (vibration motor) and the motherboard as shown in figure 4-2. The system design was partitioned into motors, EMG, motherboard, sensors and sensory feedback sections.

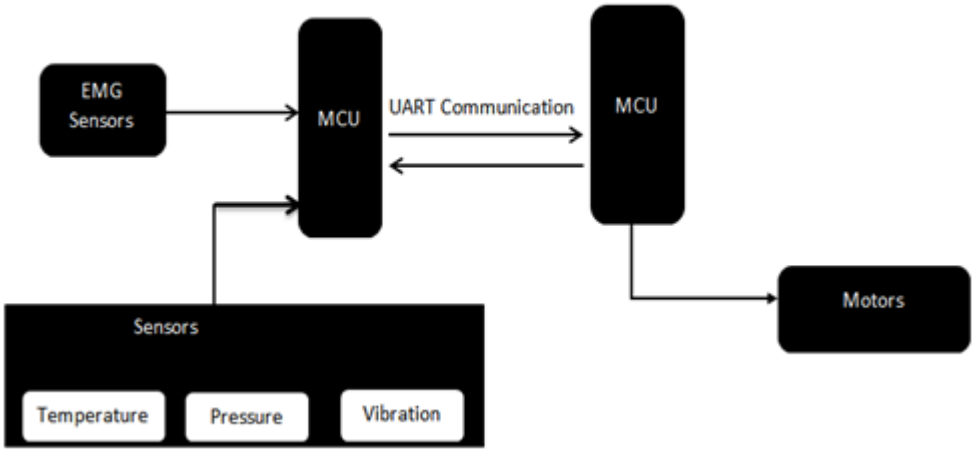

Figure 4-2: Electronic design block diagram

The hardware design of the Touch hand system comprised of the two microcontrollers, motors and power supply as shown in figure 4.2. The actuators were made up of motors to control the fingers. Torque, speed, and position measurements were supplied as feedback to the microcontroller. One microcontroller was used to analysis and transmit the EMG signals from the forearm. The another one was for receiving and decoding the signals to control the motors depending on the different grasping tasks. The H-bridge was used to regulate the speed and direction of motors by allowing the right amount of current to flow in the right direction of the motor. The PWM signals from the microcontroller enable, and disables the h-bridge. The voltage of the switching cycle was there because of frequency changes whereas the duty cycle changes the average voltage. The voltage provided by the power supply determined the peak applied motor voltage. Batteries were used as the power source, but their voltage level changes over time. The importance of this architecture was its modularity and ease assembled.

4.2. SELECTION OF THE MICROCONTROLLER FOR TOUCH HAND SYSTEM

The Touch hand system needed a microprocessor for controlling hand gestures by decoding and encoding sensory feedback information. The system required two of these microprocessors for EMG analysis and controlling of the hand motors and sensors respectively. The selection of the microcontroller was based on the availability, processing power, microcontroller size, and space.

The board shown in figure 4-3 took power from the USB connectors or from the DC plug (6 -20 V). The board had the same footprint as the Arduino/Genuino Uno and could be programmed the same way as the other Arduino boards. The microcontroller on the zero board runs at 3.3V, which meant that voltage more than 3.3 V must be applied to its inputs or outputs. In addition, the connection of the sensors and actuators to the zero always take care that the maximum voltage limits were not exceeded on the pins. However, connecting higher voltages could damage the zero board. Arduino board m0 pro was chosen because it was small, cheap, easy to use, and available and had good performance. The microcontroller was responsible for accepting user commands, monitoring measurements and controlling the motors. Each pin of the microcontroller was configured to give a good interface with the different modules.

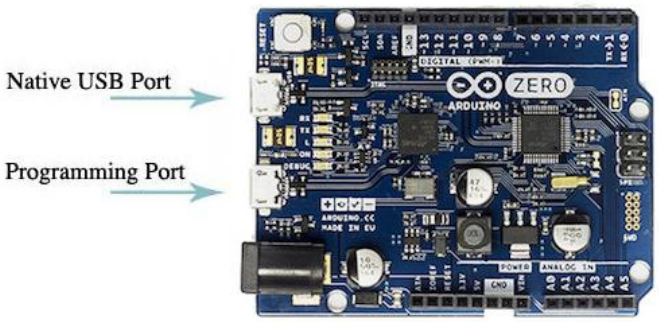

Figure 4-3: Arduino zero board

The H-bridge was connected to the digital input/output and PWM pin was to control the DC motor for effective wrist motion. The analog input channels were used for motor sensors, battery voltage motoring (1 channel) and for amplified EMG signals (2 channels). The temperature, pressure, vibration and resistive sensors used the other remaining channels on this processing board. The processing board was used to receive the output of the rectifier from the EMG sensor, interprets the impulse, and converts them to a pulse width modulated the signal to control the linear actuator.

4.3. SERIAL COMMUNICATION

The electromagnetic fields created by motors distorts the sensors readings resulting in the need to have a pair microcontroller, one set at the hand of the prosthetic and another on a command module set on the forearm as shown in figure 4-4.

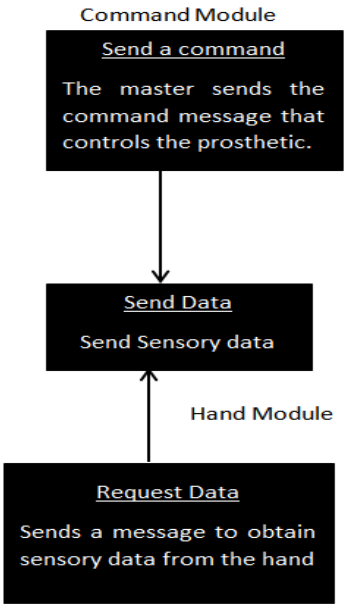

Figure 4-4: UART communication

Furthermore, the two controllers simplified the process of debugging and were easier to assemble since both were handling a variety of events to desire the outputs. In addition, fewer wires required communicating between electrodes and motor board. Each board was dedicated to a specific task. Additionally, the motor control board was used for feedback control from sensors and the actuation of motors while the other was dedicated only to the decoding of the EMG signals. The were various means of communication between the two controllers namely the controller area network (CAN), serial peripheral interfaces (SPI), integrated circuit (I2C) and universal access receiver/transmitter (UART). However, upon research and comparisons of the communication protocol, UART communication was ultimately used in the Touch hand system. Table 5 shows the advantages and disadvantages of the different communication protocols.

Table 6: Comparison of the different communication protocols

Serial protocol	Advantages	Disadvantages
UART	(1) Easy to set up. (2) Widely used. (3) Requires to lines to transmit and receive	(1) No clock, more susceptible to noise. (2) Not useful for controlling peripheral devices e.g. potential devices.
CAN	(1) No noise. (2) Reduced set of wires. (3) Can communicate with many devices.	(1) Very difficult to set up. (2) Requires a transceiver.
I2C	(1) Requires only two pins (2) Masters and slave role may be switched. (3) Good for controlling OLEDS	(1) Low speed. (2) Addressing issues. (3) Require collision protocols. (4) Finding a host to test which is difficult. (5) Require pull up resistor.
SPI	(1) Easy to set up. (2) Low power consumption. (3) No transceiver. (4) Unidirectional signals.	(1) No hardware. (2) Only short distances. (3) Only short distances. (4) No error checking protocol.

4.4. SENSOR AND DESIGN LOCATION

The number of sensors required to adequately perform tasks and their location upon the hand was determined throughout the course of this project. The three crucial sensors that were in cooperated in the Touch hand design include force, vibration and temperature sensors. The vibration sensor was used to detect and correct for the onset of slip in the grip of the prosthetic hand without the need of user intervention. As the hand initially closes around an object, the movement of the first contact between the object and the inner surfaces of the prosthetic hand was detected by dynamic force sensors located on the middle fingertip. More so, the force sensor was used to design a system, which controlled the force exerted by the artificial hand on the gripping object. As the hand continued to close, the static force sensors directly measured the forces exerted on the object.

4.4.1. Temperature sensor

Amputees often found it difficult to adjust to the surroundings. A problem often faced by amputees was the inability to sense the temperature (hotness or coldness) of the object they are touching. The endeavor here was to develop a temperature-sensing device, which could be fitted in the prosthetic hand. Touch hand 3 was capable of sensing the temperature of the object. The LM35 temperature sensor was fitted at the tip of the finger of the prosthetic hand of the amputee.

The study of different types of temperature and their effects on the prosthetic hand was carried out, before final selection of the temperature sensor.

4.4.1.1. Types of temperature sensors

Numerous kinds of temperature sensors existing have different characteristics depending on their real use. The least included the thermocouple, Resistors temperature detectors (RTD), Thermistors, semiconductors and sensor integrated circuits (ICs).

4.4.1.1.1. Thermocouple

This sensor was designed by connecting one end of the two different metals as shown in figure 4-5 (Burns *et* al., 1993). The hot junction was the joined end. Furthermore, the cold junction was the another end of the dissimilar metals that was designed using thermocouple material at the ending junction. A slight voltage was produced because of the hot junction and the cold junction differences. This voltage was the electromotive force, which was marked to show temperature (Burns *et* al., 1993).

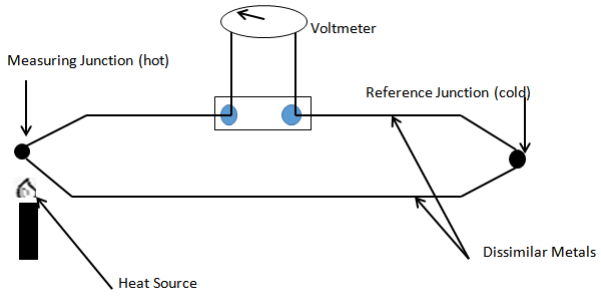

Figure 4-5: Thermocouple circuit

4.4.1.1.2. RTD

The temperature sensing device resistance changes with temperature. The RTDs have various forms such as wire wound, thin film as shown in figure 4-6 (Royal Society, 2014). The resistance of the RTD was measured by applying a continuous current to obtain the voltage readings. This sensor exhibits a direct resistance to curves over their working regions, and any nonlinearity is high likely and repeatable (Strouse, 2008).

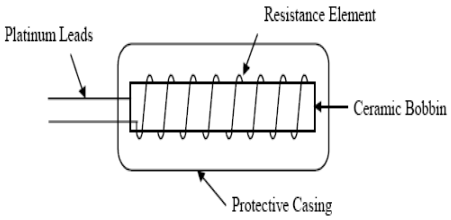

Figure 4-6: Typical RTD

4.4.1.1.3. Thermistors

Thermistors are temperature sensing device whose resistance changed with temperature. They are made from semiconductor materials as shown in figure 4-7 (Downie, 2012). Their resistance was found the same way as the RTD but they showed an extremely nonlinear resistance verse temperature curve (McGee, 1988). As a result, these sensors functioning range shows a greater change in resistance for a very slight change in temperature. This made them extremely sensitive devices, ideal for set-point applications.

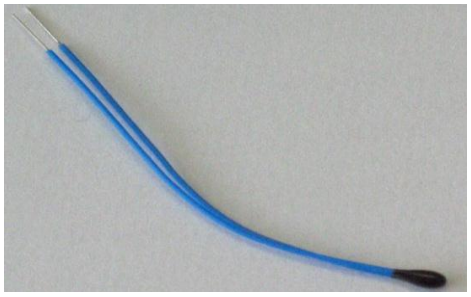

Figure 4-7: Type of thermistor

4.4.1.1.4. Semiconductors

These sensors integrated circuit were available to simplify the largest likely variety of temperature monitoring tasks as shown in figure 4-8 (James, 2008).

Figure 4-8: Type of semiconductor temperature sensor

These sensors vary considerably from the aforementioned types in a number of crucial ways such as the operating temperature range. They could work above the minimal integrated circuit range of temperature of -55°C to +150°C (Omega Engineering, 1999). In addition, there was no necessity to include biasing circuits for these integrated circuit sensors. The sensors could constantly measure and read the temperature at all the times. The processor could train the sensor to check the temperature and command the output pin to be high or low if the temperature exceeded a programming unit. The temperature threshold values could be programmed and informed the host when the temperature goes below this values (Andre, 2013). The sensor shown in figure 4-7 consisted of three pins and has a maximum supply voltage of 5.5 V (James, 2008).

The material used for this sensor works with respect to temperature changes to vary resistance (Andre, 2013). The sensor reads resistance changes to calculate the temperature.

More so, the increase in temperature result in the increase in the voltage and this could be observed by using a diode. The sensors are capable to directly communicate with the microprocessors (James, 2008).

4.4.2. Selection of LM35

The Touch hand design chose LM35 shown in figure 4-9 as a device to detect changes in temperature. This device was chosen because of easy affordability and ranges of temperature. The temperature ranges from 2˚C to 150 ˚C ("LM35 precision centigrade temperature sensors", 2000), which was appropriate for the use of artificial hand to detect object hotness or coldness.

Figure 4-9: LM35 integrated circuit

4.4.2.1. Temperature sensor and microcontroller interface

The temperature sensor circuit is as shown in figure 4-10. For the integrated circuit to work it had to receive positive DC voltage of approximately +5 V. The ground of the sensor was connected to the ground of the DC power supply. The output of the IC sensor output the analog voltage that was proportional to the temperature it measured. The microcontroller interpreted this measured analog voltage and outputs the temperature in degrees Celsius using the equation (4.1).

$$\text{Temperature} = ((\text{Celsius} * 9)/5 + 32) \quad (4.1)$$

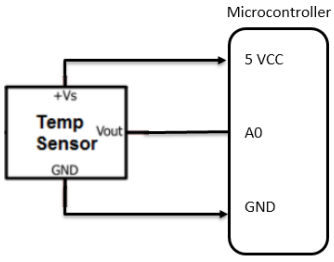

Figure 4-10: Temperature sensor and microcontroller interface

4.4.2.2. Temperature test

The sensor allowed the amputee to detect hotness and coldness of the objects resulting in differentiating between gripping a hot or cold object with an artificial hand (Drew, 2014). The LM35 sensor was positioned on the middle fingertip of the artificial hand. The hand was permitted to hold a mug cup with water of four different temperatures. The approximation of the temperature of the mug cup was in real time depending on the temperature changes experienced by the artificial hand (Drew, 2014). Figure 4-11 indicates the test outcomes that were obtained over an interval of 20 seconds (Drew, 2014). The predictable temperature refers to the predictable temperature approximations that were made each second beginning from the period of mug contact.

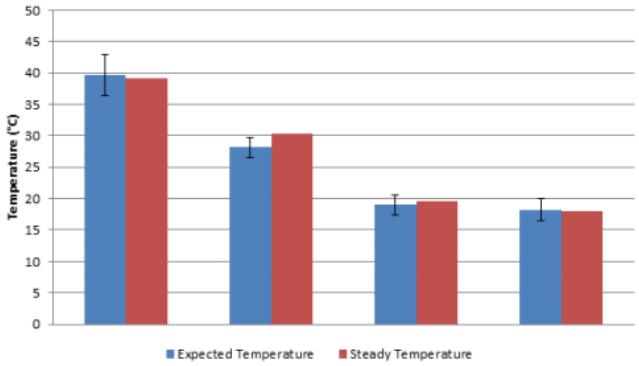

Figure 4-11: Predictable temperature versus actual temperature for a time of 20 seconds

The second test permitted the artificial hand to be in contact with very hot (150 degrees +) temperatures. To avoid injuring the hand, extreme temperatures need to be detected (Drew, 2014). The soldering gun with recognized temperatures was positioned on the middle fingertip of the artificial hand to verify this. The soldering gun was held in position for merely five seconds to avoid injuring the hand. Figure 4-12 indicates test results of final predictable temperature that was calculated 5 seconds after initial contact (Drew, 2014).

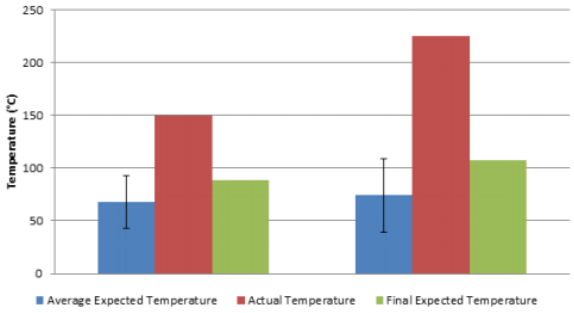

Figure 4-12: Expected temperature versus actual temperature for extreme temperature

4.4.3. Pressure sensor

This force sensor was fitted on the index finger of the touch hand 3 to control the force exerted by the hand on gripping an object. A proper pressure sensor for this hand was selected, modified, characterized and implemented on the hand.

4.4.3.1. Force sensor selection

The Touch hand 3 was designed to accommodate force sensors. These sensors can change mechanical force to an electrical signal, which differs from every load cell. Two principal choices for a load cell was either resistive or capacitive properties, which changes with applied pressure. A Force Sensing Resistor (FSR) as shown in figure 4-13 (Interlink Electronics, 2014) was finally chosen for the Touch hand design.

Figure 4-13: Force sensor resistor

This sensor was durable, which meant it could be used over a long time. In addition, the sensor was affordable and readily obtainable. The response of an FSR was simple to comprehend and describe resulting in no complications when integration with the 12-bit ADC microprocessor board. FSR comprised of a conductive polymer, which altered resistance in an expectable manner resulting in the application of force to its surface. They are usually supplied as a polymer sheet or ink that could be applied by screen-printing.

The sensing film consists of both electrically conducting and non-conducting particles suspended in a matrix. The particles were sub-micrometer sizes and were formulated to reduce the temperature dependence, improve mechanical properties and increase surface durability.

4.4.3.2. Equation of the FSR and interface with the microcontroller

The resistance of the FSR was measured by connecting one terminal to power and the other to a pull down resistor to the ground as shown in figure 4-14 (Drew, 2014). The point between the fixed pull down resistor and the variable resistor was connected to the analog input of the controller board. The configurations make the analog voltage reading ranged from ground to about 5V. The total resistance of the FSR and the pull-down resistor decreased from about 220 KΩ to 22 KΩ as the resistance of the FSR decreased. That meant the current flowing through both resistors increased

which in turn caused the voltage across the fixed 22KΩ resistor to increase. The another voltage divider was built with 4.7KΩ. The newton force was measured by the FSR to map analog voltage reading ranges to 0V to supply voltage. The FSR resistance was calculated using the following formula:

$$R_{FSR} = \frac{(V_{cc}-U)\times R1}{U} \quad (4.2)$$

Where

$R_{FSR} =$ FSR resistance

$V_{cc} =$ supply voltage

$U =$ the measured voltage.

$R1 =$ resistor.

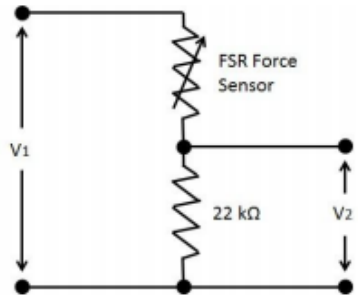

Figure 4-14: Force sensing resistor circuit

The force sensitive resistor was sensitive enough to detect rigid objects pressing against the surface of the palm without assistance from the fingers as shown in figure 4-15 (Interlink Technologies, 2016).

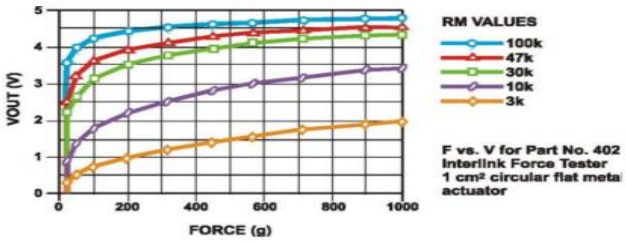

Figure 4-15: Voltage vs applied force of force sensitive resistor circuit in various resistor values.

4.4.3.3. Force sensor tests

The two voltage dividers were made up of 22 KΩ and 4.7 KΩ respectively. The two circuits with variable loads were tested by applying the supply voltage of 7.2V.

Figure 4-16 indicate that the 22 KΩ resistor made use of the full supply voltage and thus offered a better resolution of the grip force compared to the 4.7 KΩ resistor (Drew, 2014).Therefore a 22 kΩ resistor was selected for both forces sensor circuits.

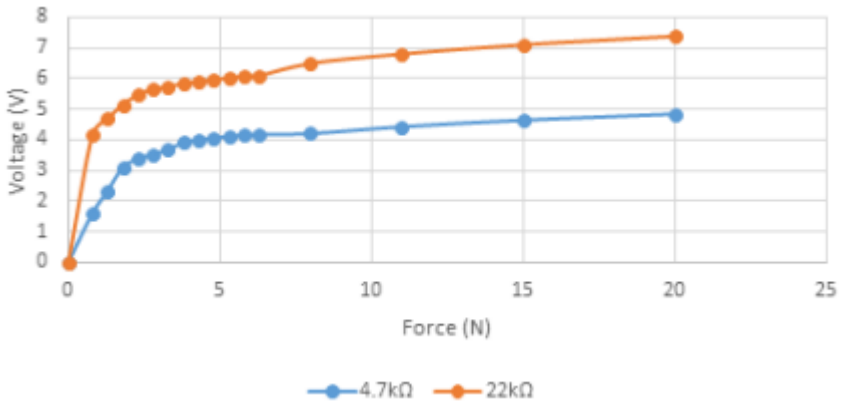

Figure 4-16: Voltage vs. force relationship for the 4.7 kΩ and 22 kΩ resistors

Once the resistances were calculated for each load point, Equation 4.2 was used to calculate the expected voltage for a 5 V supply. This was shown in figure 4-17 for the 8 mm force sensor (Drew, 2014). The equation in figure 4-17 showed the exponential change of the output voltage with respect to force sensor.

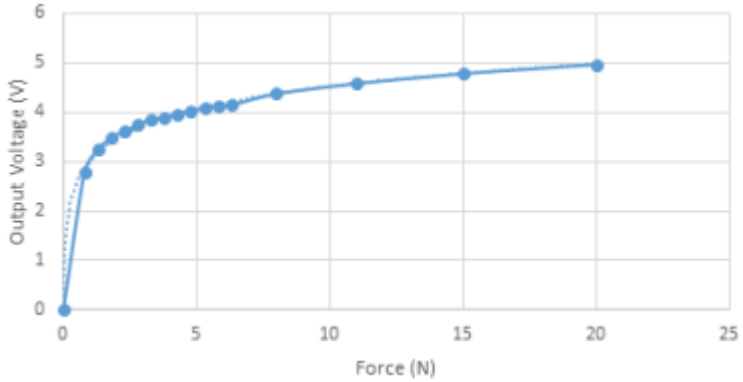

Figure 4-17: 8 mm force sensor output voltage, trend line: $y = 0.6511\ ln(x) + 3.022$

4.4.4. Vibration sensor

It worked on electrochemical principle vibration velocity sensors operate in accordance with electrodynamics principle. They were also used for measuring the bearing absolute vibration based on piezoelectric effect.

4.4.4.1. Selection of vibration sensors

The three parameters representing motion detected by vibration monitors were displacement, velocity and acceleration. These parameters were measured by a variety of motion sensors and were mathematically related (displacement was the first derivative of velocity and velocity was the first derivative of acceleration). Selection of a sensor proportional to displacement, velocity or acceleration depended on the frequencies of interest and the signal levels involved. Sensor selection and installation were the most critical determining factor in accurate diagnoses of machinery condition. Figure 4-18 shows the type of vibration sensor (Polyvinylidene fluoride- pvdf) which was used in the Touch hand system (Drew, 2014). The sensor has the following characteristics as shown in table 7:

Table 7: Characteristics of vibration sensors

Characteristics of vibration sensors
(1) Flexible PVDF Piezo Polymer Film.
(2) Wide dynamic range.
(3) Laminated for higher voltage output.

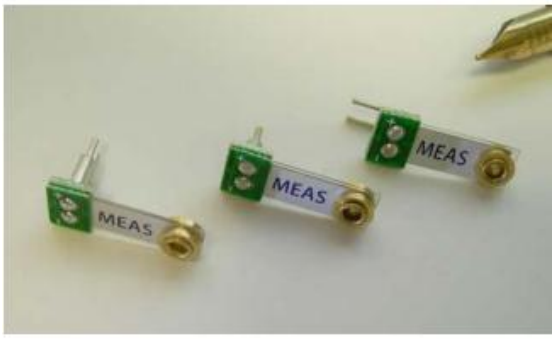

Figure 4-18: MiniSense 100 vibration sensor

4.4.4.2. Vibration sensor circuit

The sensors were a thin strip of piezoelectric material with a rivet, in the end acting as a weight. When the was a vibration, the weight moved, stressing the piezo material that produced a spike in voltage as shown in figure 4-19. The voltage that was created may be up to 90 V.

The vibration sensor was connected to a microcontroller, which read and detected some voltages that the sensor creates when there was vibration. With the resistance, which an analog terminal of an Arduino offers, these voltages of up to 90 V were brought to safety levels that were not harmful to the microcontroller.

When the microcontroller detected vibration, the LED connected to it lighted up for a second and then turned off with each vibration above a certain threshold value. This circuit was used often for impact sensing or as a flexible switch.

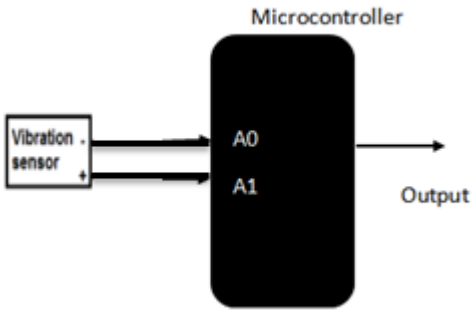

Figure 4-19: Vibration sensor connection to the microcontroller.

4.4.4.3. Vibration sensor tests

This sensor was positioned on the ring fingertip to examine the efficiency of such a sensor as slippage indicator (Drew, 2014). These sensors produce a slight voltage spike when distorted. This spike was detected during the slip of a 500 ml soda bottle from the artificial hand (Drew, 2014).

The signal was read by the microprocessor and figure 4-20 shows the minSense 100-vibration sensor 78 plotted with processing software indicating a noticeable spike in the signal when the object started to slip (Drew, 2014). This spike ranged from 0.3 to 0.8 V. There was also frequency produced by the slip, which averages around 50 Hz (Drew, 2014). However, there was a noise of approximately 50 Hz in the system as well, but this noise had an amplitude of only 0.08 V, which could be filtered out in the software (Drew, 2014).

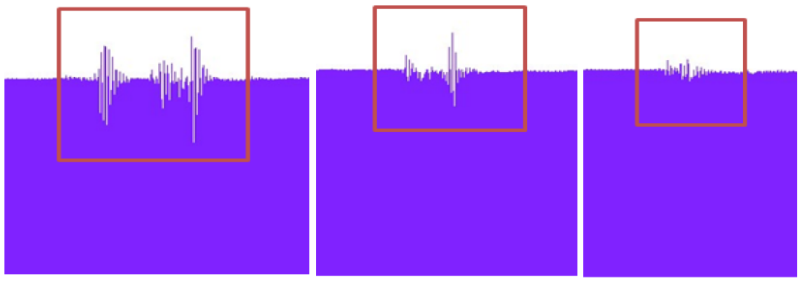

Figure 4-20: Vibration signals at the start of slip

The vibration sensor can be vulnerable to noise in two key forms namely collisions and natural jerk movements.

As a result, the noise creating situations could occur while an amputee was gripping an object (Drew, 2014). Figure 4-21 showed a plot in the way as slippage to investigate jerk movements (Drew, 2014). The natural jerk noise ranged from 0 V to 0.3 V depending on the intensity of the jerk. This noise was also observed as a spike from the plots, but its shape was very different to that of slippage (Drew, 2014).

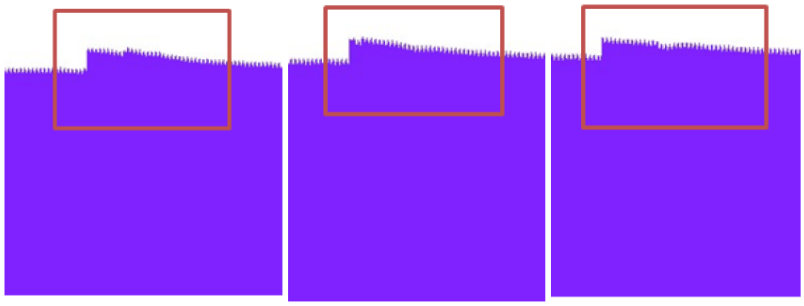

Figure 4-21: Sensor noise resulting from jerk motion

In addition, eight different surfaces were tested and their respective frequencies documented to show the difference between the different surface textures. These relationships were shown in figure 4-22 through figure 4-29 (Drew, 2014).

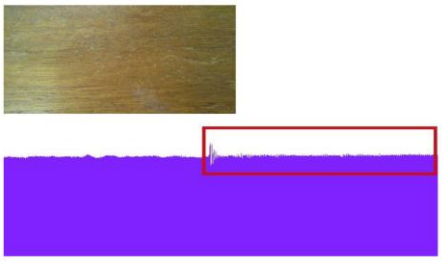

Figure 4-22: Texture vibration signal for smooth varnished wood

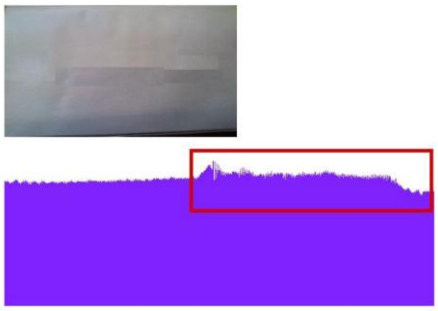

Figure 4-23: Texture vibration signal for semi-smooth plastic

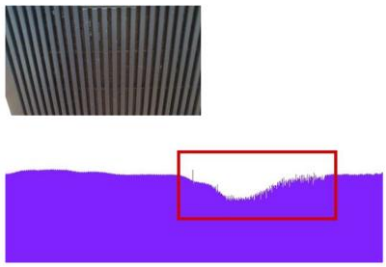

Figure 4-24: Texture vibration signal for smooth ridged plastic

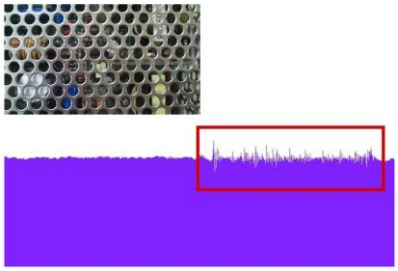

Figure 4-25: Texture vibration signal for smooth metal mesh

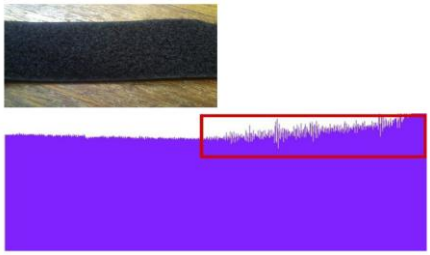

Figure 4-26: Texture vibration signal for Velcro, soft side

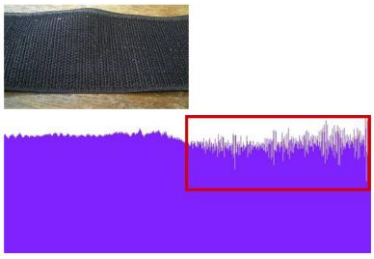

Figure 4-27: Texture vibration signal for Velcro, rough side

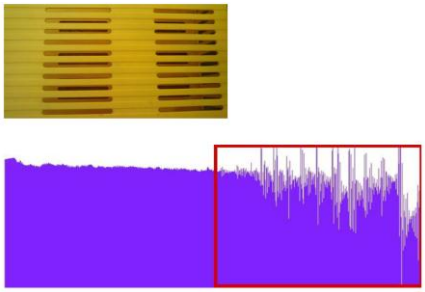

Figure 4-28: Texture vibration signal for the bumpy plastic

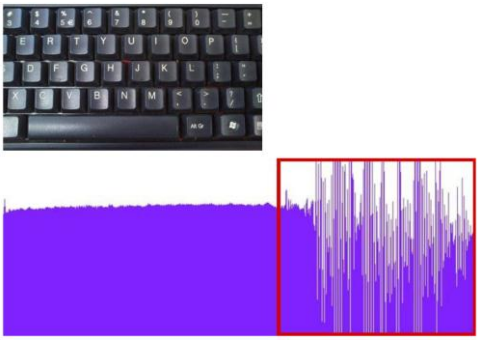

Figure 4-29: Texture vibration signal for a keyboard

Depending on the roughness of the surfaces, the vibration signals varies in both frequency and amplitude. The relative velocity between the finger and the object affects significantly the frequency of vibration of the signal. As a result, the frequency cannot accurately determine the roughness of the surface (Drew, 2014). The amplitude of the vibration signal varies proportionally to the amplitude roughness of the surface (Drew, 2014). The hand's proposed texture sensor is then capable of only distinguishing in part between different surface textures (Drew, 2014). The investigated system of texture detection is suitable for base texture discrimination between smooth, grainy and bumpy surfaces (Drew, 2014).

4.5. MOTOR SELECTION

Motors were selected to provide the best actuation method to the Touch hand 3. These selected motors would directly affect the allowable grip force and closing speed of the fingers. The motors produced the desired torque and speed for the hand to be more functional. An amputee would not have much use for the hand that did not perform to a desirable functional level. The linear actuator motors and DC motors were used in this design. The linear servo motors were used to actuate the fingers and the DC motor was used for wrist motion.

To simplify the selection process and for standardization purposes, the same motor model was selected to drive each of the actuated joints.The principal operation of brushed DC motors was first described, followed by their useful equations. Specific load cases were considered that would situate the motors in worst-case conditions. The required torques and speeds extracted from these cases were then mathematically manipulated to give values that could be compared to the data of possible motors. Three motors were evaluated and compared against one another. The PQ12 –R actuators shown in figure 4-30 were suited to be used in robotics and radio control models.

Figure 4-30: PQ12 -RC linear servo

The actuators were designed to push or pull a load along a full stroke length and the speed determined by the load applied. The actuator holds its position when the power was removed unless the applied load exceeds the back drive force. The desired actuator position was input to the actuator on lead one as a positive 5 V pulse width signal. Furthermore, a 2ms pulse commands the controller to fully retract the actuator and 1.0 ms pulse signals it to fully extend. A 1Ω- 4Ω resistor in series with the actuator's red V+ lead wire was placed if the motion of the actuator seemed to be erratic. These linear servos were designed to work with typical RC receivers and battery packs.
In addition, they were also Arduino boards, VEX microcontrollers and many other similar boards designed for robotics. The wiring of the RC linear servomotor shown in figure 4-31 is as stated in table 7:

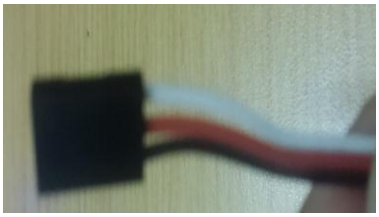

Figure 4-31: Wiring of the RC linear servo

Table 8: Linear servomotor wiring

Linear servomotor wiring
(1) RC input signal (RC servo compatible)
(2) Power (+6 VDC)
(3) Ground

4.5.1. Linear actuators

They allowed for precise control of angular or linear position, velocity, and acceleration. In addition, they consisted of a suitable motor coupled to a sensor for position feedback. They also required a relatively sophisticated controller, often a dedicated module designed specifically for use with linear actuators.

4.5.1.1. Linear actuator mechanism

A linear servo system mainly consisted of three basic components namely a controlled device, an output sensor, and a feedback system. This was an automatic closed loop control system. The device was regulated by a feedback signal produced by matching output signal and reference input signal. When reference input signal or command signal was applied to the system, it was compared with output reference signal of the system produced by output sensor, and a third signal produced by a feedback system. This third signal acts as an input signal of controlled device. This input signal to the device presented as long as there was a logical difference between reference input signal and the output signal of the system. After the device achieves its desired output, there was no longer the logical difference between reference input signal and reference output signal of the system. The third signal produced by comparing these above said signals remained enough to operate the device further. In addition, they produced a further output of the system until the next reference input signal or command signal was applied to the system. Hence, the primary task of a servomechanism was to maintain the output of a system at the desired value in the presence of disturbances.

4.5.1.2. Interface of the linear actuator and microcontroller

The linear actuator was driven by applying the voltage signal to it regular intervals. The servo was sensitive to timing variations (Sclater, 2007). A pulse of specific width was applied at specific intervals of time. Typically, the duration of pulse varied from 0 ms to 2.2 ms and the repetition rate was 50 Hz to 60 Hz (Sclater, 2007). For precise position control, the controller that was chosen had timers that required resolution. In addition, if more than one motor has to be controlled simultaneously, the processor clock must be fast enough. However, for more than one motor, a PIC, like a PIC18F or an ATMEGA was used so that its internal PWM could be utilized. However, the selection of micro-controller depended totally on the designer and the project requirements.

4.5.1.3. Controlling the linear actuator motor

The linear actuator motor angular position was controlled by applying PWM pulses of a specific width. The duration of pulse varied from about 0.5 ms for 0-degree rotation to 2.2 ms for 180-degree rotation (Sclater, 2007).

The pulses were given at frequencies of about 50 Hz to 60 Hz (Sclater, 2007). In order to generate the Pulse Width Modulation (PWM) waveform, either one can use the internal PWM module of the microcontroller or the timers could be used. Using the PWM block was more flexible as most micro-controller families design the blocks to suit the needs of application like linear actuator. For different widths of PWM pulses,the internal registers were programmed accordingly. The microcontroller was informed on how much it has to rotate. For this purpose, a simple potentiometer and an ADC to get the rotation angle or for more applications that are complex, an accelerometer were used.

4.5.2. Brushed DC motor theory

The principal operation of a brushed dc motor was the motion of looped wired in a permanent magnetic field; the current owing through it induced a force against it when a voltage was applied across its ends (Chapman, 2005). Figure 4-32 showed a sectional view of a brushed dc motor perpendicular to the shaft axis (front view) (Helms, 2011).

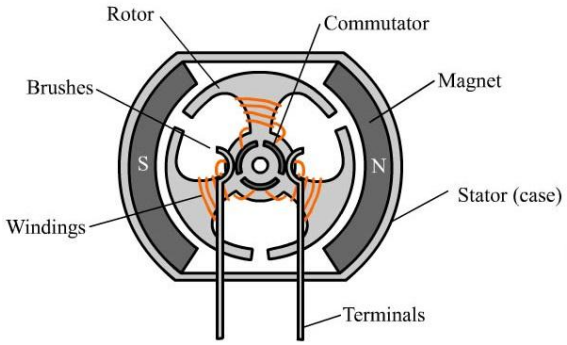

Figure 4-32: Brushed DC motor sectional front view

The north (N) and south (S) poles fixed to the stator (case), with the field directed from north to south, produce a permanent magnetic field. A rotor (also known as an armature) rotates on an axis in between the permanent magnets with windings or wire. The windings were connected to a commutator, which was in contact with a pair of brushes. This was used to synchronize the directional change of the current so that the torque on the rotor remained in one direction (Chapman, 2005). Figure 4.33 showed a sectional view of a motor from the side (2 Brothers Hobby, 2015).

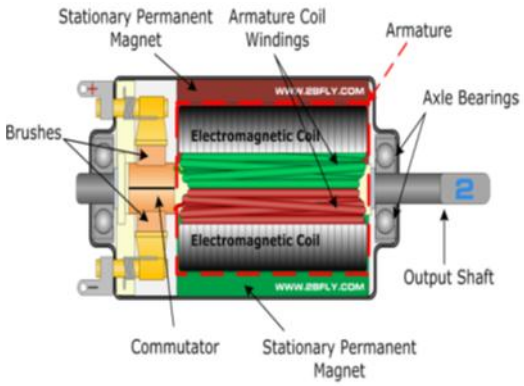

Figure 4-33: Brushed DC motor sectional view

Shaft bearings were commonly placed at the ends of the motor shaft within the casing. The image shows how the armature was a part of the shaft and how the terminals were connected directly to the brushes. An equivalent electrical circuit of a brushed dc motor was illustrated in figure 4-34 (Chapman, 2005). It consisted of an internal resistance, *Rm*, inductance, *Lm*, and back emf, V_{emf}.

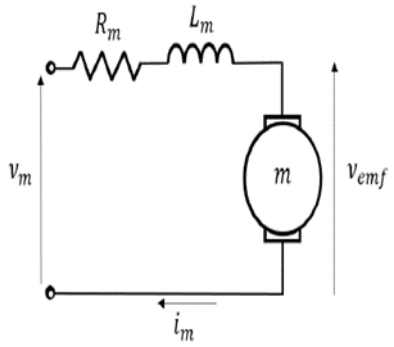

Figure 4-34: Brushed DC motor equivalent circuit

The equations described next use this circuit as a reference and were used to find important characteristics of the motor behavior under various voltages, speeds, and loads. Considering the transient voltages of the circuit and using Kirchhoff's voltage law, the terminal voltage is:

$$v_m = i_{mR_m} L_m \frac{di_m}{dt} + v_{emf} \quad (4.1)$$

Where,

v_m = transient motor terminal voltage [V]

i_m =transient motor current [A]

R_m=internal motor resistance [Ω]

L_m=internal motor inductance [H]

v_{emf}=transient motor back-emf [V]

The magnetic flux was defined by the motor constant as:

$$K_m = K_\emptyset \quad (4.2)$$

K_m=motor constant [N.m/A or V/rad.s^{-1}]

$K_\emptyset$=motor flux constant [N.m/A.Wb]

∅=motor magnetic flux [Wb]

The back emf voltage was proportional to the rotor speed through the equation:

$$v_{emf} = K_m w_m \quad (4.3)$$

v_{emf}=motor back emf voltage [V]

w_m = motor rotational speed [rad/s]

The torque generated by the shaft was proportional to the motor current through the relationship:

$$T_m = K_m i_m \quad (4.4)$$

Where, T_m=motor torque [N.m]

With no external load on the output shaft, the motor drew a no load current due to friction. Externally applied torque then follows the equation:

$$T_{m\_load} = K_m(i_m - I_0) \quad (4.5)$$

T_{m_load} = motor load torque [N.m]

I_0 = motor steady –state no load current [A]

During steady state $L_m \frac{di_m}{dt}$ and the Equation (2.3.1) reduces to:

$$v_{m} = i_{m R_m} + v_{emf} \quad (4.6)$$

Substituting Equation (4.4) and (4.3) into Equation (4.6) and rearranging to show the steady state relationship between the motor torque and speed, gives the motor a characteristic equation as:

$$w_m = \frac{V_m}{K_m} - \frac{T_m}{K^2 m} R_m \quad (4.7)$$

Where,

V_m=motor steady-state terminal voltage [V]

The electrical input power to the motor was given by:

$$P_e = V_m I_m \quad (4.8)$$

Where,

P_e= motor electrical input power [W]

I_m= motor steady state current [A]

Electrical heat losses were given by:

$$P_{loss\_elect} = {I_m}^2 R_m \quad (4.9)$$

The mechanical power produced by the motor were given by:

$$P_m = T_m \, w_m \quad (4.10)$$

Where,

P_m= motor mechanical power [W]

Mechanical losses were due to friction and was determined using the no-load current by:

$$P_{loss\_mech} = K_m I_o w_m \quad (4.11)$$

Where,

P_{loss_mech}= motor mechanical power losses [W]

Mechanical power output after frictional losses drive the external load and was determined by:

$$P_{m\_out} = P_m - P_{loss_{mech}} = T_m \, w_m - K_m I_o w_m \quad (4.12)$$

Where,

P_{m_out}=motor mechanical output power [W]

Electrical and mechanical losses were the combinational losses:

$$P_{loss\_comb} = P_{loss\_elect} + P_{loss_{mech}} = {I^2}_m \, R_m + K_m I_o w_m \quad (4.13)$$

Where,

P_{loss_comb}= motor combinational power losses [W]

P_{loss_elect}= motor electrical power losses [W]

$P_{loss_{mech}}$= motor mechanical power losses [W]

The motor efficiency was defined as the useful mechanical output over the electrical input as:

$$n_m = \frac{P_m - P_{loss\_mech}}{P_e} \; x \; 100 \qquad (4.14)$$

Where,

η_m=motor efficiency [%]

4.5.2.1. Selection criteria

The DC motor selected was chosen to actuate the wrist motion. As a result, the criteria that were used to evaluate whether a motor gearbox combination would satisfy the load requirements (Faulhaber, 2015). The selection procedure with conditional equations was described (Faulhaber, 2015). The motor was considered first, followed by the gearbox. The power of the motor was calculated using Equation (4.15). The rated mechanical power of possible motors for selection was then calculated using Equation (4.16). The motor power would need to satisfy the condition of Equation (4.17).

$$P_{g\_out\_max} = T_{g\_out\_max\_int} W_{g\_out\_max} \qquad (4.15)$$

$$P_m^R = T_m^R \, W_m^R \qquad (4.16)$$

$$1.5 \leq \frac{P_m^R}{P_{g\_out\_max}} \leq 2.5 \qquad (4.17)$$

Where,

$P_{g\_out\_max}$ = gearbox maximum mechanical output power [W]

$T_{g\_out\_max\_int}$ = gearbox maximum intermittent output torque [N.m]

$w_{g\_out\_max}$ = gearbox maximum output speed [rad/s]

P_m^R = motor rated mechanical power [W]

T_m^R = motor rated torque [N.m]

w_m^R = motor rated speed [rad/s]

The width and height dimensions were then checked against the space requirements. The available voltage supply should have a nominal value greater than the rated voltage of the motor, using Equation (4.18).

$$V_{supply\_nom} \leq V_{m\_nom}^R \qquad (4.18)$$

Where,

V_{supply} = nominal power supply voltage [V]

$V_{m\_nom}^R$ = motor rated nominal voltage [V]

The gearbox rated output torques should be higher than the required torques. This is checked using Equation (4.19) and (4.20) for the continuous and intermittent conditions, respectively.

$$T^{R}_{g\_out\_max_{cont}} \geq T_{g\_out\_max\_cont} \quad (4.19)$$

$$T^{R}_{g\_out\_max\_int} \geq T_{g\_out\_max\_int} \quad (4.20)$$

Where,

$T^{R}_{g\_out\_max\_cont}$ = rated gearbox maximum continuous output torque [N. m]

$T_{g\_out\_max\_cont}$ = gearbox maximum continuous output torque [N. m]

$T^{R}_{g\_out\_max\_int}$ = Rated gearbox maximum intermittent output torque [N.m]

$T_{g\_out\_max\_int}$ = gearbox maximum intermittent output torque [N.m]

The gearbox speed ratio was then determined using Equation 4.21. The closest available gearbox ratio that satisfied the dimensional requirements was selected, represented by G_{g_select}.

$$G_{g=} \frac{w^{R}_{g\_in\_max}}{w_{g\_out\_max}} \quad (4.21)$$

Where

$w^{R}_{g\_in\_max}$ = Rated gearbox maximum input speed [rad/s]

The maximum required gearbox input speed by the motor was then calculated, using Equation (4.22), and compared against the rated speed using Equation (4.23).

$$w_{g\_in\_max} = G_g w_{g\_out\_max} \quad (4.22)$$

$$w^{R}_{g\_in\_max} \geq w_{g\_in\_max} \quad 4.23)$$

Where,

$w_{g\_in\_max}$ = gearbox maximum input speed [rad/s]

Considering the efficiency of the gearbox, the required torques to be produced by the motor was calculated using Equation (4.24) and (4.25).

$$T_{g\_in\_max\_cont} = \frac{T_{g\_out\_max\_cont}}{G_g n_g} \quad (4.24)$$

$$T_{g\_in\_max\_int} = \frac{T_{g\_out\_max\_int}}{G_g n_g} \quad (4.25)$$

Where,

$T_{g\_in\_max\_cont}$ = gearbox maximum continuous input torque [N. m]

$T_{g\_in\_max\_cont}$ = gearbox maximum intermittent input torque [N.m]

n_g = gearbox efficiency [%]

The maximum motor speed was equivalent to the maximum gearbox input speed, and the maximum motor torques were equivalent to the maximum gearbox input torques. These relationships were shown in Equation (4.26), (4.27) and (4.28).

$$w_{m\_max} = w_{g\_in\_max} \quad (4.26)$$

$$T_{m\_max} = T_{m\_int} = T_{g\_in\_max\_int} \quad (4.27)$$

$$T_{m\_cont} = T_{g\_in\_max\_cont} \quad (4.28)$$

Where,

w_{m_max}= motor maximum speed [rad/s]

T_{m_max}= motor maximum torque [N.m]

T_{m_int}= motor intermittent torque [N.m]

T_{m_cont}= motor continuous torque [N.m]

The required continuous torque was a crucial aspect to minimize heat problems and should be less than the rated continuous torque of the motor. In equation form

$$T_{m\_cont} \leq T_m^R \quad (4.29)$$

Where,

$T_m^R = \text{rated motor torque [N. m]}$

Once the required torques and speeds of the motor via the gearbox were determined, further optimization could be made to improve the motor operational life.

This involved a comparison of the motors required maximum speed against the no load speed, and a comparison of the motor required maximum torque against the stall torque. These comparisons were represented in Equation (4.30) and (4.31).

$$w_{m\_max} \geq \frac{w_{m\_0}}{2} \quad (4.30)$$

$$T_{m\_max} \leq \frac{T_{m\_stall}}{2} \quad (4.31)$$

If both conditions were not met, then a motor with the next rated voltage up should be evaluated (Greg, 2015). If the torque condition was met but the speed condition was not, then a motor with the next lower rated voltage or with a smaller frame size should be evaluated (Greg, 2015). The radial and axial shaft loads on the gearbox should be determined to be compared against the rated bearing loads. Additional selection factors considered were cost and weight. If a number of motor gearbox combinations satisfied the requirements, then these were the final determining factors (Greg, 2015).

4.6. H-BRIDGE

An H-bridge circuit was an electronic power circuit that was used to control electric motors, such as dc motors for automotive applications.

The H-bridge was used to control the speed and direction of motors by allowing the right amount of current to flow in the right direction of the motor. The H-bridge consisted of four MOSFETS that were controlled by Pulse Width Modulation control signals. Generally, a motor can be either

switched ON or OFF (uni-directional rotation) based on the needs and direction of rotation depends on the polarity. A combination of these two schematics gives an H-bridge circuit and the switching between polarities was done using transistors (electronic switches) as shown in figure 4-35.

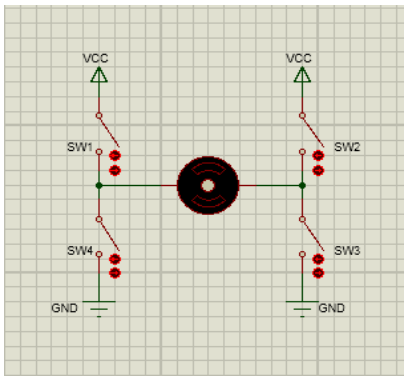

Figure 4-35: H-bridge

The H-bridge controlled the average voltage applied to the motors. The PWM signals from the microcontroller enabled, and disabled the H-bridge. From figure 4-35 circuit, it was seen that when (SW1 and SW3) were closed, the motor was in one polarity and when the switches (SW2 and SW4) were closed while the other switches were open, the motor was in another polarity. This was how an H-bridge circuit worked to control the DC motor in wrist motion of the touch hand system.

4.6.1. H-bridge selection

Due to the variance of operating voltages, in order to provide the ideal solution, it was important to pick the correct H-bridge as shown in figure 4-36. One of the keys to choosing an H-bridge was to determine what maximum current the DC motor being used will draw. The stall current, in which the motor needs to initially run, was also considered. The H-bridge that was chosen need to be rated to handle that much current, otherwise the integrated circuit will burn out.

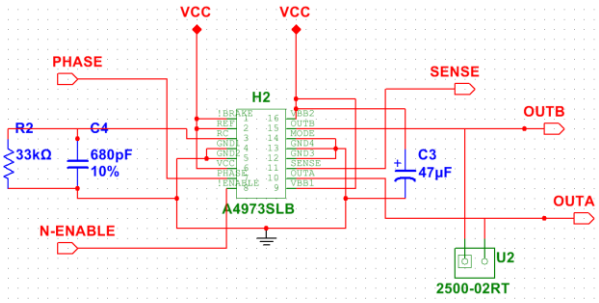

Figure 4-36: H-bridge circuit

4.7. BATTERY AND CHARGING

Most upper-limb prosthetic devices (terminal devices and wrists) were designed to operate on 7.2 V (nominal) with the exception of the powered elbows. Some can tolerate slightly higher voltages, but caution should be used here to avoid products and loss of the manufacturer's warranty.

4.7.1. Section objectives

The hand needed to run off a battery to allow for easy and safe charging and battery capacity monitoring. The battery was either connected externally, in the socket or strapped to the arm. It was also either removable or charged in a charger or plugged in on hand /socket and charged, and maximize battery life for full day's use.

4.7.2. Battery

The battery was essential in the design of the Touch hand system. Only Rechargeable batteries were used because the hand was to be used on a day-to-day basis. Commonly available rechargeable battery technologies include Nickel Cadmium (NiCd), Nickel-Metal Hydride (NiMH), Lead Acid, Lithium-Ion (Li-ion), and Lithium-Ion Polymer (Li-Po). The battery to be used in this project was selected according to its high density and lightweight to minimize the additional load the amputee would have a carry. Li-ion shown in figure 4-37 was used because it was cheap and easily available (Stopforth, 2010).

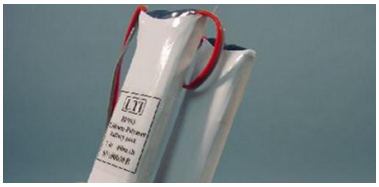

Figure 4-37: Li-ion battery

4.7.3. Advantages of Li-ion

The Li-ion had many advantages in the design of the Touch hand 3. The advantages of Lithium-ion Phosphate batteries were shown in table 9 (Stopforth, 2010):

Table 9: Advantages of Li-ion

Advantages of Li-ion
(1) The battery needs to be charged regularly and easy to maintain.
(2) The battery comparatively discharge slowly.
(3) Less weight for same size.
(4) More energy.
(5) Inherently safe.
(6) Rechargeable.
(7) Lithium-ion chemistry with no thermal runaway.
(8) Remains thermally stable.
(9) Virtually zero maintenance over the service life of the battery.
(10) No battery memory effect.
(11) Low Peukert's Effect – low capacity loss as discharge rates increases.
(12) Low self-discharge.
(13) No sudden death syndrome.
(14) No explosive hydrogen gases (vital for the environment that the robot will operate in).
(15) No corrosion on battery terminals.
(16) No need to refill electrolyte.

4.7.4. Limitations Li-ion

However, the battery had minor flaws in the operation. These flows were shown in table 10.

Table 10: Limitations of the Li-ion

Limitations of the Li-ion
(1) Requires protection circuit to maintain voltage and current within safe limits.
(2) Subject to aging, even if not in use - storage in a cool place at 40% charge reduces the aging effect.
(3) Transportation restrictions - shipment of larger quantities may be subject to regulatory control. This restriction does not apply to personal carry-on batteries.
(4) Expensive to manufacture - about 40 percent higher in cost than nickel-cadmium.
(5) Not fully mature - metals and chemicals are changing on a continuing basis.

4.7.5. Protection of the battery

The voltage of the battery pack needed to be selected. The minimum input voltage was supposed to be at least 6.0V.The battery had cells of the nominal voltage of 3.6 V. However, the instantaneous voltage changes over the discharge cycle, starting at approximately 4.2 V and ending at 3.0V (Simpson. 2006). A two-cell battery pack with the cells in series was being selected to provide a voltage range of 6.0 V - 8.4 V. The selected battery pack had a capacity of 2.6A.h. The battery voltage was supposed to be monitored for more precise motor voltage control. This was important

because the voltage would change over time. A voltage divider circuit shown in figure 4-38 was used in this project.

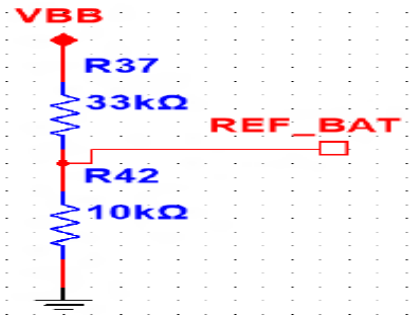

Figure 4-38: Protection of the battery

The VBB power rail was connected directly to the battery and the output REF_BAT was connected to the microcontroller. The resistor values were selected to convert the maximum battery voltage of 8.4V below the analog reference value of 3.3V.

4.8. VOLTAGE REGULATORS

A voltage regulator was designed to automatically maintain a constant voltage level. The regulator also provides a great amount of stability and protection for the Touch hand system. There are various popular series of voltage regulators for example LM78XX and LM79XX (Grainger et al., 1994). The LM78XX voltage regulators were regulating and outputting positive voltage while the LM79XX were series of regulators for negative voltage. A voltage regulator with three terminal devices as shown in figure 4-39 (Grainger et al., 1994).

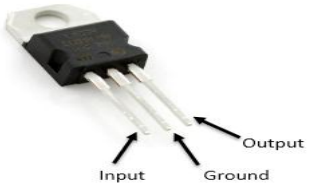

Figure 4-39: A voltage regulator

The output voltage of the of the Lithium ion battery was regulated down from 7.4 V to 5V for the Arduino m0 pro. The ground was essential so that the voltage would have electric potential and the circuit would have a return path. The advantages of the LMXXXX family were shown in table 11.

Table 11: Advantages of the LMXXXX family

Advantages of the LMXXXX family
(1) They have short circuit protection.
(2) They have thermal overload protection.
(3) Output current up to1A, which is a safe value with respect to the demands of the circuit.

The voltage regulator circuit was shown in figure 4-40 (Grainger et al., 1994).

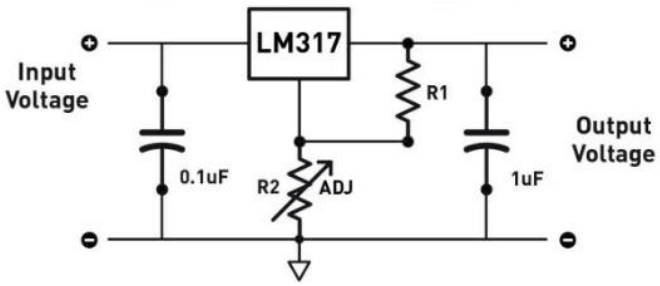

Figure 4-40: Voltage Regulator

The 0.33 µF after the lithium ion battery and before the input of the voltage of the regulator. This capacitor was there to filter out any coming noise from the voltage source (the battery).The voltage regulator was the most efficient when clean DC signal was fed to it.

The DC line was protected from any noise. The 0.1 µF was hooked after the voltage regulator. This capacitor was there again to filter out any noise or high-frequency signals that may be on the DC voltage line.

4.9. EMG AMPLIFIERS

The EMG circuits and sensors have found their way into prosthetics, robotics, and other control systems. In the design of the prosthetic hand, two amplifiers as shown in figure 4-41 were used to process the signals from the forearm.

Figure 4-41: Touch hand 3 EMG amplifier

EMG signal was acquired through differential amplification technique. The differential amplifier should have high input impedance, very low output impedance. Ideally, a differential amplifier had infinite, and zero output (2009) Instrumentation Amplifier Application Note, Intersil Incorporated. An instrumentation amplifier as shown in figure 4-42 had a high impedance to achieve differential amplification.

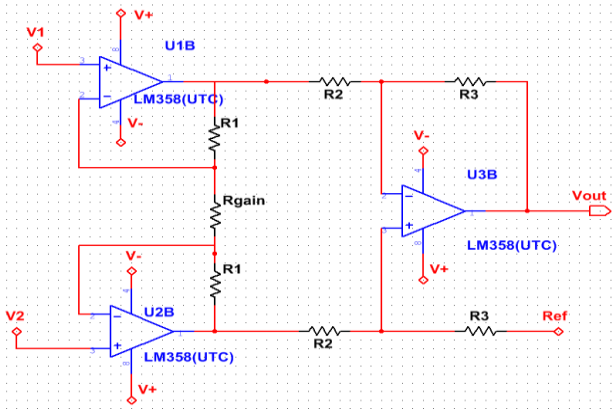

Figure 4-42: Instrumentation amplifier

4.9.1. EMG amplifiers filtering

A major signal acquisition using surface EMG and circuit design considerations for robotic prosthesis role in hampering the recording of the EMG signal was noise. Therefore, the signal has to be filtered, even after differential amplification (Gianluca De Luca., 2001). The noise frequencies that contaminates the raw EMG signal could be either high or low. Low frequency noise could be caused by amplifier DC offsets, sensor drift on skin and temperature fluctuations and could be removed using a high-pass filter. High-frequency noise could be caused by nerve conduction and high-frequency interference from radio broadcasts, computers, cellular phones etc. and could be deleted using a low pass filter. In order to remove these high and low frequencies, high pass and low pass bio-filters could be used. The EMG amplifier had a high pass filter as shown in figure 4-43 to remove low-frequency component from a particular electrical signal (Gianluca De Luca., 2001).

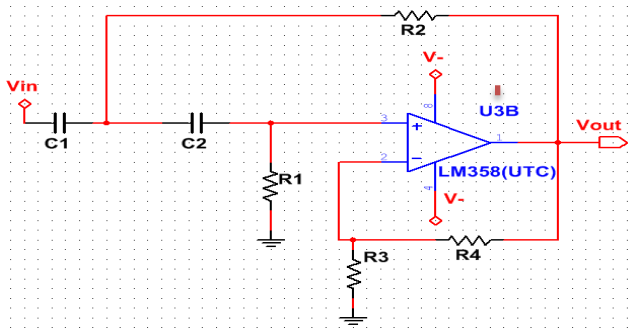

Figure 4-43: A second order high pass filter

In addition, the amplifier had a low pass filter as shown in figure 4-44 to allow frequencies that were less than the cut-off frequency to be transmitted and above to be removed (Gianluca De Luca., 2001).

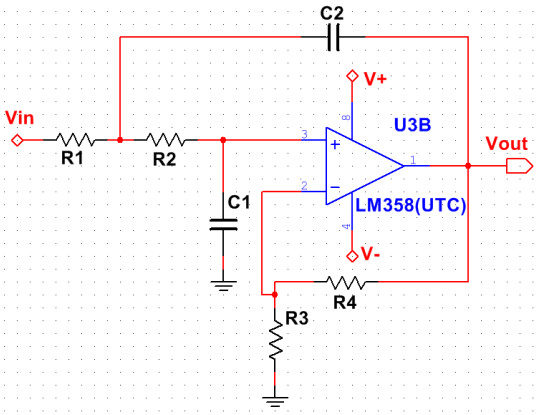

Figure 4-44: A second order low pass filter

4.9.2. EMG amplifier connectivity

The pin out of the EMG amplifier shown in figure 4-45 (Gianluca De Luca., 2001) was important in connecting it to the power supply, electrodes, and microcontroller.

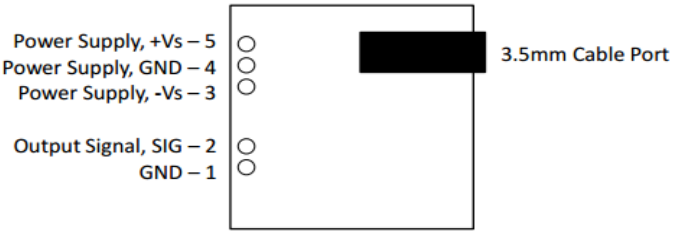

Figure 4-45: EMG amplifier pinout

4.9.2.1. Connecting to the electrodes

The electrodes were connected as below:

(1) After determining which muscle group, you want to target (e.g. bicep, forearm, and calf), clean the skin thoroughly.

(2) Place one electrode in the middle of the muscle body, connect this electrode to the RED Cable's snap connector.

(3) Place the second electrode at one end of the muscle body, connect this electrode to the Blue Cable's snap connector.

(4) Place a third electrode on a bony or non-muscular part of your body near the targeted muscle, connect this electrode to the Black Cable's snap connector.

4.9.2.2. Connecting to the microcontroller

The microcontroller was connected to the amplifier as follows:

(1) Connect the SIG pin of your sensor to an analog pin on the microcontroller (e.g. A0).
(2) Connect the GND pin of your sensor to a GND pin on the microcontroller.

4.9.2.3. Connecting to the power Supply

The power supply was connected to the microcontroller as follows:

(1) Connect the positive terminal of the first 9V battery to the +Vs pin on your sensor.
(2) Connect the negative terminal of the first 9V battery to the positive terminal of the second 9V battery. Then connect to the GND pin on your sensor.
(3) Connect the negative terminal of the second 9V battery to the –Vs pin of your sensor.

4.10. OVERALL CIRCUIT SCHEMATIC

The overall schematic circuit shown in figure 4-46 show high electrical connections through the Touch hand 3.The circuit consisted of two microcontrollers that communicated through UART. The master microcontroller was used to decode EMG signals and was for haptic feedback.

Two EMG sensors were used to acquire the muscle signals from the forearm. The hand microcontroller was used to decode the temperature, pressure, and vibration sensor. The Touch hand 3 had a single pressure, temperature and vibration sensor attached to the index, middle and ring finger respectively. This schematic was powered by a Lithium-ion battery that supplies 6 volts. In addition, Voltage regulators were used to regulating the power supplied to the other circuit to avoid overheating. Three linear actuators were used to actuate the thumb, index and middle depending on the command interpreted from the EMG signals. The DC Motor was used to rotate the wrist via a motor drive.

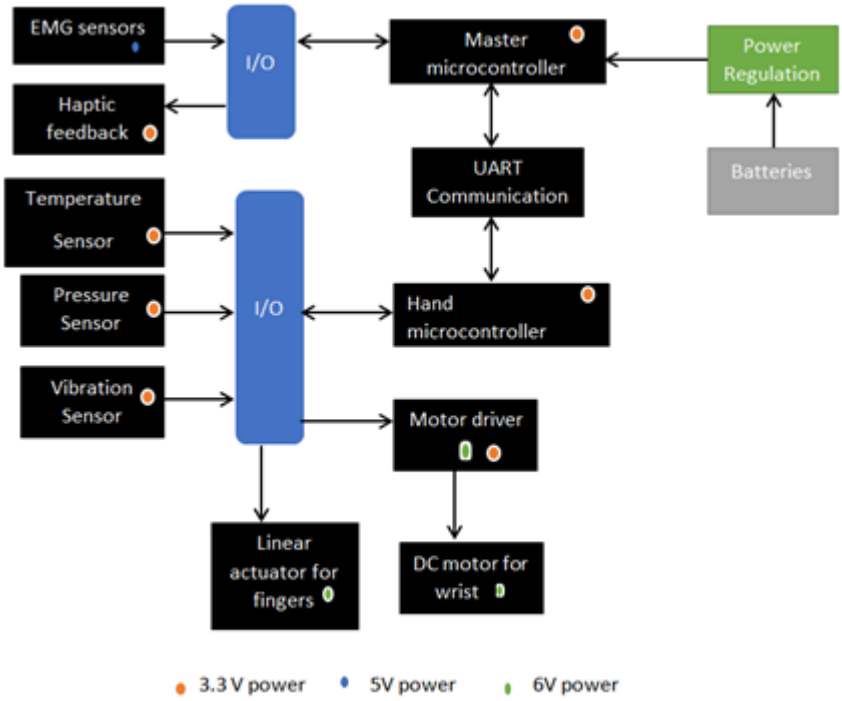

Figure 4:46: High-level electrical connections of the touch hand system

4.11. PCB DEVELOPMENT

The modular printed circuit board were designed. The PCBs were created to support and electrically connects electronic components using conductive tracks, pads, and other features etched from copper sheets laminated onto a nonconductive substrate (Tavernier, 2015). The components that were soldered on the PCB were capacitors, resistors or active devices. The PCB could be single (one copper layer), double sided (two copper layers) and or multi-layer (outer and inner layers) (Tavernier, 2015). Touch hand PCB designs were designed manually using ultiboard. The PCBs that were designed include the motherboards to hold the two microcontrollers and allowed multiple other PCBs for the sensory system (Temperature, Pressure and vibration sensors) and EMG sensors.

The Touch hand PCBs were designed with dedicated layout software. Schematic capture through the Multisim 12 was created as shown in figure 4-47

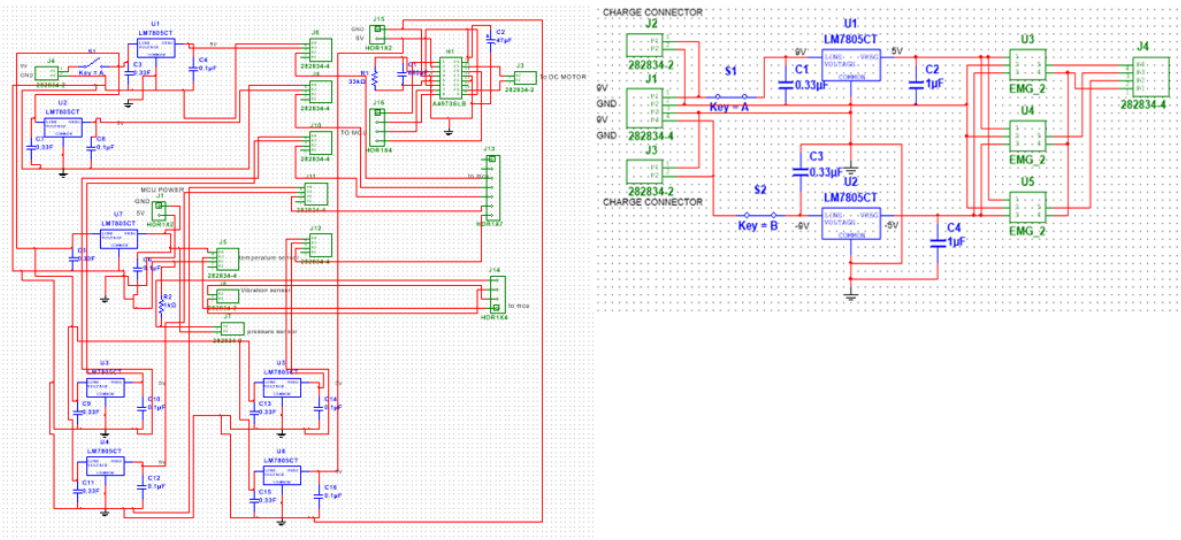

(a) (b)

Figure 4-47: Multism circuit diagrams for (a) Motor and sensors control board (b) EMG control board

The modular printed circuit board were designed. The PCBs were created to support and electrically connects electronic components using conductive tracks, pads, and other features etched from copper sheets laminated onto a nonconductive substrate (Tavernier, 2015). The PCBs that were designed include the motherboards for stalking with the Arduino M0 Pro to accommodate the EMG sensors, motors and sensory system (Temperature, Pressure and vibration sensors) as shown in figure 4-48. The double copper layer Touch Hand PCB was designed using Ultiboard. The PCBs have the dimensions of the Arduino M0 Pro (53.34 mm x 68.58 mm) to allow proper stalking.

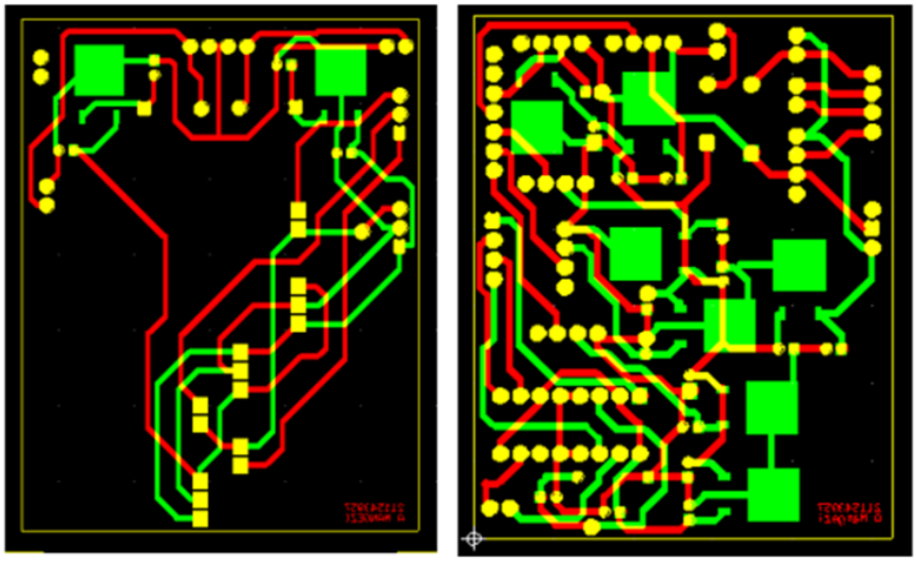

(a) (b)

Figure 4-48: (a) EMG amplifiers PCB (b) Motors and sensory system PCBs

The modular PCB for the motors and sensory system were designed as shown in figure 4.49. The PCB was designed to drive 6 motors, 5 linear servomotors for the fingers and one DC Motor for the wrist. It was made to accommodate one temperature, one vibration, and two force sensors.

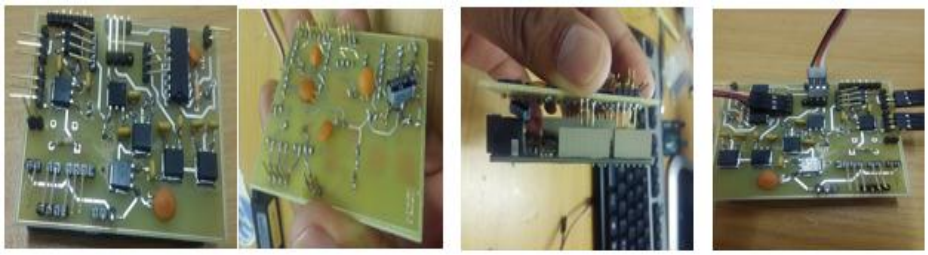

Figure 4-49: Motor and sensory PCB (a) Top view (c) Bottom view (d) Connecting the PCB to arduino m0 pro (d) Connecting motor and sensors example

Furthermore, the EMG amplifiers PCB were designed as shown in figure 4-50. The PCB was made to be connected to three amplifiers but the Touch hand system used four channel EMG amplifiers to acquire the forearm muscle signals for every grasping motion of the arm. The PCB was modular for easy connections, repair, and maintenance.

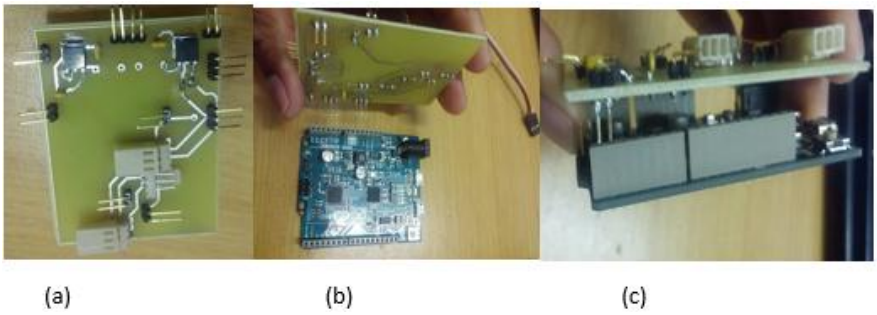

Figure 4-50: EMG amplifiers PCB (a) Top view (b) Bottom view (c) Connecting the PCB to arduino m0 pro

4.12. TOUCH HAND 3 PCB MANUALS

The manual was designed to assist users to connect the electronic PCB boards to the Touch hand 3 without complications. It shows final product connections for the motor and EMG contro board. The motor control board was made to accommodate 5 micro linear actuators (PQ12) to actuate the fingers, 1 dc motor for the wrist, and 3 sensors (1 temperature sensor (LM35), 1 vibration sensor (MEAS) and 1 force sensor). The EMG control board can accommodate maximum of 3 amplifiers. In Touch hand 3 design, 2 EMG channels were used to analysis and acquire signals from the foearm.

4.12.1. Motor control board final PCB connections

Figure 4-51 shows the final motor and sensor control PCB that was made for Touch Hand 3.The labeled parts on the PCB shows all the connections that can be done as follows:

(a) Micro linear actuator motor 1 connected to the thumb of the Touch hand 3.

(b) Micro linear actuator motor 2 connected to the index finger of the Touch hand 3.

(c) Micro linear actuator motor 3 connected to the middle finger of the Touch hand 3.

(d) Micro linear actuator motor 1 connected to the Ring finger of the Touch hand 3.

(e) Micro linear actuator motor 1 connected to the Pinky finger of the Touch hand 3.

(f) DC motor connections for the wrist motion.

(g) Force sensor connections for the index finger.

(h) Vibration sensor connections for the palm.

(i) The temperature sensor connections for the middle finger.

(j) The GND wire that is connected to the EMG board.

(k) The UART(Tx,Rx) for serial communication with the EMG board.

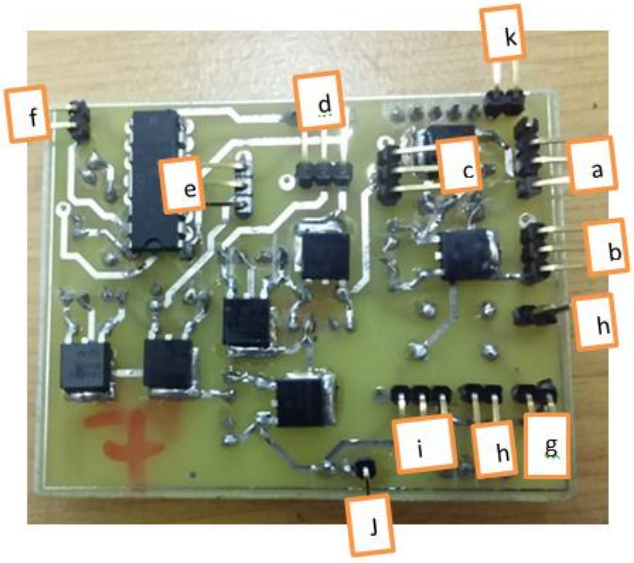

Figure 4-51: Motor and sensor control PCB

The connections in Figure 4-52 showed how the micro linear actuators were connected to the PCB board. Take note of the wiring of the motor as:

Black implies Ground

Red implies Positive

White implies Signal

N/B: The connections should be exactly done as shown in figure 4-52.

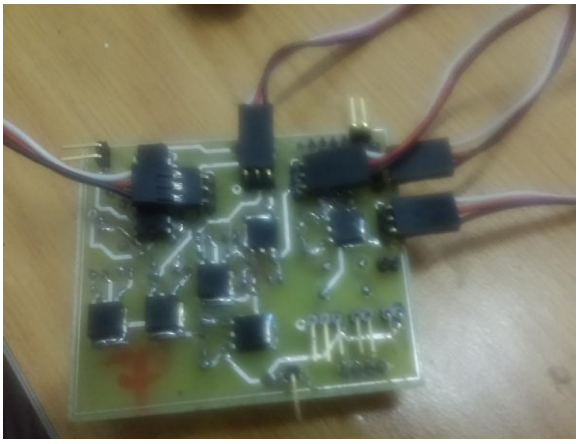

Figure 4-52: PCB showing connections for the micro linear actuators

Figure 4-53 shows how the battery was connected to the board.

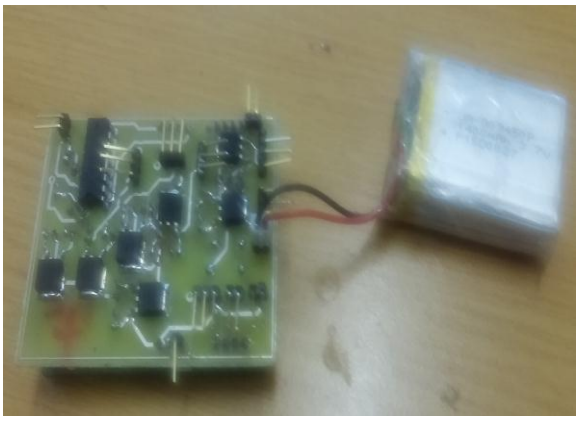

Figure 4-53: PCB showing battery connections

The diagram figure 4-54 shows how the temperature, vibration, and force sensors were connected to the electronic PCB board.

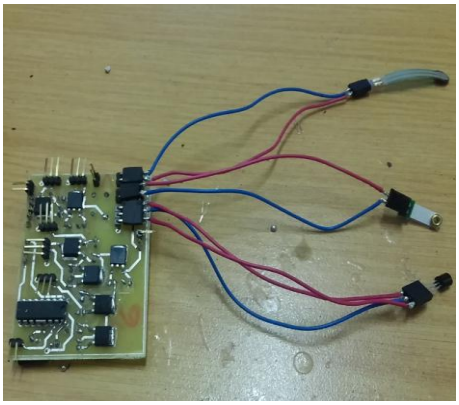

Figure 4-54: PCB showing connections for the sensors

4.12.2. EMG control board final PCB connections

Figure 4-55 shows how the different amplifiers were connected on the EMG control board as follows:

(a) EMG 1 (V+, GND, V-) is connected.
(b) EMG 1(GND,Signal) is connected.
(c) EMG 2 (V+, GND, V-) is connected.
(d) EMG 2 (GND,Signal) is connected.
(e) EMG 3 (V+, GND, V-) is connected.
(f) EMG 3 (V+, GND) is connected.
(g) Battery connections.
(h) UART(Tx, Rx) connections.
(i) Battery charging port(negative voltage).
(j) Battery charging port(positive voltage).
(k) GND be connected to the Motor and sensors control board.

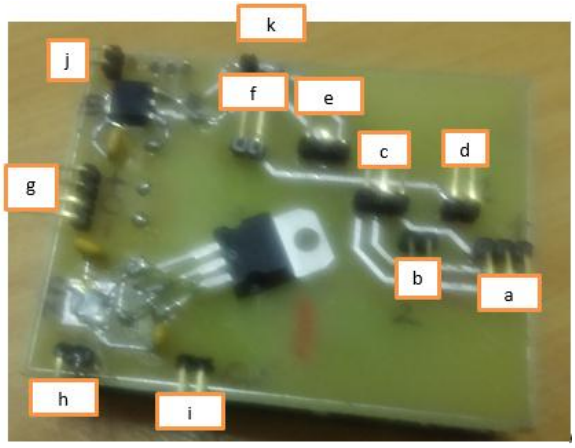

Figure 4-55: The EMG control board connections.

The connections in figure 4-56 show how the EMG control board connected to the EMG amplifiers.

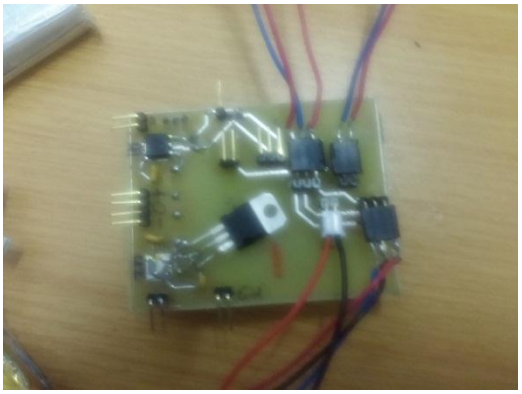

Figure 4-56: EMG control board connections

Figure 4-57 shows how the batteries are connected to the EMG control board.

Figure 4-57: Battery connections to the EMG control board

4.13. CHAPTER SUMMARY

A modular and compatible electronic system was designed for the Touch hand system. A full understanding of the different components that was used in this project was acquired through research. A full sensory system namely the temperature ,pressure and vibration sensor was designed. The right type of the motors was chosen to actuate the fingers and the wrist motion. Furthermore, the battery that was used was able to power the Touch hand system. The overal schematic systemof the Touch hand system was fully understood.

CHAPTER 5: TESTS AND RESULTS

5.0. INTRODUCTION

Various tests were performed in order to evaluate the prosthetic hand and subsystems designed. The investigations were done to find the best electrodes to be used for Touch hand system. In addition, the correlation between the EMG electrodes and antenna, considering yagi-patch antenna configuration was investigated. Furthermore, the sensory system was tested to evaluate its effectiveness in interpreting and quantifying environmental conditions of object temperature and grip strength. The various gripping types were investigated by placing two sets of electrodes on the forearm muscles. The methods for the filtering of the EMG signals noise e.g. Kalman filter were discussed. Different algorithms that were implemented to design the touch hand system were also discussed. Finally, the test results of the overall system with the amputee were included. Additionally, these testing results were to prove the theory behind the development of the touch hand system.

5.1. EMG RESULTS AND DISCUSSION

With the need to find the best EMG electrodes to use for Touch hand 3, a number of experiments were carried to determine the correlation between EMG and antenna configuration. The experiments that were carried by the volunteers include investigations of the effect of the development electrodes (direct and indirect contact), embroidered electrodes (direct and indirect contact) and comparison of “big” and “small” covidien electrodes. In addition, the overall comparison of the different configuration of the different type of the electrodes was done. Furthermore, the different gripping types on each volunteer were investigated, taking into account the voltage ratios of the two muscles in the forearm.

5.1.1. Developed contactless electrodes

This experiment was carried to compare direct and indirect electrodes in contact with the different volunteer forearm muscles. Silver/silver chloride (Ag/AgCl) electrodes were used for direct contact. However, indirect contact electrodes were constructed with the combination Ag/AgCl electrodes and aluminum foil as an insulator. These indirect contact electrodes were five different combinations of layered electrodes that include single layer, two layers, three layers, four layers and five layers, each tested one at a time on different volunteers. The different layered electrodes were placed and monitored on the forearm muscles of the volunteers. The single layer consisted of an aluminum foil and AgCl electrode. All the other electrodes layers were made by combining many single electrodes. In addition, different layers of the non-contact electrodes with the combination

silicon layer were also tested. In every experiment, there are rare cases to obtain accurate readings and result criterions are used to obtain approximately correct readings. In this case, Chauvenet's criterion was used to eliminate dubious results. Figure 5-1 shows the graph for non-contact stick-on electrodes that was obtained before applying the criterion. The graph has plotted the voltage against the number of the electrode layers for these volunteers. The effect of increasing the number of layers was investigated and analyzed on the volunteers to give the best electrode layers combination. The observations and analysis were as shown in table 12.

Table 12: Discussion, analysis, and evaluation of developed contactless electrodes

Number of volunteers(9)	Discussion, analysis and evaluation
Volunteer1	The voltage increased approximately from 0.1 V to 0.3 V, proportionally with respect to the number of electrode layers. The 5 layers electrodes corresponded to the highest voltage value of 0.3 V. This concluded that 5 layers were the best electrodes combination to use by volunteer1.
Volunteer2	The voltage decreased approximately from 0.2 V to 0.05 V between 1 layer and 3 layer electrodes. It started to increase approximately from 0.05 V to 0.27 V, which corresponded to 5 layers. This concluded that 5 layers were the best electrode combination to use by volunteer2.
Volunteer3	The voltage increased approximately from 0.11 V to 0.27 V, which corresponded between 1 layer and 4 layer electrodes respectively. It started to decrease to approximately 0.1 V on layer 5. This concluded that 4 layers were the best electrodes to be used by volunteer3 since they were corresponding to the highest voltage value.
Volunteer4	There was a slight increase in voltage of approximately 0.02 V between 1 layer and 2 layer electrodes. A sharp increase in voltage of approximately 0.39V between 2 layers and 3 layer electrodes followed. The voltage decreased by approximately 0.39 V between 3 layers and 4 layers. It started to increase approximately from 0.09 V to 0.255 V between 4 layers and 5 layers. This concluded that 3 layers were the best electrode to be used by volunteer3 because it corresponds to the highest voltage value.

Number of volunteers(9)	Discussion, analysis, and evaluation
Volunteer5	The voltage decreased by approximately 0.32 V between 1 layer and 2 layer electrodes. It started to increase approximately from 0.27 V to 0.57 V between 2 layers and 4 layers. It then decreased by approximately 0.2V between 4 layers and 5 layers. This concluded that 4 layers were the best electrodes to use by volunteer5.
Volunteer6	The voltage increased approximately from 0.24 V to 0.42 V between 1 layer and 2 layers. It started to decrease approximately from 0.42 V to 0.04 V between 2 layer and 4 layers. It further increases slightly by approximately 0.1 V between 4 layers and 5 layers. This concluded that 2 layers were the best electrodes to use by volunteer6.
Volunteer7	The voltage increased approximately from 0.1 V to 0.25 between 1 layer and 3 layers. It then decreased approximately by 0.15 V between 3 layers and 4 layers. The voltage increased slightly by approximately 0.4 V between 4 layers and 5 layers. This concluded that 3 layers were the best electrodes to use by volunteer7.
Volunteer8	The voltage increased approximately from 0.09 V to 0.3 V between 1 layer and 4 layers. There was a constant change in voltage between 4 layers and 5 layers. This concluded that either 5 layers or 4 layers could be used by volunteer8.
Volunteer9	The voltage increased approximately from 0.05 V to 0.59 V between 1 layer and 5 layers. This concluded that 5 layers were the best electrodes to use by volunteer9 since they corresponded to the highest voltage value.

To verify the correctness of the above analysis, Chauvenet's criterion was applied. Dubious results from the volunteers were eliminated. In addition, the analysis above could not find the best suitable electrode layers for all the volunteers. The best electrode layer varied on each volunteer which gives rise to queries, resulting in chauvenet's criterion application.

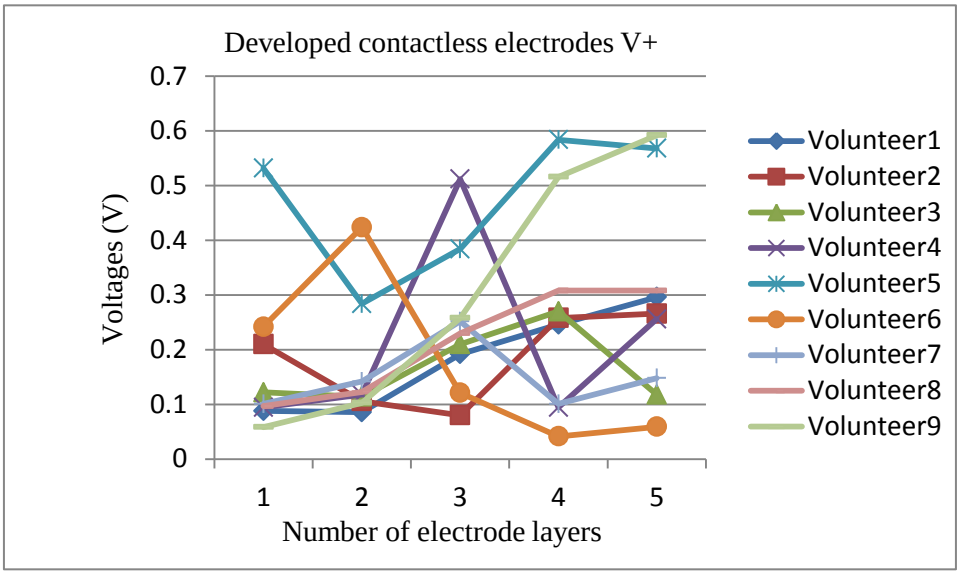

Figure 5-1: Non-contact electrodes before Chauvenet's criterion

The graph in figure 5-2 showed how some dubious results were eliminated after applying Chauvenet's criterion. This criterion used statistical probability by calculating the mean and standard deviation of the observed data of the volunteers. In this case, the mean and standard deviation of the 10 volunteers were calculated depending on the positive voltage values obtained on a different layer of the electrodes. Volunteers with dubious results were eliminated namely volunteer4, volunteer5, and volunteer6 as shown in figure 5-1. Considering the voltages and number of electrode layers, one could conclude that layer 5 was the best electrode layer to use by volunteers. Furthermore, one volunteer tested the effect of placing the developed contactless electrodes on the silicon layer. The results obtained in figure 5-1 graph showed that 4 layer electrodes were the best since it corresponded to the highest voltage. This explained the patch-yagi antenna theory of the effect of increasing electrode layers and aluminum foil.

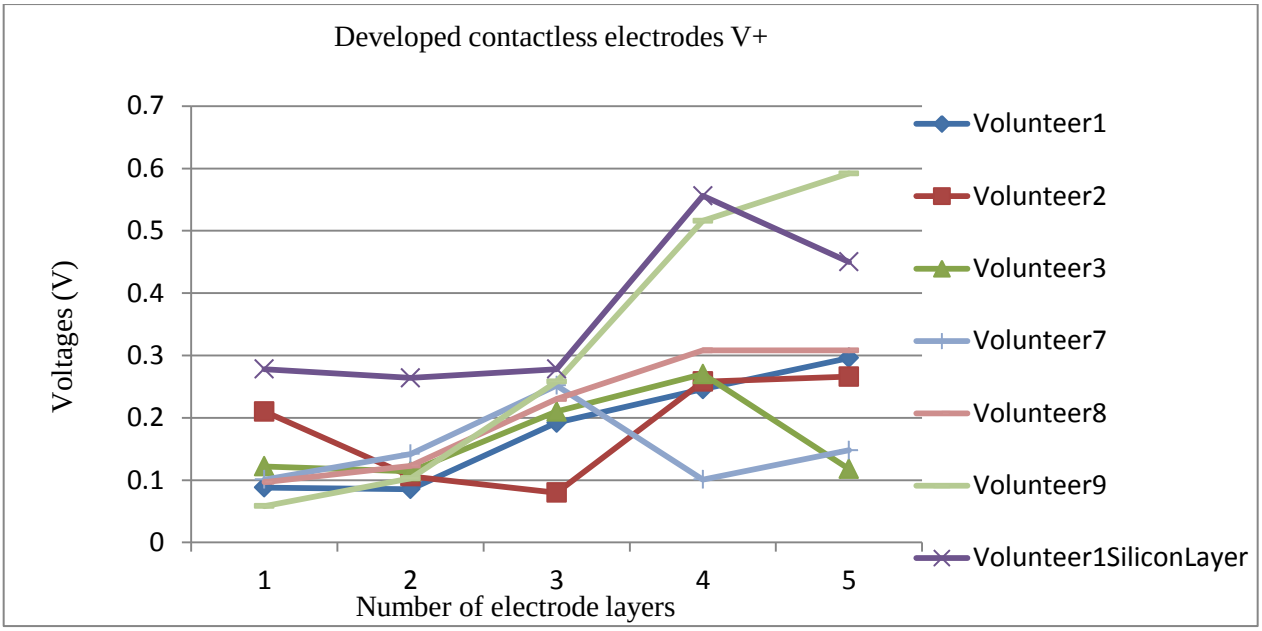

Figure 5-2: Non-contact electrodes after Chauvenet's criterion

The average positive voltage (V+) and average voltage (Vp-p) for developed contactless electrodes were crucial in finding the best electrode layer to use for Touch hand system. As a result, figure 5-3 showed the V+ and Vp-p results that were obtained from the volunteers in a relationship with the number of electrode layers.

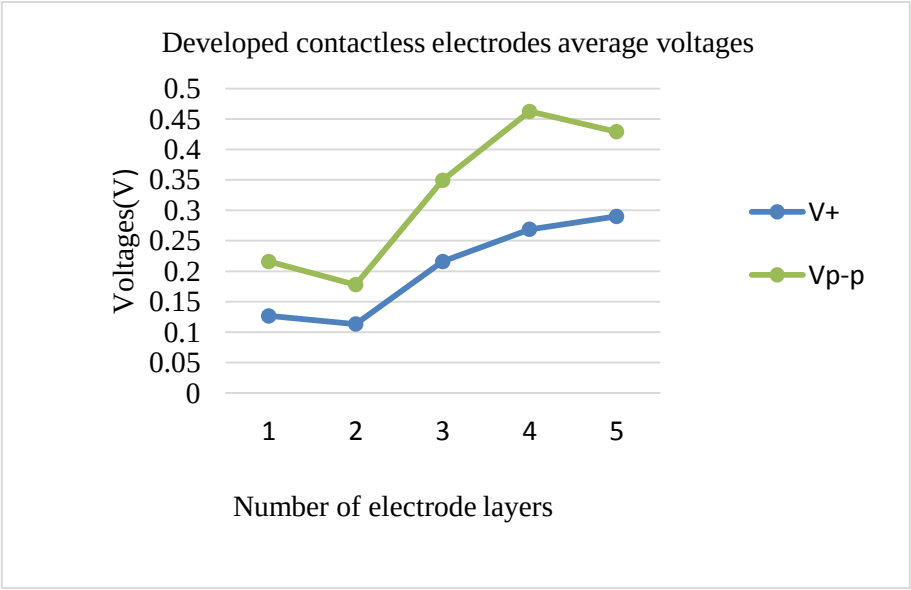

Figure 5-3: Average voltages for developed contactless electrodes

The observations and analysis were stated as shown in table 13.

Table 13: Developed contactless electrodes V+ and Vp-p discussion, analysis and evaluation

Developed contactless electrodes	Discussion, analysis and evaluation
(1) V+	The V+ decreased approximately by 0.1 from 0.12 V to 0.11 V between 1 layer and 2 layers. It started to increase approximately from 0.11 V to 0.29 V between 2 layers and 5 layers. Furthermore, 5 layers corresponded to the highest voltage value. The higher the voltage value the better the electrode layer.
(2) Vp-p	The Vp-p decreased approximately from 0.21 V to 0.17 V between 1 layer and 2 layers. It then started to increase approximately from 0.17 V to 0.46 V between 2 layers and 4 layers. There was a slight decrease from 0.46 V to 0.42 V between 4 layers and 5 layers. By comparing the average voltage values of the electrodes, one could conclude that non-contact electrodes were better that the contact electrodes.

5.1.2. Embroidery electrodes

The experiment was done to determine the best combination of the different layered embroidered electrodes. The investigation focused on both contact and non-contact electrodes with and without cloth. In addition, the combination of the non-contact electrodes with the silicon electrodes was also investigated. Direct contact was done to determine the effect of thickness of the embroidered electrodes on the forearm muscles. Figure 5-4 showed the results that were obtained from determining the effect of thickness on the electrodes.

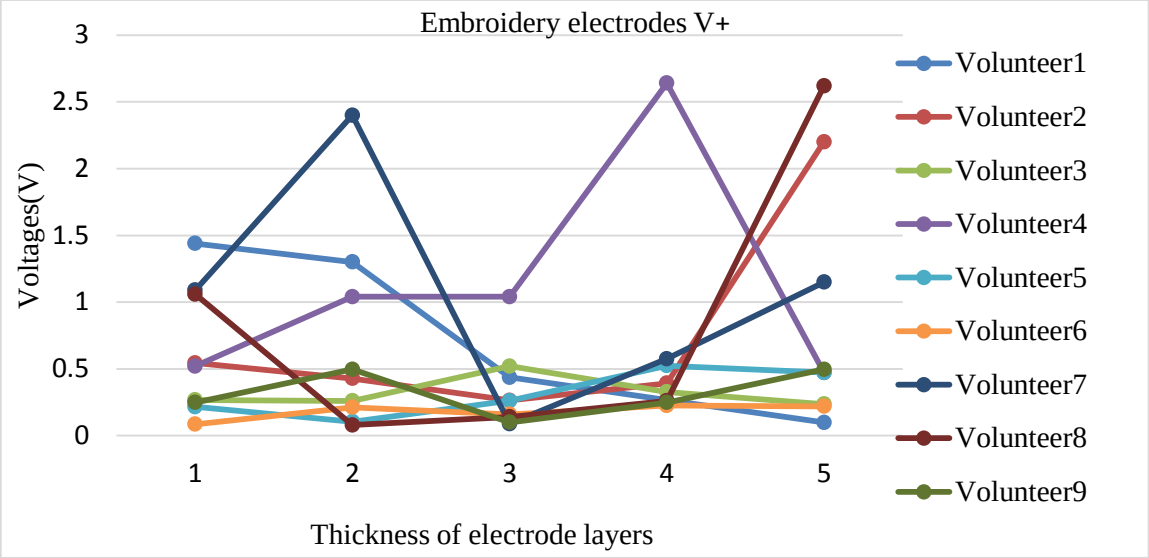

Figure 5-4: Non-contact embroidery electrodes before Chauvenet's criterion

The analysis and observations were done as stated in table 14.

Table 14: Discussion, analysis, and evaluation of embroidery electrodes

Number of volunteers(9)	Discussion, analysis, and evaluation
Volunteer1	The voltage decreased approximately from 1.45 V to 0.09 V, proportionally with respect to the thickness of the embroidery electrodes. This concluded that 1 layer had the priority to be used by volunteer1 since it corresponded to the highest voltage value.
Volunteer2	The voltage decreased approximately from 0.55 V to 0.26 V between 1 layer and 3 layer electrodes. It then started to increase approximately by 0.12 V between 3 layers and 4 layers. There was a sharp increase of voltage approximately from 0.35 V to 2.0 V between 4 layers and 5 layers. This concluded that 5 layers were the most preferred thickness of electrodes to use by volunteer2.
Volunteer3	The voltage increased approximately from 0.25 V to 0.50 V between 1 layer and 3 layer electrodes. It then decreased approximately from 0.5 V to 0.2 V between 3 layers and 5 layers. This concluded that 3 layers were the best thickness layer to be used by volunteer3 since they were corresponding to the highest voltage value.

Number of volunteers(9)	Discussion, analysis and evaluation
Volunteer4	The voltage increased approximately from 0.5 V to 2.6 V between 1 layer and 4 layers. It then decreased from 2.6V to 0.4 V between 4 layers and 5 layers. This concluded that 5 layers were the best thickness layer to use by volunteer4 because they corresponded to the highest voltage value.
Volunteer5	The voltage slightly increased approximately from 0.2 V to 0.5 V between 1 layer and 4 layers. It then started to decrease approximately to 0.4V. This concluded that 4 layers were the best thickness layer to use by volunteer5.
Volunteer6	The voltage increased approximately from 0.08 V to 0.16 V between 1 layer and 5 layers. This concluded that there was no effect in increasing the thickness of the embroidery electrodes. The difference was negligible.
Volunteer7	The voltage increased approximately from 1.2 V to 2.52V between 1 layer and 2 layers. It then sharply decreased approximately to 0.08 V between 2 layers and 3 layers. The voltage increased approximately from 0.08 V to 1.1V between 4 layers and 5 layers. This concluded that 2 layers with highest voltage was the proper thickness to use by volunteer7.
Volunteer8	The voltage decreased approximately from 1.0 V to 0.08 V between 1 layer and 2 layers. It then started to increase approximately by 0.18 V between 2 layers and 4 layers. There was a sharp change in voltage approximately from 0.25 V to 2.2 V between 4 layers and 5 layers. This concluded that 5 layers with the highest voltage was the proper thickness to use by volunteer8.
Volunteer9	The voltage increased approximately from 0.24 V to 0.4 V between 1 layer and 5 layers. This concluded that there was no effect in increasing of the embroidery electrodes thickness.

To verify the correctness of the above analysis, Chauvenet's criterion was applied. Dubious results from the volunteers were eliminated. Figure 5-5 shows the graph that was obtained after applying Chauvenet's criterion. Dubious results of Volunteer4 and Volunteer7 were eliminated. The graph is showing a slight change in voltage values, which concludes that thickness, has an effect on the embroidered electrodes.

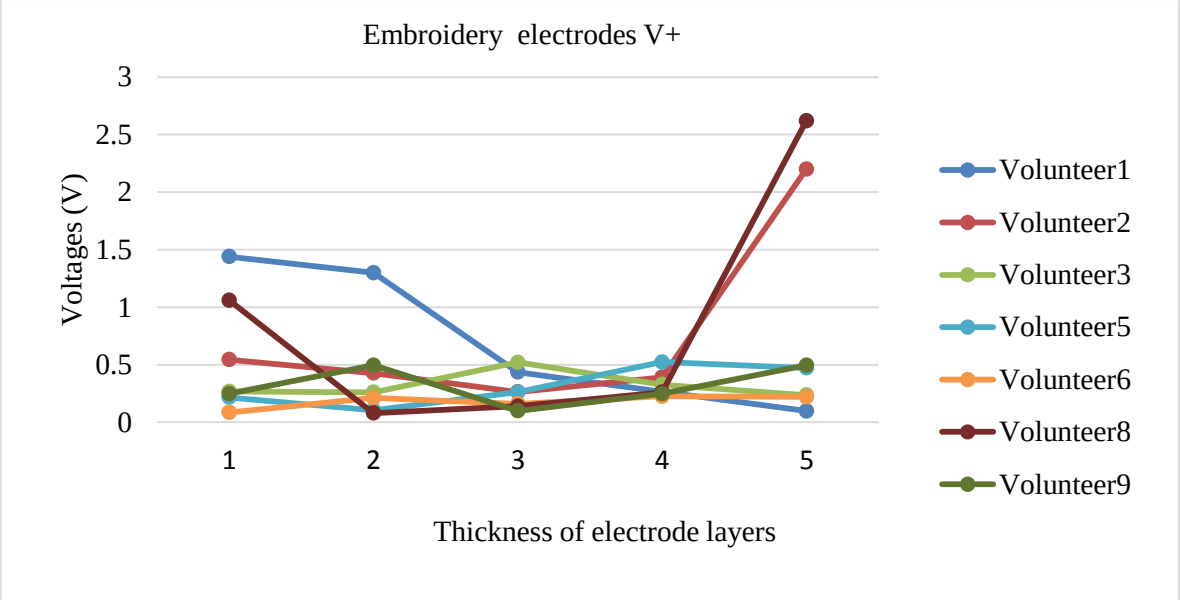

Figure 5-5: Non-contact embroidery electrodes after Chauvenet's criterion

The average V+ and Vp-p were critical parameters in determining the effect of thickness on the embroidered electrodes. Figure 5-6 showed the embroidered electrodes averages.

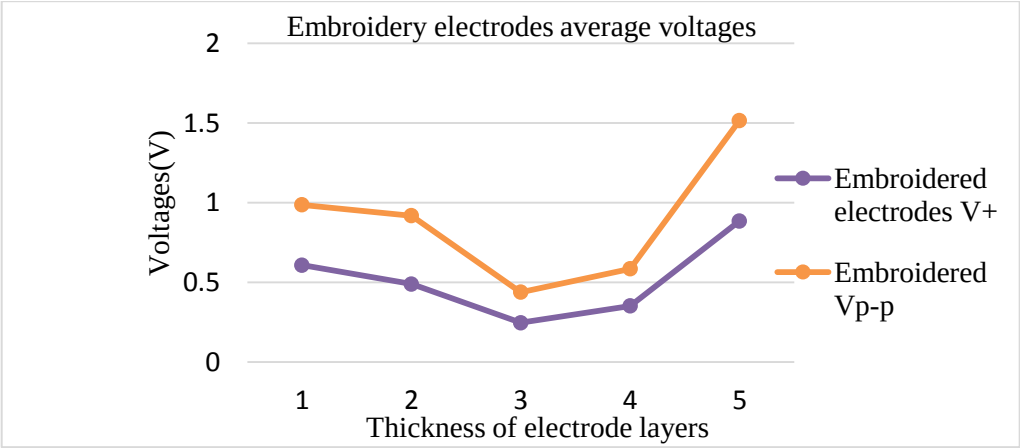

Figure 5-6: Average voltages for embroidery electrodes

The parameters were observed and analyzed as stated in table 15.

Table 15: Embroidery electrodes V+ and Vp-p discussion, analysis and evaluation

Embroidery electrodes	Discussion, analysis and evaluation
V+	The V+ decreased approximately from 1.0 V to 0.4 V between 1 layer and 3 layers. It then started to increase approximately from 0.40 V to 0.85 V between 3 layers and 5 layers. The highest average voltage corresponded to thickness of 5 layers.
Vp-p	The Vp-p decreased approximately from 0.6V to 0.24 V between 1 layer and 3 layers. It then started to increase approximately from 0.24 V to approximately 0.90V. The highest average voltage corresponded to thickness of 5 layers.

Indirect contact consisted of the different combination of the embroidery electrodes with the cloth in between. Figure 5-7 shows the graph of the embroidery electrodes plus cloth in between. The voltage values increase between 1 layer and 2 layers on all the volunteers. In addition, there is a slight change in voltage between 4 layers and 5 layers. The positive voltage values increase as the number of layers of embroidered electrodes increases. However, the combination of the embroidered electrodes gives the best results on average with the second layer than all the other layers. The 5 layers indicate a small improvement compared to 2 layers, yet the average improvement was 0.183 V. The cost factor has to be considered to justify that the more layers are needed for the small average value obtained with the increase in the voltage.

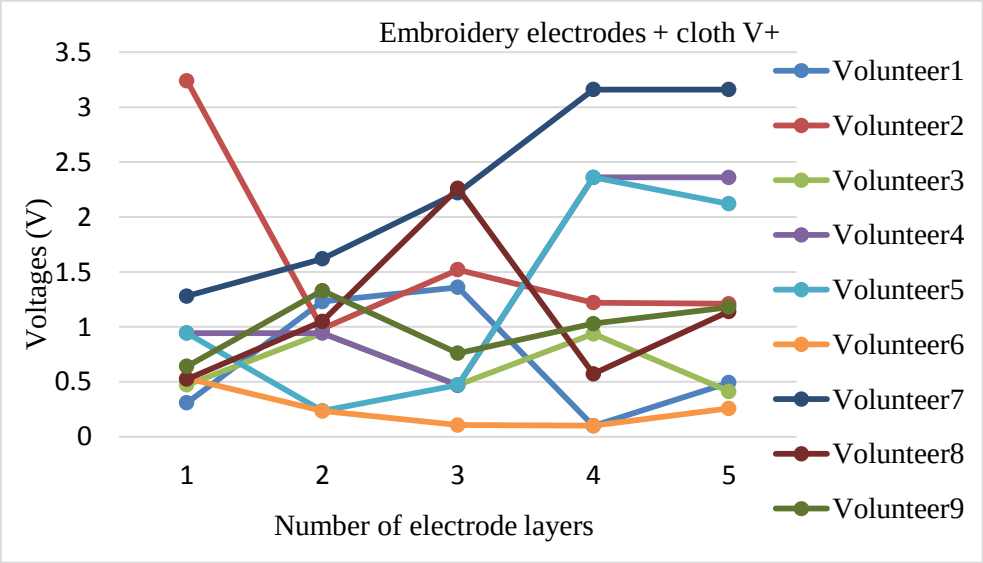

Figure 5-7: Non-contact embroidery + cloth electrodes before Chauvenet's criterion

In every experiment, there are rare cases to obtain accurate readings and result criterions were used to obtain approximately correct readings. Hence, in this experiment, the mean and standard deviation of the observed data of volunteers was calculated using the Chauvinist's criteria to eliminate dubious results as shown in figure 5-8. Dubious points were removed from the plotted graph. The conclusion was that layer 2 combination was the best to use as embroidered electrodes because of their better voltages on all the volunteers. Furthermore, one volunteer tested the effect of placing the developed contactless electrodes on the silicon layer. The results obtained in

figure 5-8 graph shows that layer 2 was the best since it corresponds to the highest voltage.

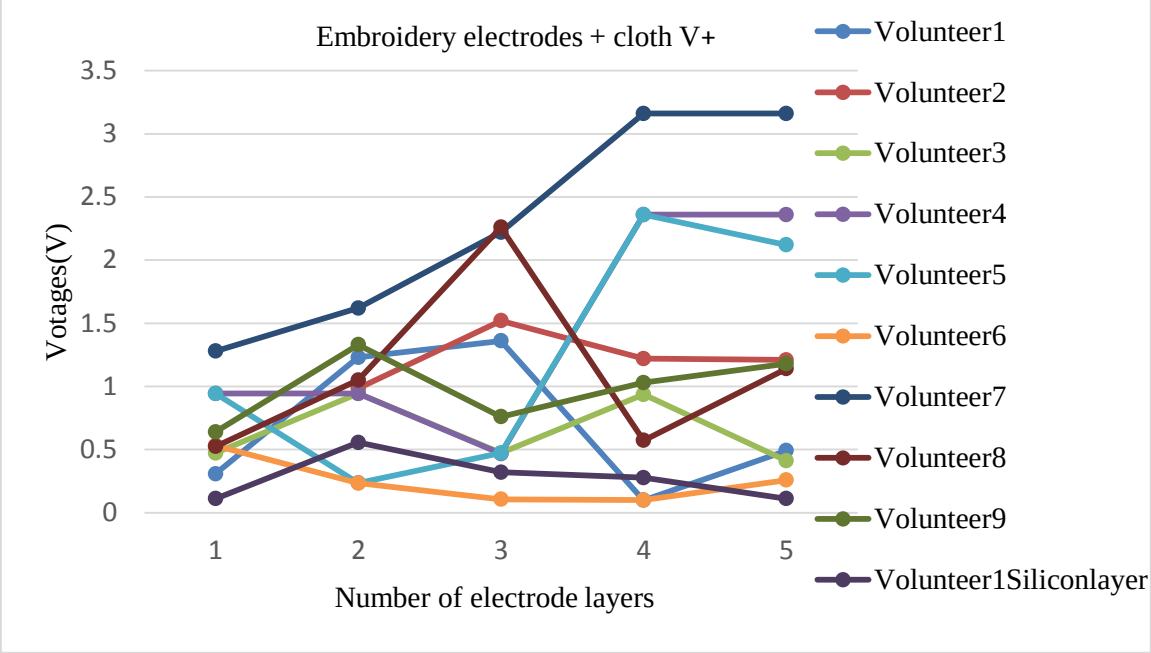

Figure 5-8: Non-contact embroidery + cloth electrodes after Chauvenet's criterion

In addition, the average voltage value (V+) for the embroidered electrodes plus cloth ranges approximately from 0.7V - 1.3 V respectively as shown in figure 5-9. Furthermore, the Vp-p ranges approximately from 1.1 V to 1.9 V. The V+ and Vp-p values obtained from this experiment concludes that non-contact embroidered electrodes are the best electrodes to use.

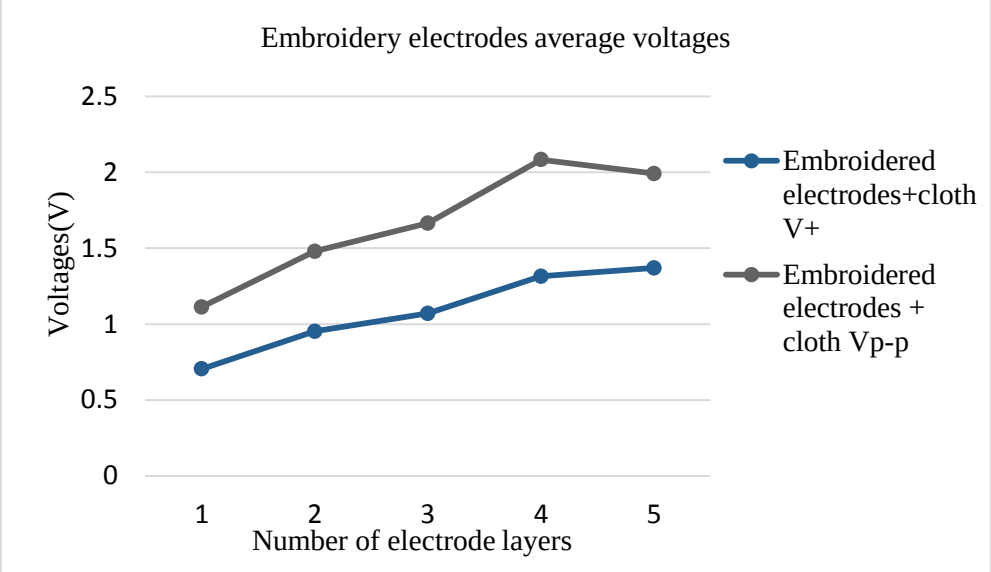

Figure 5-9: Embroidery electrodes average voltages

5.1.3. Overall comparison of the electrodes for the touch hand system

The series of EMG experiments were carried out to determine the electrodes used for the Touch hand system. The results obtained from the experiments shows that non-contact electrodes were an obvious choice to be implemented for Touch hand 3. These electrodes are not sensitive to skin, could be embedded in clothing and can eliminate the risk of delivering high currents to the test study since they are capacitive and non-contact. The comparison was based on the positive voltages and average voltages obtained from the volunteers as shown in figure 5-10. The higher the voltage and average voltage, the better the non-contact electrode layer. As a result, the non-contact stick-on electrode was chosen for the Touch hand system because they were inexpensive to construct and easily available.

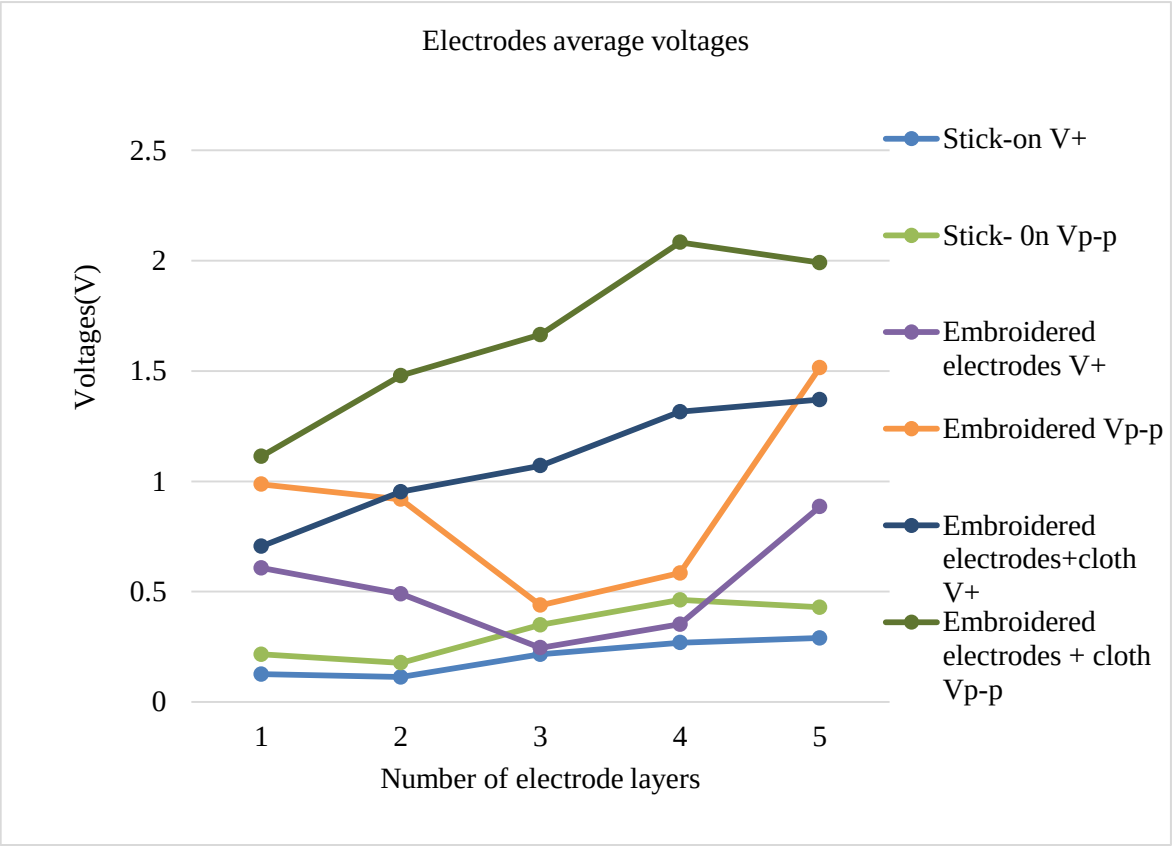

Figure 5-10: Average voltages of the electrodes

5.1.4. Comparison of "big" and "small" covidien (sticky) electrodes

The experiment was done to compare the effect size on the sticky electrodes. The criteria to choose the best electrode was based on the output voltage (V+) and average voltage (Vp-p).Volunteers were asked to lift a weight and monitor the voltage changes on an oscilloscope. Figure 5-11 showed the bar graph to compare the "big" and "small" covidien electrodes. The V+ and Vp-p for the small sticky electrodes are 0.08 V and 0.172 V respectively. The V+ and Vp-p for the big covidien electrodes are 0.0632 V and 0.143 V respectively. The higher the voltage value, the better the electrode. Comparing the voltages, one can conclude that the small covidien electrodes are the best choice to use for Touch hand system.

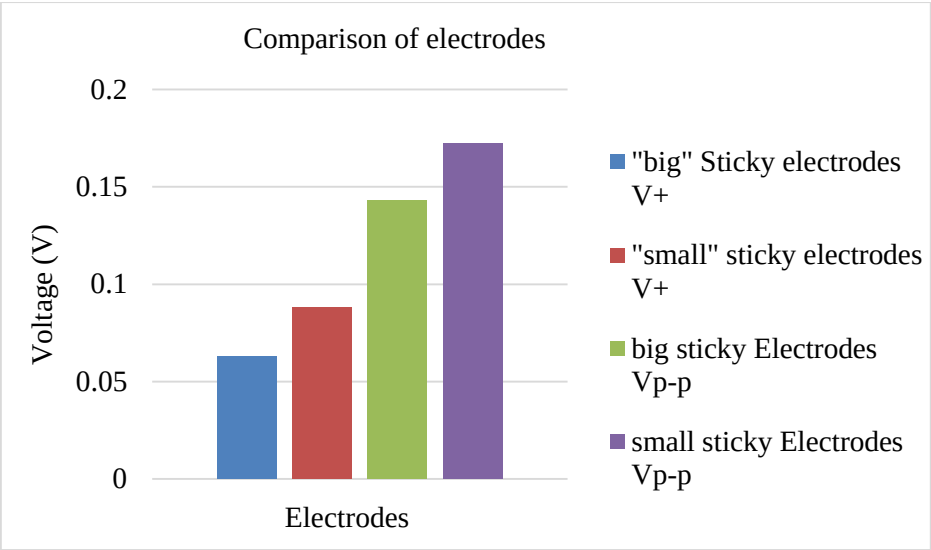

Figure 5-11: Comparison of "big" and "small" covidien electrodes

5.1.5. Investigation of the different gripping types

The experiment was carried out to determine if there was some relationship with some percentage value that each muscle group generated when a person wants to do something. Two set of sticky electrodes were placed on the two different of the forearm muscles and their inputs were monitored on the oscilloscope. Five volunteers were allowed to perform gripping such a picking a pencil, holding a key, turning a wrist left and right etc. For each gripping type, the voltage values and their averages were noted for each muscle group. The bar graph in figure 5-12 shows the average voltages that were obtained by one volunteer for different gripping types. The bar graph shows that muscle group strength differs depending on the gripping type performed.

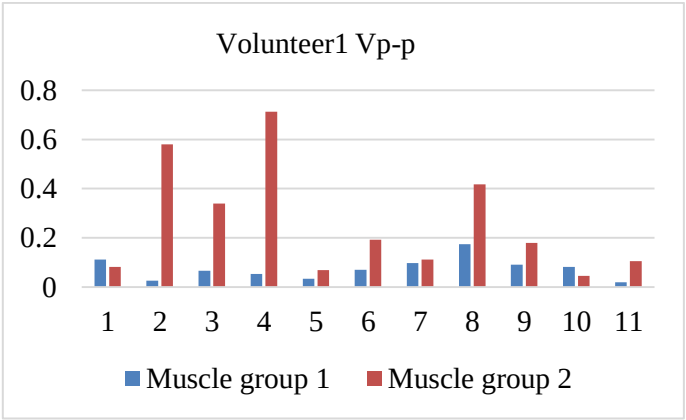

Figure 5-12: Average voltages for a volunteer

Furthermore, figure 5-13 shows the bar graph for voltage (V+) against muscle groups. The graph shows that one set of muscle is strong that the other. This was observed by the high voltage values that correspond to the muscle group. The gripping types performed by the volunteer verifies the coordination of the muscles in the forearm.

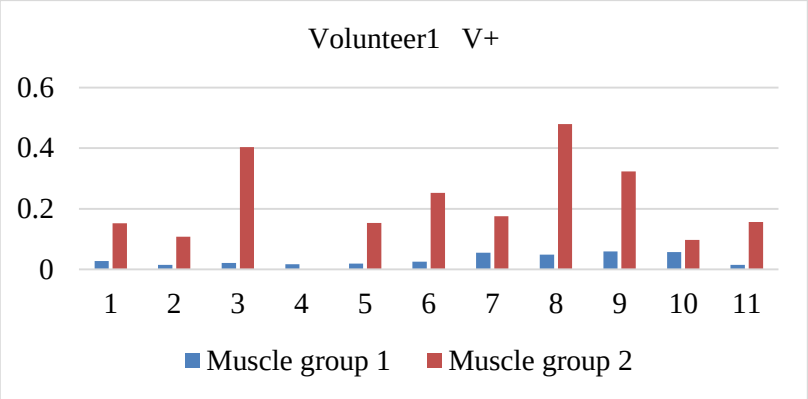

Figure 5-13: Positive voltages (V+) for a volunteer

In addition, the calculation of the voltage ratios shown in table 16, regroup the different gripping types in similar categories using alphabetical letters. The table shows an example of gripping pencil, holding the key, carrying a bag etc. as same gripping type represented by letter "g". However, voltage ratios differ for each volunteer. This implies that volunteers have different muscle strength resulting in a difference in the values of the voltages that were obtained on each different gripping type. Furthermore, the results show a relationship of some percentage value that each muscle group generates on performing a respective task.

Table 16: Volunteer muscle group and voltage ratios

Volunteer 1	V + 1 ratio (Muscle group 1)	V + 2 ratio (Muscle group 2)	Correlation
Gripping a pencil	18.01189465	81.98810535	g
Holding a key	18.97565071	81.02434929	g
Wrist right	12.82051282	87.17948718	wr
Wrist left	0	100	wl
Pick up a spoon	29.62962963	70.37037037	g
Pick up a plate	17.27272727	82.72727273	g
Pick up a cup	6.976744186	93.02325581	g
Grab a light bulb	18.64555849	81.35444151	lb
Grab a knife	24.75728155	75.24271845	k
Push a clothes peg	6.542056075	93.45794393	g
Carry a bag	20.19837692	79.80162308	g

Where,

g = pinch grip.

wr = wrist right rotation

wl = wrist left rotation

lb = spherical grip

k = hook grip

5.2. KALMAN FILTER RESULTS

With the need to eliminate the EMG signal noise from the forearm muscles, the Kalman filter approach was used. This mathematical power tool was used for stochastic estimation from the EMG sensors. The implementation of the predictor-corrector type estimator minimized the estimated error covariance when some presumed conditions were met. The amputee was allowed to perform different grasping tasks whilst a set of electrodes were placed on the forearm muscles. A number of 500 V readings were taken from the set of forearm arms. The idea was to find the Kalman variance, which was determined by reading samples of the raw data and using excel. The Kalman variance obtained from the two forearm muscles were 46.05 V and 13.4 V respectively. The values differ between amputees because of the difference in muscle strength, hence generating different voltage values from the EMG sensors. The Kalman filters variables e.g. Process noise covariance, measurement noise covariance, the value of interest, estimation error covariance and Kalman gain were introduced in the C programming to define the state of the filter.

5.3. DIFFERENT ALGORITHMS IMPLEMENTED

A number of algorithms were implemented in designing the Touch hand 3. The algorithms that were implemented includes the EMG, temperature, force, vibration and motor algorithms. The C programming language was used written to represent each algorithm. The EMG algorithm was successfully implemented because the prosthetic hand was able to perform different grasping tasks by open and closing the fingers. Touch hand 3 was programmed in such a way to allow the amputee to perform the different grasping tasks. In this case, the Touch hand was able to perform wrist rotation, closing and opening fingers using the EMG signals. The signals were analyzing when the amputee was performing different grasping tasks and a statistical probability was formulated to create a range of filtered Kalman values for each grasping task.

Furthermore, the algorithms formulated for the temperature, force sensor and vibration sensors were successful in that Touch hand 3 was able to sense external heat, force, and vibration respectively. The variables were introduced in C programming language to accommodate and calculate the raw value readings from these sensors. In addition, the motor algorithm was formulated to control the movement of the fingers and wrist depending on the EMG command received. This algorithm that was implemented enabled the Touch hand 3 fingers and wrist to respond to the EMG signals.

5.4. TESTS WITH THE AMPUTEE

The amputee tested the Touch hand 3 with the idea of proving the myoelectric concepts behind the Touch hand system. The system was designed for amputees with the aim to fully restore human like features. The initial step was testing how the prosthetic Touch hand 3 responses to the amputee's hand using the EMG signals as shown in figure 5-14. The Touch hand system was able to open and close in response to the amputee actions.

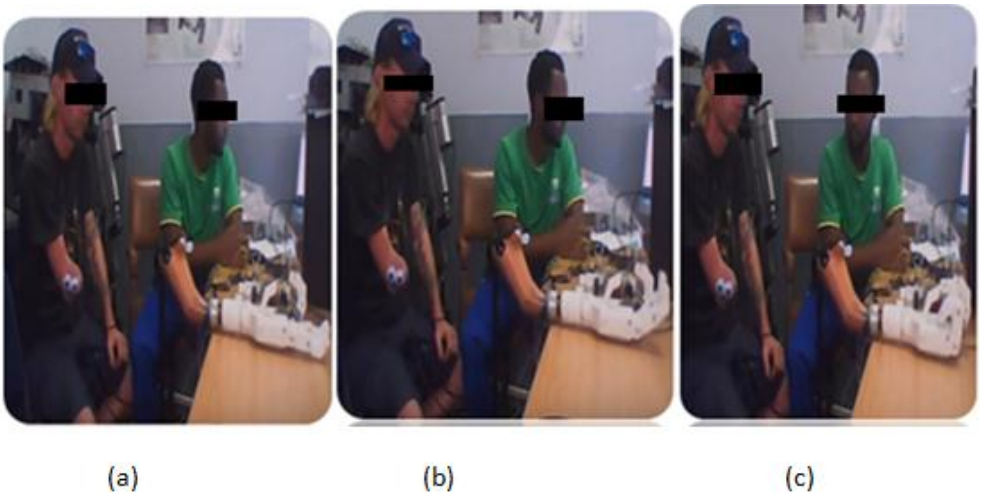

Figure 5-14: (a) Open position (b) middle way position (c) close position of the Touch Hand as controlled by the amputee

Furthermore, figure 5-15 shows how the amputee was preparing to fit the Touch hand 3.The forearm socket was designed specifically for the amputee to feel comfortable and flexible when performing different tasks.

Figure 5-15: (a) Fitting the socket to the hand (b) The amputee putting inner part of the socket on his arm (c) The amputee fitting on the Touch hand

The amputee was able to attach his arm into the socket. The first task was to pick up a chalk dust as shown in figure 5-16. It was not easy since that was his first time to use it, hence the chalk dust slipped from his hand.

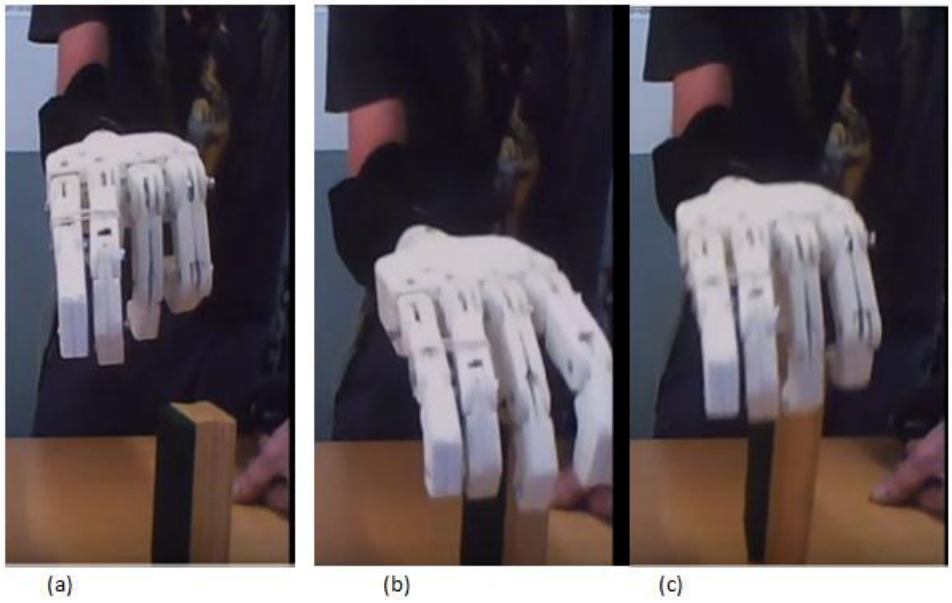

Figure 5-16: (a) The amputee attempting to open the hand using EMG signals (b) Opened hand and ready to pick up the chalk dust (c) The amputee holding the chalk dust.

The second task was to pick up a chalk dust and place it on top the plastic container as shown in figure 5.17. The amputee was able to balance it quite nicely on top of the plastic container. This was nice for the building of puzzles and other similar tasks to be performed by the amputee.

Figure 5-17: (a) Open hand (b) Touch hand holding the chalk dust (c) Touch hand balancing the chalk dust on a plastic container

The next task was to place the chalk duster on top of the small cylinder. This was a more challenging task and more coordination was needed to be in contact with the robotic hand such as the Touch hand 3 as shown in figure 5-18. In addition, the wrist was able to rotate so that the hand was able to perform many tasks. The amputee was able to perform a different task using EMG signals. This proved the myoelectric concepts behind the Touch hand 3.

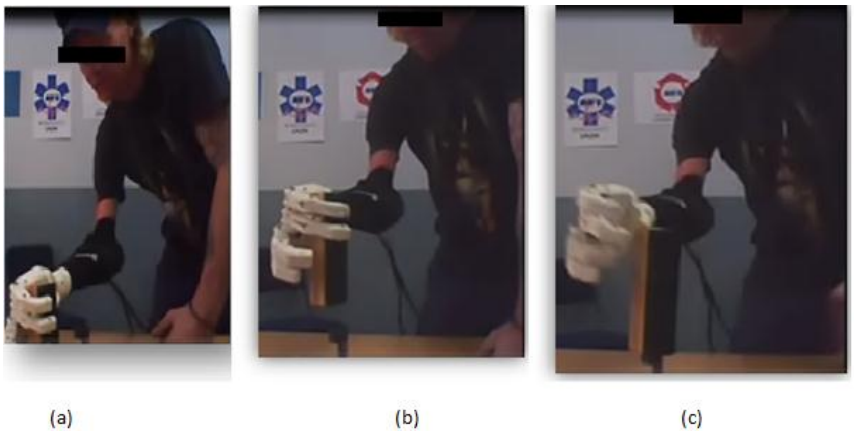

Figure 5-18: (a) Touch hand picking up the chalkdust (b) Touch hand placing the chalkdust on the small cylinder (c) Amputee balancing the chalkdust on a small cylinder.

5.5. CHAPTER SUMMARY

Successful investigations of the correlation between the EMG electrodes and antenna following the Yagi patch antenna configuration were observed. This was proved through the experiment that was carried to determine the type of EMG electrode for the Touch hand system. The comparison between the direct and non-contact electrodes was done. However, non-contact electrodes proved to have many advantages over contact electrodes. This is because non-contact electrodes are not sensitive to skin, can be embedded in clothing and can eliminate the risk of delivering high currents to the test study since they are capacitive. From the EMG experiments that were carried out to determine the best electrode for Touch hand 3, it was concluded that the combination of the developmental contactless electrode layer 4 and silicon was the best. The comparison was based on the output voltage from the amplifiers. The higher the voltage, the better the electrode. The EMG experiment also helps to choose between big and small sticky electrodes to use for constructing the developmental contactless electrodes. The algorithm that was formulated helped in the development of the Touch hand 3.In addition, the testing results obtained from the amputee proved the myoelectric idea behind the Touch hand system. The amputee was able to perform different gripping tasks like picking up of the chalk dust and perform the building of puzzles.

CHAPTER 6: DISCUSSION OF THE OVERALL SYSTEM, CONCLUSION, AND FUTURE WORK

6.0. CONCLUSION

On testing the Touch hand system with the amputee, its performance was satisfactory and has the proficiency to grip a number of objects with many shapes. The amputee was able to the balance object on plastic containers and cylinder, which was quite nice for the building of puzzles. However, the amputee had a fatigue since it was his fist time with EMG prosthetics. In addition, the amputee needed strength, endurance, and skill to continually using the hand. The EMG, electronics, and sensory systems form the modularity for the Touch hand system. The design objectives were met and stated as shown in table 17.

Table 17: Discussion and analysis of the design objectives

Design objectives	Discussion and analysis
(1) Controlling the prosthetic hand using only two channels.	The two set of EMG electrodes were placed on the forearm muscles to analysis the movement of the muscles according to the gripping type performed by the hand. These EMG signals were then decoded to suit the exact gripping actions.
(2) Investigation of the non-contact and non-contact electrodes for the Touch hand system.	Touch hand system used non-contact electrodes because of their indirect contact between the electrode surface and skin. They were also easier to use and more comfortable since capacitively coupled the need for conductive gel. It was observed that the was a correlation between the EMG electrodes and antenna, thus obtaining the best reading in a patch-yagi antenna configuration. This was proved in the experiment to determine the effect of increasing the number of electrode layers and antenna effect. As a result, 2 layers of the embroidery electrodes with a combination of the cloth were chosen.

Design objectives	Discussion and analysis
(3) To measure the temperature of objects, slippage, and texture of the hand.	The sensors of the hands proved to satisfactorily detect temperature and grip force. The ability of the hand to detect extreme temperatures quickly was inaccurate. The hand's prediction grew more accurate as the time passed, especially after the 4-second window lag time. The hand could satisfactorily determine when it was in contact with dangerously hot objects.
(4) The system should be aesthetically pleasing, low-cost and lightweight.	The Touch hand 3 electronics cost USD 500.This was a lost cost mechatronic system compared to the Touch hand 2 which cost USD 700.The hand was aesthetically pleasing because of the modular electronics and sensory system that was designed.

As mentioned in table 17, the choice of the best non-contact electrodes were based on the higher amplitudes values of the V+ and Vpp. The table 18 shows that the combination of the developed contactless and embroidery electrodes with silicon were giving similar results. As a result of that, embroidery electrodes proved to be the best choice because they were less noisy.

Table 18: Comparison of the non-contact electrodes

Best combination non-contact electrodes	V+(V)	Vpp(V)
Developed contactless electrodes 4 layers	0.269	0.463
Developed contactless electrodes + Silicon 4 layers	0.56	0.56
Embroidery electrodes + cloth 2 layers	1	1.51
Embroidery electrodes + cloth + Silicon layer 2 layers	0.56	0.56

The results obtained in table 18 shows that 2 layers were the best since it corresponds to the highest voltage. The results with 1 embroidery sensor on silicon layer were less than that of a single embroidery sensor against the skin. It was noted that the non-contact electrodes have many advantages over contact electrodes.

The first advantage was that non-contact method provides an indirect contact between the electrode surface and skin. The non-contact measurement is also suitable for long-term measurements since conductive gel desiccation can result in loss of contact between the electrodes. Less noisy and smoother graphs were observed for non-contact electrodes than contact electrodes. The features implementation of non-contact electrodes for amputees have been obtained, because of their sophisticated, comfortable and non-obtrusive EMG measurements and it can be concluded that there is value in using them.

The study of the relation between EMG and biomechanical variables including the joint motion, force, muscle fatigue, and velocity. It was concluded that the measure of tension was the mean value of the corrected EMG signal. From an electromyographically point of view, fatigue has been found to not only reduce the muscle force but also to alter the shape of the motor action potentials. It was found that the EMG amplitude increased with increasing walking speed and that the EMG activity was minimized with subjects walking at their comfortable speed. Furthermore, Kalman filtering that uses Gaussianity assumption and other EMG signals were used for EMG decoding to minimize noise. The algorithms for the EMG, temperature, pressure and vibration sensors were formulated to designing a working prosthetic hand with human-like features.

The prosthetic hand consisted of the two microprocessor and circuitry allowing it to control the linear actuators for the fingers and a DC motor for the wrist motion. The hand used flex sensors to measure the degree of closure in each finger and is equipped with a modular sensory system. The sensory system consists of pressure, temperature and vibration sensors, which were used to detect grip force, temperature, object slippage, and texture. These sensors could accurately detect grip force (to 0.1 N) and temperature (to the nearest degree Celsius). Methods for detecting object slippage and texture using the vibration sensors were proposed. The hand was controlled with a 2-channel EMG control system.

For future recommendations, the hand should be equipped with vibrotactile to display sensory feedback control to the amputee. The hand should also communicate navigation information from the human user interface control method.

7. REFERENCES

Alsayegh O.A., 2000. “EMG-based human-machine interface system,” Multimedia and Expo, 2000. ICME 2000. 2000 IEEE International Conference on, vol. 2, pp. 925 – 928.

Andre Luiz Aita and Cesar Ramos Rodrigues. "PTAT CMOS Current Sources Mismatch over Temperature". The 26th Symposium on Integrated Circuits and System Design (SBCCI 2013). 2013.

Aicha Zerbet, Mikhail Nikulin. A new statistics for detecting outliers in exponential case, Communications in Statistics: Theory and Methods, 2003, v.32, pp. 573–584.

Andersen, Jesper L. "Muscle, Genes and Athletic Performance." Scientific American 283, no. 3 (2000): 48–55.

Ascoli, G.A. (Ed). (2002). Computational Neuroanatomy: Principles and Methods. Totowa, New Jersey: Humana Press.

Antonis Papachristodouluo and Ali Jadbaaie, “Delay Robustness of Nonlinear Internet Congection Control Schemes”, IEEE Transaction on automatic control, Volume 55, pp- 1421-1427, (2010).

Antonios G. Angoules, MD; Konstantine C. Balakatounis, PT, MSc; Kalomoira A. Panagiotopoulou, PT; Andreas F. Mavrogenis, MD; Evanthia A. Mitsiokapa, MD; Panayiotis J. Papagelopoulos, MD, DSc (2008). Effectiveness of Electromyographic Biofeedback in the Treatment of Musculoskeletal Pain. ORTHOPEDICS 2008; 31:980.

Baldwin, K. M. & Haddad, F. (2014) The Muscular System: Muscle Plasticity. History of Exercise Physiology, p. 337

Barreto A. B., Scargle S. D., and Adjouadi M, 1999. “A Real-Time Assistive Computer Interface for Users with Motor Disabilities,” ACM SIGCAPH Computers and the Physically Handicapped, pp. 6-16.

Bear, M., *et* al. Neuroscience: Exploring the Brain. Baltimore: Williams & Wilkins, 1996.

Balanis, Constantine A. (2011). Modern Antenna Handbook. John Wiley and Sons. pp. 2.17-2.18.

Basmajian JV, de Luca CJ. Muscles Alive - The Functions Revealed by Electromyography. The Williams & Wilkins Company; Baltimore, 1985.

Burns, G.W., et al., Temperature-Electromotive Force Reference Functions and Tables for the Letter-Designated Thermocouple Types Based on the ITS-90, NIST Monograph 175, National Institute of Standards and Technology, 1993.

Broman, H., Bilotto, G., & De Luca, C.1. (1985). A note on non-invasive estimation of muscle fiber conduction velocity. IEEE Transactions on Biomedical Engineering, 32, 341-344.

Bufalari S., Mattia D., Babiloni F., Mattiocco M., Marciani M. G., Cincotti F., 2006 "Autoregressive spectral analysis in Brain Computer Interface context," Engineering in Medicine and Biology Society, 2006. EMBS '06. 28th Annual International Conference of the IEEE, pp. 3736 – 3739.

Basu, Dipak (2010). Dictionary of Pure and Applied Physics, 2nd Ed. CRC Press. p. 21.

Basmajian, J.V., & De Luca, C.J. (1985). Muscles alive (5th ed.). Baltimore: Williams & Wilkins.

Broman, H., Bilotto, G., & De Luca, C.1. (1985). A note on non-invasive estimation of muscle fiber conduction velocity. IEEE Transactions on Biomedical Engineering, 32, 341-344.

C. A. Balanis, Antenna Theory, Analysis and Design, John Wiley & Sons, Inc., New Jersey, 2005.

Cheng M., Gao X. R., Gao S. G., and Xu D. F., 2002. "Design and implementation of a brain computer interface with high transfer rates," IEEE Transactions on Biomedical Engineering, vol. 49, pp. 1181-1186

Doyle T. E., Kucerovsky Z., Greason W. D., 2006. "Design of an Electroocular Computing Interface", Electrical and Computer Engineering, 2006. CCECE '06. Canadian Conference on, pp. 1458-1461.

Downie, Neil A, 'The Ultimate Book of Saturday Science' (Princeton 2012)

D.J. Atkins and R.H. Meier, Comprehensive Management of the of the Upper-Limb Amputee, Springer-Verlag Publishing, 1988.

David K. Cheng, Field and Wave Electromagnetic, AddisonWesley Pub. Co., New York, 1989.

Day SJ (1997) The Properties of Electromyogram and Force in Experimental and Computer Simulations of Isometric Muscle Contractions: Data from an Acute Cat Preparation. Dissertation, University of Calgary, Calgary.

De Luca, CJ., & Van Dyk, EJ. (1975). Derivations of some parameters of myoelectric signals recorded during constant-force isometric contractions. Biophysical Journal, 15, 1167-1180.

De Luca, CJ. (1984). Myoelectric manifestations of localized muscular fatigue. CRC Critical Reviews in Biomedical Engineering, 11, 251-279.

Drew van der Reit (2014). A Modular prosthetic arm with haptic interfacing for transradial amputees

E. Huigen, A. Peper, and C. A. Crimbergen, “Investigation into the origin of the noise of surface electrodes,” Medical & Biological Engineering & Computing, vol. 40, pp. 332–338, 2002.

Fernández, M. and Pallás-Areny, R. (2000). Ag-AgCl electrode noise in high-resolution ECG measurements. Biomed. Instrum. Technol., 34, 125-130.

Fawwaz T. Ulaby, Applied Electromagnetics, Prentice-Hall, Inc., New Jersey, 2007.

Fernández, M. and Pallás-Areny, R. (2000). Ag-AgCl electrode noise in high-resolution ECG measurements. Biomed. Instrum. Technol., 34, 125-130.

Ferris, C.D. (1972). Introduction to bioelectrodes. Plenum Press, New York.

Graf, Rudolf F. (1999). Modern Dictionary of Electronics (7 ed.). Newnes. p. 858.

Gopi E.S., Sylvester Vijay R., Rangarajan V., Nataraj L., 2006. “Brain Computer Interface Analysis using Wavelet Transforms and Auto Regressive Coefficients,” Electrical and Computer Engineering, 2006. ICECE '06. International Conference on, pp. 169 – 172.

Guger C., Edlinger G., Harkam W., Niedermayer I., and Pfurtscheller G., 2003. “How many people are able to operate an EEG-based brain-computer interface (BCI),” IEEE Trans. Rehab.Engng, vol 11(2), pp. 145-147.

Gregory Kyle Jones (2015). Mechatronic Design and optimisation of a low cost prosthetic hand.

Grainger, John J and William D Stephenson (1994). Power System Analysis and Design. New York: McGraw-Hill. pp. 51–54

Jonghwa Kim, Stephan Mastnik, Elisabeth André, 2008. “EMG-based hand gesture recognition for real-time bio signal interfacing,” International Conference on Intelligent User Interfaces, Proceedings of the 13th international conference on intelligent user interfaces, pp. 30-39.

J.Nguyen, Valence Technology, Austin, Texas, USA Gianluca De Luca (2001) “Fundamental Concepts in EMG Signal Acquisition”, Delsys Incorporated

Kandel, Eric R., James H. Schwartz, and Thomas M. Jessell. Principles of Neural Science, 4th Ed. New York: McGraw-Hill, 2000.Dalley, Keith L. Moore, Anne M.R. Agur (2010). Clinically oriented anatomy (6th ed., [International Ed.]. Ed.). Philadelphia [etc.]: Lippincott Williams & Wilkins, Wolters Kluwer. pp. 48–55.

Kamen, Gary. Electromyography Kinesiology. In Robertson, DGE et al. Research Methods in Biomechanics. Champaign, IL: Human Kinetics Publ., 2004.

Lippert, L.S. (2011). Clinical Kinesiology and Anatomy, 5th ed. Philadelphia, PA: F.A. Davis.

L.H. Han and H.P. Huang Department of Mechanical Engineering of Taiwan University, Development of A Modular Prosthetic Hand- NTU-Hand III ,Dec(2014).

Mansfield, P.J., & Neumann, D.A. (2009). Essentials of Kinesiology for the Physical Therapist Assistant. St. Louis, MO: Mosby Elsevier.

Malmivuo, Jaakko, Robert Plonsey (1994). Bio electromagnetism*:* principles and applications of bioelectric and biomagnetic fields. New York: Oxford University Press

Marieb, Elaine; Hoehn, Katja (2007). Human Anatomy & Physiology (7th Ed.). Pearson Benjamin Cummings. p. 317

Microstrip antenna design handbook/ Ramesh G. Artech house 2001, ISBN 0-89006-513-6

Millan J. D., Renkens F., Mourino J., and Gerstner W., 2004. "Non-invasive brain-actuated control of a mobile robot by human EEG," IEEE Transactions on Biomedical Engineering, vol.51, pp. 1026-1033.

Miami, FL; 1997. p. 56-60. & In 1998. Webster JG, editor. Medical instrumentation: application and design, 3rd Ed. Boston: Houghton Mifflin Company.

McGee, Thomas (1988). "Chapter 9". Principles and Methods of Temperature Measurement. John Wiley & Sons. p. 203

Milligan Thomas A. Modern antenna design, Second edition. Published 2005

Mital A Gandhi, and Lamine Mili, "Roust Kalman Filter based on a Generalized Maximum- Like good-Type Estimator", IEEE Transaction on Signal Processing, Volume 58, pp-2509-2520,(2010).

Performance of Phosphate Lithium-ion Batteries in Motive Applications,

P.R.S. Sanches, A.F. Müller, L. Carro, A.A. Susin, P. Nohama (2007) "Analog Reconfigurable Technologies for E Bancroft, R. Microstrip and Printed Antenna Design Noble Publishing 2004, chapter 2-3

Patton HD, Fuchs AF, Hille B, Scher AM, Steiner R (eds.) (1989): Textbook of Physiology, 21st ed., 1596 pp. W. B. Saunders, Philadelphia.

Pfurtscheller G, Flotzinger D, Pregenzer M, Wolpaw JR, McFarland D., 1996. "EEG-based brain computer interface (BCI)". Med Progr Technol, 21.

Palaniappan R., 2005. "Brain Computer Interface Design Using Band Powers Extracted During Mental Tasks," Neural Engineering, 2005. Conference Proceedings. 2nd International IEEE EMBS Conference on, pp. 321 – 324.

Qiuping Ding, Kaiyu Tong, Guang Li, 2005. “Development of an EOG (Electro-Oculography) Based Human-Computer Interface,” 27th Annual International Conference of the Engineering in Medicine and Biology Society, IEEE-EMBS 2005, pp. 6829 – 6831.

RSLSteeper (2013a). Bebionic3 precision open grip. Available online: http://www.wired.com/images_blogs/wiredscience/2012/11/bebionic3-precision-open.jpg, [2014, September 15].

Wolff Christian (2010). "Yagi Antenna". Radar Basics. Radartutorial.eu. Retrieved September 18, 2014.

W.H. Ko, M.R. Neumann, R.N. Wolfson and E.T. Yon,”Insulated Active Electrodes”, IEEE Transactions on Industrial Electronic Control Instruments, 17, 1970, pp. 195-197

Taberner A. M., Barreto A. B., 1997. “Real-time signal processing towards an EEG-based human-computer interface,” Proceedings of the 1997 Florida Conference on Recent Advances in Robotics, Wolpaw J. R. and McFarland D. J., 1994. "Multichannel EEG-based brain-computer Communication," Electroencephalography and Clinical Neurophysiology, vol. 90, no. 6, pp. 444-449.

Winder, Steve; Joseph Carr (2002). Newnes Radio and RF Engineering Pocket Book, 3rd Ed. Newnes.

W. L. Stutzman and G. A. Thiele, Antenna Theory and Design, Wiley, New York, 1998.

John D. Kraus, Antennas, McGraw-Hill, New York, 1988.

Tavernier, Karel. "PCB Fabrication Data - A Guide". Ucamco. Retrieved 8 January 2015.

Siemens, William (1871). "On the Increase of Electrical Resistance in Conductors with Rise of Temperature, and Its Application to the Measure of Ordinary and Furnace Temperatures; Also on a Simple Method of Measuring Electrical Resistances". The Bakerian Lecture (Royal Society). Retrieved May 14, 2014.

Strouse, G.F. (2008). Standard Platinum Resistance Thermometer Calibrations from the Ar TP to the Ag FP. Gaithersburg, MD: National Institute of Standards and Technology.

James Bryant. "IC Temperature Sensors". Analogue Devices. 2008.

Omega Engineering, 1999. Practical Guidelines for Temperature Measurement, Online Technical Report.

Sclater, N., Mechanisms and Mechanical Devices Source book, 4th Edition (2007), 25, McGraw-Hill

S. Au, M. Berniker, and H. Herr, “Powered ankle-foot prosthesis to assist level-ground and stair-descent gaits,”Neural Netw., vol. 21, no. 4, pp. 654–666, 2008.

Appendix A: MOTOR AND GEAR BOX

a. Miniature linear motion series

PQ12 Specifications

Gearing Option	30:1	63:1	100:1
Peak Power Point	15N@15mm/s	30N @ 8mm/s	40N @ 6mm/s
Peak Efficiency Point	8N @ 20mm/s	12N@12mm/s	20N @ 8mm/s
Max Speed (no load)	28mm/s	15mm/s	10mm/s
Max Force (lifted)	18N	45N	50N
Max Side Load	5N	10N	10N
Back Drive Force	9N	25N	35N
Stroke	20 mm		
Input Voltage	6 or 12 VDC		
Stall Current	550mA @ 6V, 210mA @ 12V		
Mass	15g		
Operating Temperature	-10°C to +50°C		
Positional Repeatability	±0.1mm		
Mechanical Backlash	0.25 mm		
Audible Noise	55dB @ 45cm		
Ingress Protection	IP-54		
Feedback Potentiometer	5kΩ±50%		
Limit Switches	Max. Current Leakage: 8uA		
Maximum Duty Cycle	20%		

b. Load curves and Current curves

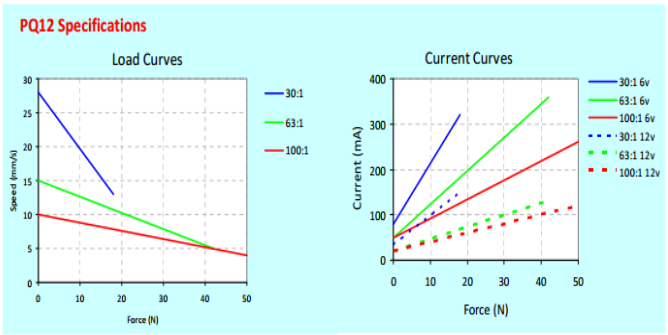

c. Mechanical drawings of the linear actuator

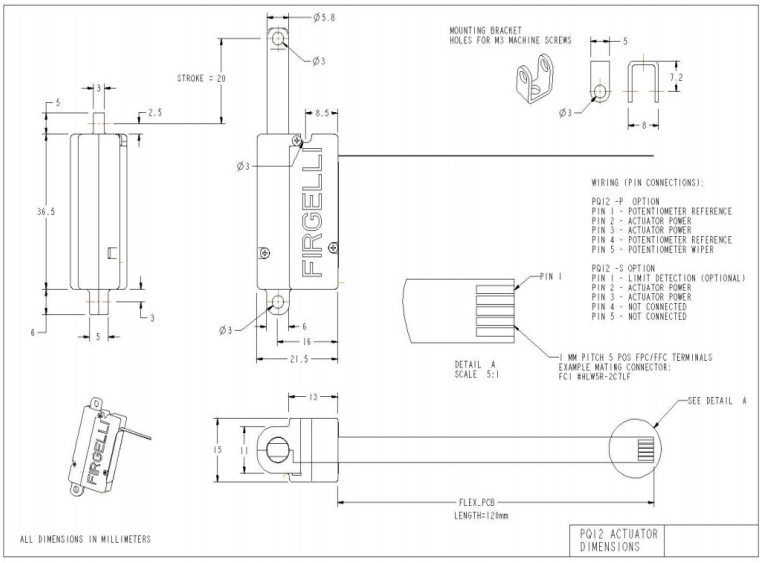

Appendix B: COST ESTIMATIONS

Item Name	Cost per item/m	No. of items	Cost	Specs	Supplier	Part Number	Ref Design
Regulators, MC7805	R 4.00	4	R 16.00		Mantech	14k5237	U19
Diode 1n4001	R 0.20	1	R 0.20		Mantech	14k5217	D13
ZENER, 1N5226B	R 0.35	12	R 4.20	3.3 V, 500 mW, 1N5226	Mantech	14K1531	D1, D2, D3, D4, D5, D6, D7, D8, D9, D10, D11, D12
RESISTOR, 33kΩ	R 0.20	15	R 3.00		Mantech	14k7898	R25, R26, R27, R28, R29, R30, R31, R33, R34, R37, R38, R43, R48, R53, R58
RESISTOR, 10kΩ	R 0.20	1	R 0.20		Mantech	14k7854	R42
RESISTOR, 20kΩ	R 0.25	6	R 1.50		Mantech	14k8035	R32, R39, R44, R49, R54, R59
CAPACITOR M/L, 22nF	R 0.35	7	R 2.45		Mantech	14k2755	C25, C26, C27, C28, C29, C30, C31
RESISTOR, 27Ω	R 0.25	12	R 3.00		Mantech	14k7890	R4, R10, R14, R15, R23, R24, R36, R41, R46, R51, R56, R61
RESISTOR, 6.8kΩ	R 0.25	19	R 4.75		Mantech	14k7917	R1, R3, R6, R7, R9, R11, R13, R16, R18, R19, R20, R22, R35, R40, R45, R47, R50, R55, R60
Op-amp, LM358(UTC)	R 1.00	7	R 7.00		Mantech	lm358d	U1, U11, U13, U14, U16, U20, U21
CAPACITOR, 680pF 10%	R 0.20	6	R 1.20		Mantech	14k2574	C13, C15, C17, C19, C21, C23
CAP_ELECTROLIT, 47µF	R 1.00	6	R 6.00		Mantech	14k9486	C14, C16, C18, C20, C22, C24
Drivers, A4973SLB	R 29.38	4	R 117.52		Mantech	99k0231	H1, H2, H3, H4, H5, H6
Headers, 2500-02RT	R 0.18	7	R 1.26		Mantech	14k0898	MC1, U3, U4, U6, U7, U8
RESISTOR, 0.1Ω 5%	R 1.00	6	R 6.00		Mantech	14k7918	Rs1, Rs2, Rs3, Rs4, Rs5, Rs6
RESISTOR, 220Ω 5%	R 0.20	3	R 0.60		Mantech	14k8287	R2, R12, R21
CAPACITOR, 47nF	R 0.35	12	R 4.20		Mantech	14k5810	C1, C2, C3, C4, C5, C6, C7, C8, C9, C10, C11, C12
RESISTOR, 220Ω 5%	R 0.25	3	R 0.75		Mantech	14k7883	R5, R8, R17
Arduino M0	R 693.20	10	R 6 932.00		Micro Robotics, Mantech		U5
PCB board material	R 20.00	1	R 20.00		UKZN Elect.		
Header SIL R/A 40W	R 5.10	1	R 5.10		Mantech	14k1173	
Header SIL STR 40 W	R 4.00	1	R 4.00		Mantech	70k1005	
Wick Desolder 1.9 mm	R 33.00	1	R 33.00		Mantech	14k2716	
Twin Flex Black/Black (Power Cable)	R 3.95	1	R 3.95		Mantech	70k0657	
Hous Sil F/Lock 2W (Motor Plug Housing)	R 0.10	7	R 0.70		Mantech	14k3756	
Terminals 2510 T Loose	R 0.20	25	R 5.00		Mantech	70k0163	
Socket DC In-line R/A (Power Cable Attached Socket)	R 4.50	1	R 4.50		Mantech	14k8966	
Wire M/S 0.34 O=1.6 BLUE	R 2.50	2	R 5.00		Mantech	70k0779	
Wire M/S 0.2 O=1.6 ORANGE	R 1.35	2	R 2.70		Mantech	70k0454	
Sleeve heat-shrink 1.5mm BK	R 2.50	1	R 2.50		Mantech	55k0002	
Temperature Sensor (LM35)	R 18.38	5	R 91.90		Manitech		
Solder	R 30.00	1	R 30.00		Mantech		
		electronics total	**R 7 270.68**				

Appendix C: EMG TESTS

a. Developed Contactless Electrodes

"Stick-on" electrodes															
1 Layer			2Layer			3Layer			4 Layer			5 Layer			
V+	V-	Vp-p	V+	V-	Vp-p	V+	V-	Vp-p	V+	V-	Vp-p	V+	V-	Vp-p	
0.088	-0.092	0.18	0.0856	-0.0944	0.18	0.192	-0.064	0.256	0.246	-0.204	0.45	0.296	-0.118	0.414	
0.21	-0.086	0.296	0.106	-0.0736	0.1796	0.08	-0.0336	0.1136	0.258	-0.192	0.45	0.266	-0.184	0.45	
0.122	-0.044	0.166	0.114	-0.05	0.164	0.21	-0.108	0.318	0.27	-0.18	0.45	0.118	-0.136	0.324	
0.0944	-0.0344	0.1288	0.118	-0.0616	0.1796	0.512	-0.212	0.712	0.0944	-0.048	0.1424	0.256	-0.194	0.45	
0.532	-0.368	0.9	0.284	-0.172	0.456	0.384	-0.328	0.712	0.584	-0.504	1.088	0.568	-0.168	0.736	
0.242	-0.238	0.48	0.424	-0.476	0.9	0.121	-0.0592	0.1802	0.0416	-0.032	0.0736	0.0592	-0.0584	0.1176	
0.101	-0.0792	0.1802	0.142	-0.04	0.182	0.252	-0.198	0.45	0.101	-0.0576	0.1586	0.148	-0.052	0.2	
0.0968	-0.132	0.2288	0.123	-0.0568	0.1798	0.23	-0.086	0.316	0.308	-0.142	0.45	0.308	-0.142	0.45	
0.0584	-0.0096	0.068	0.103	-0.0768	0.1798	0.258	-0.192	0.45	0.516	-0.384	0.9	0.592	-0.128	0.72	
0.1716222	-0.120356	0.2919778	0.1666222	-0.122356	0.28897778	0.24877778	-0.1423111	0.38975556	0.26877778	-0.1937333	0.46251111	0.29013333	-0.1311556	0.42906667	

b. Embroidered electrode

Embroidered electrodes														
Direct contact			2 Layer			3 Layer			4 Layer			5 Layer		
1 Layer														
V+	V-	Vp-p	V+	V-	Vp-p	V+	V-	Vp-p	V+	V-	Vp-p	V+	V-	Vp-p
1.44	-0.78	2.22	1.3	-1.6	2.9	0.436	-0.464	0.9	0.266	-0.178	0.444	0.0984	-0.0816	0.18
0.544	-0.356	0.9	0.428	-0.276	0.704	0.264	-0.248	0.508	0.392	-0.204	0.594	2.2	-1.52	3.72
0.268	-0.192	0.46	0.26	-0.16	0.42	0.52	-0.38	0.9	0.328	-0.24	0.564	0.236	-0.214	0.45
0.52	-0.38	0.9	1.04	-0.76	1.8	1.04	-0.76	1.8	2.64	-1.16	3.8	0.472	-0.428	0.9
0.216	-0.12	0.336	0.105	-0.0752	0.1802	0.262	-0.124	0.386	0.524	-0.376	0.9	0.472	-0.428	0.9
0.0848	-0.0952	0.18	0.212	-0.098	0.31	0.16	-0.102	0.262	0.226	-0.224	0.45	0.22	-0.112	0.332
1.09	-0.648	1.77	2.4	-1.08	3.48	0.0888	-0.052	0.1408	0.576	-0.324	0.9	1.15	-0.648	1.798
1.06	-0.7	1.76	0.08	-0.054	0.134	0.14	-0.094	0.234	0.26	-0.116	0.376	2.62	-1.84	4.46
0.248	-0.104	0.352	0.496	-0.404	0.9	0.0992	-0.0808	0.18	0.248	-0.202	0.45	0.496	-0.404	0.9
0.60786667	-0.3750222	0.98644444	0.70233333	-0.5008	1.20313333	0.33444444	-0.2560889	0.59008889	0.60666667	-0.336	0.942	0.88493	-0.63062	1.51556

c. Embroidered electrodes + Cloth

Embroidered Electrodes + Cloth														
Direct														
1 Layer			2 layer			3 Layer			4 Layer			5 Layer		
V+	V-	Vp-p	V+	V-	Vp-p	V+	V-	Vp-p	V+	V-	Vp-p	V+	V-	Vp-p
0.308	-0.142	0.45	1.23	-0.568	1.798	1.36	-1.3	2.66	0.0992	-0.0472	0.1464	0.492	-0.408	0.9
3.24	-0.68	3.92	0.984	-0.816	1.8	1.52	-0.54	2.06	1.22	-0.2	1.42	1.21	-0.592	1.802
0.472	-0.428	0.9	0.944	-0.472	1.416	0.472	-0.428	0.9	0.936	-0.856	1.792	0.412	-0.18	0.592
0.944	-0.856	1.8	0.944	-0.44	1.384	0.468	-0.432	0.9	2.36	-1.52	3.88	2.36	-1.14	3.5
0.944	-0.856	1.8	0.236	-0.104	0.34	0.472	-0.428	0.9	2.36	-1.52	3.88	2.12	-1	3.12
0.532	-0.368	0.9	0.234	-0.046	0.28	0.106	-0.0736	0.1796	0.1	-0.0272	0.1272	0.258	-0.076	0.334
1.28	-0.24	1.52	1.62	-0.94	2.56	2.22	-1.14	3.36	3.16	-1.64	4.8	3.16	-1.2	4.36
0.524	-0.256	0.78	1.05	-0.584	1.934	2.26	-0.8	3.06	0.572	-0.328	0.9	1.14	-0.608	1.748
0.64	-0.112	0.752	1.33	-0.472	1.802	0.76	-0.2	0.96	1.03	-0.768	1.798	1.18	-0.38	1.56
0.98711	-0.43756	1.42467	0.95244	-0.49356	1.47933	1.07089	-0.59351	1.6644	1.31524	-0.76738	2.08262	1.37022	-0.62044	1.99067

d. Monitoring Muscle group in Volunteers

1. Volunteer1

	Direct contact									
	Muscle group 1(yellow signal)			Muscle group 2		blue signal				
Volunteer 1	V+	V-	Vp-p	V+	V-	Vp-p	Sum		V+1 ratio	V+2 ratio
Gripping a pencil (to pick it up)	0.028	-0.084	0.112	0.152	0.07	0.082	0.18	18	15.5555556	84.4444444
gripping/holding a key	0.0152	-0.0104	0.0256	0.108	0.05	0.58	0.1232	12.32	12.3376623	87.6623377
Turning wrist to the right	0.022	-0.044	0.066	0.404	0.064	0.34	0.426	42.6	5.16431925	94.8356808
Turning write to the left	0.0176	-0.036	0.0536	0.808	0.096	0.712	0.8256	82.56	2.13178295	97.8682171
pick up a spoon	0.019	-0.0147	0.0337	0.154	0.0848	0.0692	0.173	17.3	10.982659	89.017341
Pick up a plate	0.0259	-0.0443	0.0702	0.253	0.0608	0.192	0.2789	27.89	9.28648261	90.7135174
Pick up a cup	0.0553	-0.0427	0.098	0.176	0.0644	0.1116	0.2313	23.13	23.9083441	76.0916559
Grab a light bulb (or some ball ob	0.0495	-0.125	0.1745	0.48	0.062	0.418	0.5295	52.95	9.34844193	90.6515581
Grip a knife	0.0599	-0.0312	0.0911	0.323	0.143	0.18	0.3829	38.29	15.6437712	84.3562288
Push a clothes peg	0.057	-0.0251	0.0821	0.098	0.052	0.046	0.155	15.5	36.7741935	63.2258065
Carry a bag	0.0148	-0.00456	0.01936	0.157	0.052	0.105	0.1718	17.18	8.61466822	91.3853318
AVERAGE VOLTAGES	0.3642	0.46196	0.82616	3.113	0.794	2.8358	3.4772	347.72	10.4739446	89.5260554

2. Volunteer2

	Direct contact										
	Muscle group 1(yellow signal)			Muscle group 2		blue signal					
Volunteer 2	V+	V-	Vp-p	V+	V-	Vp-p	Sum		V+1 ratio	V+2 ratio	
Gripping a pencil (to pick it up)	0.018	-0.006	0.0078	0.264	0.212	0.052	0.282	28.2	6.38297872	93.6170213	g
gripping/holding a key	0.14	-0.016	0.156	0.205	0.111	0.094	0.345	34.5	40.5797101	59.4202899	g
Turning wrist to the right	0.102	-0.052	0.154	0.178	0.08	0.098	0.28	28	36.4285714	63.5714286	wr
Turning write to the left	0.0152	-0.0048	0.02	0.86	0.16	0.7	0.8752	87.52	1.73674589	98.2632541	wl
pick up a spoon	0.0912	-0.012	0.1032	0.848	0.068	0.78	0.9392	93.92	9.71039182	90.2896082	g
Pick up a plate	0.0288	-0.0208	0.0496	0.32	0.14	0.18	0.3488	34.88	8.25688073	91.7431193	g
Pick up a cup	0.0248	-0.0104	0.0352	0.272	0.088	0.184	0.2968	29.68	8.35579515	91.6442049	g
Grab a light bulb (or some ball ob	0.044	-0.018	0.062	0.192	0.068	0.124	0.236	23.6	18.6440678	81.3559322	lb
Grip a knife	0.036	-0.022	0.058	0.412	0.112	0.3	0.448	44.8	8.03571429	91.9642857	k
Push a clothes peg	0.02	-0.01	0.03	0.178	0.134	0.044	0.198	19.8	10.1010101	89.8989899	g
Carry a bag	0.0624	-0.0152	0.0766	0.776	0.164	0.612	0.8384	83.84	7.44274809	92.5572519	g
AVERAGE VOLTAGES											